

STUDY AND DEVELOPMENT OF TECHNIQUES FOR 3D
DENTAL IDENTIFICATION

ZHONG XIN

(B. Eng., M. Sc., Sichuan University)

A THESIS SUBMITTED
FOR THE DEGREE OF DOCTOR OF PHILOSOPHY
DEPARTMENT OF MECHANICAL ENGINEERING
NATIONAL UNIVERSITY OF SINGAPORE

2013

DECLARATION

I hereby declare that the thesis is my original work and it has been written by me in its entirety. I have duly acknowledged all the sources of information which have been used in the thesis.

This thesis has also not been submitted for any degree in any university previously.

A handwritten signature in black ink, reading "Zhong Xin". The signature is written in a cursive, flowing style. The first name "Zhong" is written with a large, sweeping 'Z' and the second name "Xin" is written with a large, sweeping 'X'.

Zhong Xin

26 December 2013

Acknowledgements

I praise my LORD for HIS steadfast love. HE provides me wisdom and unfailing faith in making my ideas come true. All obstacles and sufferings became blessings of my work. Thank for this character refinement journey. Thank for disciplining me to put a belief in my research work. Thank for arranging helpful people along the way. ‘Your word is a lamp to my feet and a light to my path.’- Psalm 119:105. I believe that ‘The fear of the LORD is the beginning of wisdom, and knowledge of the Holy One is understanding.’- Proverbs 9:10.

I am grateful for Singapore government and National University of Singapore for providing the great opportunity and financial support in my Ph.D. program.

I take great joy in expressing my deepest gratitude to my supervisor Professor Wong Yoke San and Dr. Alan Cheng Ho-lun for their invaluable guidance, support, criticisms and inspirations throughout the entire project.

Also, I am grateful for the productive interactions with Prof. Terence Sim, Prof. Kelvin Weng Chiong Foong , Prof. Lu Weng Feng and forensic dentists Prof. John Clement, Colonel Tan Peng Hui. I could not finish a multi-discipline project without their expertise.

I would like to thank my seniors and colleagues for their fruitful discussions, encouragement. In particular, Dr. Yu Deping, Dr. Zhu Kunpeng, Mr. Zhang Li, Mr. Zhang Zhiyuan, Mr. Ji Dongxu and other members in manufacturing lab in Department of Mechanical Engineering. I would also like to thank visiting scholar Mr. Christian Schwarz for his help in database construction.

Lastly, I wish to thank my parents, relatives, my discipleship study teacher, my church friends for their everlasting support and unconditional love throughout my Ph.D. journey.

Table of Contents

DECLARATION	i
Acknowledgements.....	ii
Table of Contents.....	iii
Abstract.....	v
List of Tables	viii
List of Figures	ix
Nomenclature.....	xii
Chapter 1 Introduction	1
1.1 Human Forensic Identification	1
1.2 Forensic Dental Identification.....	4
1.3 Research Gaps and Problem Statement	8
1.4 Research Objectives and Scopes.....	9
1.5 Research Significance.....	12
1.6 Thesis Structure	12
Chapter 2 Literature Review	13
2.1 Comparative Dental Identification Using Dental Chart.....	13
2.2 Dental Identification Using Computer-aided Software	13
2.3 A Radiograph-based Automated Dental Identification System (ADIS).....	18
2.3.1 Image Segmentation.....	21
2.3.2 Feature Extraction.....	24
2.3.3 Tooth Classification	25
2.3.4 Matching	27
2.5 Dental Identification Trend.....	31
2.6 Summary	32
Chapter 3 Point-based Matching and Identification	33
3.1 Introduction.....	33
3.2 System Approach Overview	33
3.3 Algorithm Overview	34
3.4 Data Preparation.....	36

3.5 Dental Feature Point Extraction	42
3.6 Point Feature Descriptions	45
3.7 Coarse-to-fine Matching	49
3.8 Experiments and Discussion	51
3.9 Computational Time	65
3.10 Summary	66
Chapter 4 Arch-based Matching and Identification and A Hierarchical Ranking Identification Scheme (HRIS).....	69
4.1 Introduction.....	69
4.2 System Approach Overview	71
4.3 Algorithm Overview	73
4.4 Data Preparation.....	74
4.5 Dental Arch Extraction	75
4.5 Arch Feature Description.....	81
4.6 Dental Arch Matching.....	82
4.7 Demonstration of the Hierarchical Ranking Identification Scheme	84
4.8 Experiments and Discussion	85
4.9 Computational Time of HRIS	95
4.10 Summary	97
Chapter 5 Single Tooth Classification and Identification.....	100
5.1 Introduction.....	100
5.2 System Approach Overview	103
5.3 Classification Algorithm Overview	104
5.4 Data Preparation.....	105
5.5 Eigenteeth Calculation	110
5.6 Experiments and Discussion	112
5.7 Summary	117
Chapter 6 Conclusions and Future Work.....	119
6.1 Conclusions.....	119
6.2 Future Work.....	123
List of Publications	125
BIBLIOGRAPHY	126

Abstract

Human forensic identification is the process of establishing the identities of deceased persons from their remains. Dental records have been regarded as one of the primary identifiers from recovered remains under severe conditions and mass disasters when other biological samples, such as DNA and fingerprint, cannot be suitably obtained. The commonly used approach is through manual comparison of dental features in dental charts and radiographs, which is inefficient and prone to errors. The need for computer-facilitated dental identification becomes particularly significant when handling huge volume of samples taken from dental remains after mass disasters, such as the recent Asian tsunami and the earthquake in Japan. The primary objective of this thesis is to develop computer-based 3D identification approaches that overcome key hurdles in those based on 2D radiographs, including inaccurate tooth feature extraction from blurred images and the incorrect matching due to differences of imaging angles since radiographs are 2D projections of 3D objects.

Three approaches are proposed and investigated: point-based matching and identification, arch-based matching and identification, and single-tooth classification and identification. A primary performance index used in the evaluation of the approach is the identification accuracy based on the correctly identified Post-mortem (PM) samples relative to the total number of PM samples tested. Matched Ante-mortem (AM) samples are ranked, whereby rank-1 match using the evaluated technique indicates that the AM sample from the database has been identified to be the most likely match to the PM sample being identified. If it is rank-2 matched, it means that it is the next likely match, and likewise for subsequent ranking.

The point-based matching and identification approach is a pose invariant dental identification (PIDI) technique involving algorithms for feature extraction, description and correspondence on digitized dental casts. Salient point features are first extracted from mesh representations of the digitized dental casts. A saliency shape descriptor is assigned to each extracted point. Then a coarse-to-fine correspondence algorithm is developed to match PM records to a database of AM records. 60 PM samples and 200 AM samples taken from multi-ethnic Asian groups (Chinese, Indian and Malay) are used in the evaluation of the approach. The 60 PM

samples consist of 50 genuine PM samples (which mean that these samples have corresponding AM samples in the AM database) and 10 imposter PM samples (which do not have corresponding AM samples in the AM database). Three types of genuine PM samples are involved: 7 complete PM samples, 11 partial PM samples (with missing teeth compared to the corresponding AM samples), and 32 noisy PM samples. Using the approach, the rank-1 accuracy is 100% for the 7 complete PM sample. The rank-1 identification accuracy of matching 11 partial PM sample is 72.7% and 78.1% for 32 noisy PM samples.

The proposed arch-based matching and identification approach aims to improve the identification speed of the point-based method, whereby dental arches are first extracted from the digitized dental casts using a developed Radial Ray Algorithm (RRA). A Hierarchical Ranking Identification Scheme (HRIS), using arch feature first and then point feature, in matching has been developed with improved identification speed. Arch-based ranked matches serve as pre-filtered set for the more accurate point-based matching. The 7 complete samples achieved 100% rank-1 identification accuracy with a more than 6 times improved identification speed using HRIS. The rank-1 identification accuracy of matching 11 partial PM sample is 54.5% and 59.4% for 32 noisy PM samples.

The third proposed technique is targeted for 3D single-tooth identification. This is applied to cases where only significantly partial jaw features are found, typically with few teeth in the jaw. From previous partial sample identification experiments, it is very difficult to correctly align significantly partial PM jaws with AM samples. Eigenteeth feature and the K Nearest Neighbourhood (KNN) algorithm are applied to first classify different types of human teeth: anterior (incisor and canine), posterior (premolar and molar). Then Iterative Closest Point (ICP) is applied to identify a classified PM single tooth or tooth crown from an indexed AM sub-database. The classification accuracy achieved is 96% and the final rank-1 identification accuracy is 76% in tooth crown identification experiment in the 2-class scheme. The classification accuracy achieved is 90% and the final rank-1 identification accuracy is 80% in complete single tooth (crown and root) identification experiment in the 2-class scheme. The classification accuracy achieved is 88% and the final rank-1 identification accuracy is 68% in tooth crown identification experiment in the 4-class scheme. The classification accuracy achieved is 80% and

the final rank-1 identification accuracy is 70% in complete single tooth (crown and root) identification experiment in the 4-class scheme.

In summary, the study and development of methods presented in this thesis aims towards effective 3D dental identification. They are suitable for computer-facilitated decision support in dental identification by expert investigators. The study shows that identification of partial dental sets, noisy sets and single tooth is feasible in 3D, with certain limitations that are discussed. Further studies, establishment of a comprehensive database, and the development of more robust approaches and techniques are needed to achieve high identification efficiency. The study also serves to provide some of the issues and challenges in computer-assisted dental identification when extending 2D dental identification to 3D dental identification.

List of Tables

Table 1.1 Biometric identifiers comparison.....	4
Table 2.1 Tooth segmentation algorithm comparison	23
Table 2.2 Tooth contour extraction algorithm comparison	25
Table 2.3 Tooth classification algorithm comparison.....	27
Table 2.4 Tooth matching algorithm comparison.....	29
Table 3.1 Main steps of pose invariant dental identification (PIDI) technique	35
Table 3.2 Identification of 7 genuine PM complete samples from 200 AM samples .	52
Table 3.3 Identification of 7 genuine PM complete samples from 100 AM samples .	52
Table 3.4 Genuine matching error at first four ranks (7PM vs 200AM)	52
Table 3.5 Imposter matching error at first four ranks (10PM&200AM).....	54
Table 3.6 Identification of 11 PM genuine partial samples from 200 AM samples	56
Table 3.7 Correspondence algorithm comparison	62
Table 3.8 Shape descriptor comparison	64
Table 3.9 Computational time in Experiment I [Unit: Second (s)]......	66
Table 4.1 comparison of the literature study on dental arch.....	71
Table 4.2 Main steps of Radial Ray Algorithm (RRA) and the Hierarchical Ranking Identification Scheme (HRIS).....	73
Table 4.3 1-200 arch rank list	84
Table 4.4 Arch identification of 11 simulated PM complete samples to 200 AM samples.....	86
Table 4.5 Arch identification of 11 simulated PM complete samples to 200 AM samples.....	88
Table 4.6 Identification of 11 PM partial samples from 200 AM samples (HRIS).....	92
Table 4.7 Identification of noisy samples (1-19) from 200 AM samples (HRIS)	93
Table 4.8 Identification of noisy samples (20-38) from 200 AM samples (HRIS)	94
Table 4.9 Computational time comparison in identification of complete samples [Unit: Second (s)]	96
Table 5.1 Tooth crown data details.....	106
Table 5.2 Complete tooth data details.....	109
Table 5.3 Identification of single tooth crown.....	113
Table 5.4 Identification of complete single tooth	116

List of Figures

Figure 1.1 (a) forensic finger print identification[1] (b) forensic DNA identification [2] (c) forensic dental identification [3]	2
Figure 1.2 Three types of dental radiographs: (a) A bitewing radiograph (b) a periapical radiograph (c) a panoramic radiograph [11]	7
Figure 1.3 Forensic dentist Dave Antunovic of New Plymouth in the police uniform identifying bodies for the Christchurch coroner [12]	7
Figure 1.4 An example of mismatched X-ray tooth contours due to imaging angle change [34].....	9
Figure 1.5 3D-ADIS identification overview flow diagram	10
Figure 1.6 Scenarios and scopes of study	11
Figure 2.1 An example of PM dental chart [7]	13
Figure 2.2 An example of a dental chart produced by WinID[14]	17
Figure 2.3 Match matrix for DVI[15]	18
Figure 2.4 Systematic structures of ADIS [42].....	20
Figure 2.5 Main components in ADIS and identification with user interaction [34] ..	21
Figure 3.1 An overview of the point-based approach.....	34
Figure 3.2 Sample illustration.....	41
Figure 3.3 Manual segmentation of a human skull (a) a human skull (b) the expected detected interstices (solid line) and the interstices obtained by minima curvature rule (dash line) (c) a set of manual segmented mandibular teeth of a human skull (d) PCA-plane (e) segmented tooth crown (f) bottom part of a dental plaster	42
Figure 3.4 Bounding box and diagonal length of a dental surface (b) neighbourhood determination using a query ball for vertex v (c) 6 differently Gaussian-filtered models of a molar from the dental arch	45
Figure 3.5 (a) Saliency descriptor (b) Gaussian curvature descriptor(c) Integral volume descriptor.....	47
Figure 3.6 One ring connectivity for mean curvature estimation	48
Figure 3.7 Differences in genuine sample identification and imposter sample identification (a) genuine sample (b) imposter samples.	50
Figure 3.8 Matching error comparison of genuine samples at first four ranks.....	53
Figure 3.9 Matching error comparison of imposter samples at first four ranks	54
Figure 3.10 (a) manual PM9 ICP (b) manual PM9 this work $\epsilon=0.25\%$ (c) manual PM9 this work $\epsilon=0.15\%$ (d) manual PM13 ICP (e) manual PM13 this work $\epsilon=0.25\%$ (f) manual PM13 this work $\epsilon=0.15\%$ (g) manual PM15 ICP (h) manual PM15 this work $\epsilon=0.25\%$ (i) manual PM17 ICP (j) manual PM17 this work $\epsilon=0.25\%$ (k) auto PM8 ICP (l) auto PM8 this work $\epsilon=0.25\%$ and $\epsilon=0.15\%$	56
Figure 3.11 Noisy sample specific rank.....	57

Figure 3.12 (a) manual PM50 ICP error=1.39 (b) manual PM50 this work error=0.67 (c) auto PM29 ICP error=1.08 (d) auto PM29 this work error=1.05 (e) auto PM50 ICP error=1.42 (f) auto PM50 this work error=1.24	58
Figure 3.13 Identification accuracy comparison of 50 genuine samples	59
Figure 3.14 Feature points on complete, partial and noisy dental meshes (left to right): upper row existing work; lower row: this work	60
Figure 3.15 Possible initial rotations	61
Figure 4.1 (a) Dental arch (b) Dental brace	70
Figure 4.2 Calibration (a, b) and manual arch mark point specification (c) in literatures [62, 80]	70
Figure 4.3 An overview of Arch-based Identification and A Hierarchical Ranking Identification Scheme	72
Figure 4.4 Sample illustration	75
Figure 4.5 Principal axes	76
Figure 4.6 Four possible results after PCA alignment	77
Figure 4.7 Anatomical planes of human body	77
Figure 4.8 Boundary points on X-Y plane	79
Figure 4.9 Dental arch extraction	80
Figure 4.10 Under described (upper row) and over described (lower middle and right) dental arches	81
Figure 4.11 Extracted anterior dentition arch	81
Figure 4.12 PM dental arch, flipped PM dental arch and AM dental Arch before matching	83
Figure 4.13 (a) AM and PM arch matching (b) AM and flipped PM arch matching ..	83
Figure 4.14 Difference of genuine arch matching error (top left) and imposter arch matching error (the other three)	84
Figure 4.15 Simulated arch averaged matching errors at the first 10 ranks	86
Figure 4.16 An example of samples are not identified at rank-1 after arch matching (a) PCA alignment of AM and PM samples (b) extracted arches before matching (c) arches after matching	87
Figure 4.17 Arch matching errors and final matching errors of complete PM samples	89
Figure 4.18 Arch matching errors and final matching errors of 10 imposter PM samples	90
Figure 4.19 Dental arches of top 10% identified partial samples	92
Figure 4.20 Identification accuracy comparison of total samples in Chapter 3 and Chapter 4	94
Figure 4.21 Identification accuracy comparison of only complete samples in Chapter 3 and Chapter 4	95
Figure 5.1 (a) a few pieces of single tooth are found at crime scene (b) a partial jaw with a few teeth (c) samples found in anthropology and archaeology investigations (d) arch shape change due to orthodontic surgery	101

Figure 5.2 Four types of teeth in jaws [86]	102
Figure 5.3 An adult dentition in universal tooth numbering system [87]	103
Figure 5.4 Single tooth classification and identification flow chart	104
Figure 5.5 Single tooth classification algorithm	105
Figure 5.6 Four types of segmented teeth from laser-scanned dental plasters (a) incisor (b) canine (c) premolar (d) molar	106
Figure 5.7 Four types of segmented teeth from laser-scanned dental plasters (a) molar (b) premolar (c) canine (d) incisor (e) upper and lower jaw teeth reconstructed from CBCT image	107
Figure 5.8 3D reconstruction of single tooth from CBCT image (a) one layer of CBCT image (b) specify an initial contour for level set evolvement (c) a clearly defined edge after level set evolvement (d) segmented part lighted in red (e) under segmentation (f) correction of under segmentation (g) over segmentation (h) correction of over segmentation (i) 3D mesh of a single tooth before smoothing (j) smoothed mesh ...	109
Figure 5.9 (a) genuine tooth crowns (b) imposter tooth crowns	113
Figure 5.10 (a) genuine complete single tooth (b) imposter complete single tooth ..	115

Nomenclature

AM	Ante-mortem
PM	Post-mortem
RRA	Radial Ray Algorithm
HRIS	Hierarchical Ranking Identification Scheme
PCA	Principal Component Analysis
ICP	Iterative Closest Point
CBCT	Cone Beam Computed Tomography
AM samples	samples acquired during the lifetime of individuals
PM samples	samples obtained of deceased individuals
Mandibular teeth	teeth in lower jaw
Genuine samples	paired AM and PM samples from the same person
Genuine identification	identification of AM and PM sample comes from the same person
Imposter samples	AM and PM samples belonging to different persons
Imposter identification	identification of AM and PM samples belonging to different persons
Anterior teeth	incisors and canines
Posterior teeth	premolars and molars
Orthodontics	specialty of dentistry that is concerned with the study and treatment of malocclusions

Chapter 1 Introduction

Human forensic identification is the process of establishing the identities of deceased persons from their remains. Dental records have been regarded as one of the primary identifiers from recovered remains under severe conditions and mass disasters when other biological samples, such as DNA and fingerprint, cannot be suitably obtained. This chapter begins with a brief survey of human forensic identification methods, and then introduces the development of forensic dental identification methods. Research gaps and problems are also stated. Finally, research objectives, scopes and contributions are presented.

1.1 Human Forensic Identification

Biometric identifiers have been exploited for decades for human forensic identification. Post-mortem (PM) identification is more difficult than Ante-mortem (AM) identification due to the fact that few biometric identifiers can be used. The objectives of human forensic identification are suspect identification and victim identification. Evidence of biometric identifiers such as fingerprints, DNAs, and dental records are collected at crime scenes and disaster scenes. The identities of suspects and victims could be established by matching the PM and AM records of the collected biometric identifiers. Figure 1.1 shows PM and AM records in human forensic identification.

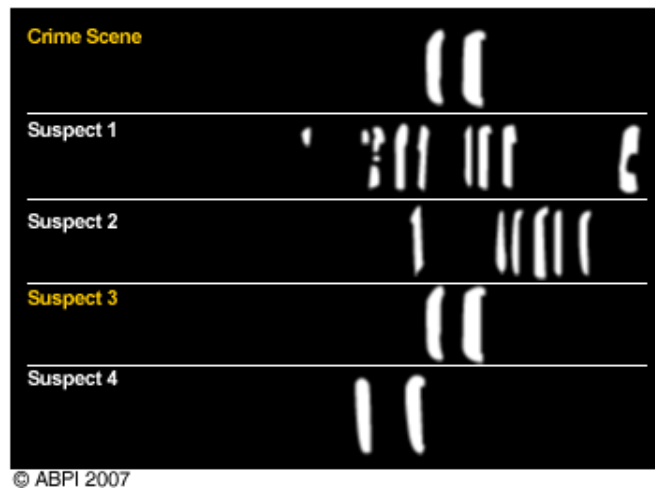
- Fingerprints

Fingerprints have been a popular standard for human identification within the forensic community. Fingerprint identification is a valid and efficient technique in suspect identification, but it is not popular in victim identification, especially in disaster victim identification because in most cases it is impossible to obtain PM fingerprints from decomposed, burnt or skeletonized bodies. For instances, a body that remains immersed in fresh water can decompose rapidly; bodies found in 911 attacks, 2004 Asian tsunami, 2010 Japan earthquakes, airplane crashes, hurricanes, wars were subject to high destructive energy disasters. In such cases, soft tissues of the human

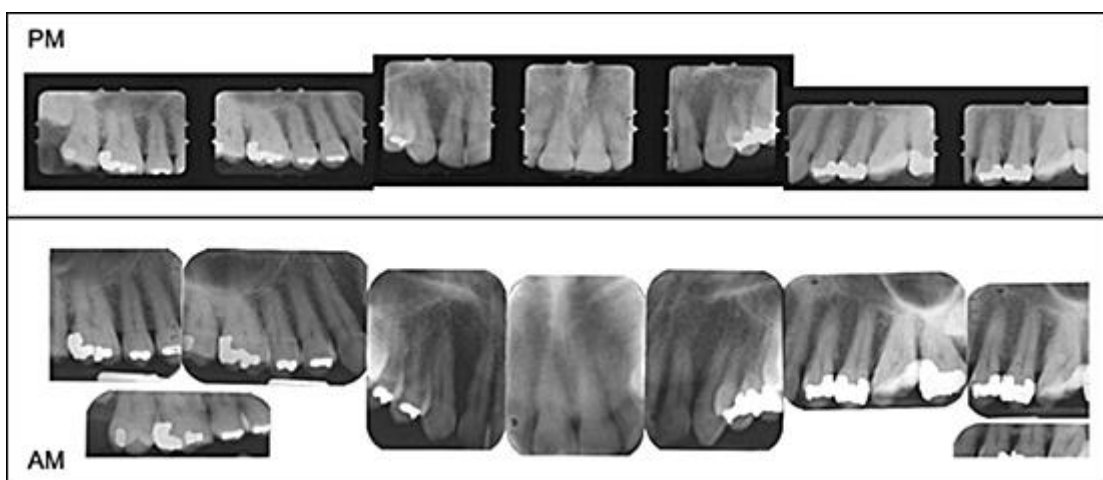
body would have damaged to unidentifiable status; therefore fingerprints cannot be properly obtained for identification.



(a)



(b)



(c)

Figure 1.1 (a) forensic finger print identification[1] (b) forensic DNA identification [2]
(c) forensic dental identification [3]

- DNA

DNA identification has become an increasingly popular forensic technique and is considered to be an accurate identification method. The ability of acquiring AM DNA samples even after an individual's death is an extraordinary advantage of DNA analysis over other ways of identification. A DNA sample from a close relative's stored blood or material from the decedent's hairbrush or toothbrush may provide sufficient comparison material. However, the major limitations are the time required and the costs involved. In addition, DNA from any tissue is only useful if the DNA structure is not altered or destroyed through time, heat, chemical or other forces.

- Dental records

DNA matching is accurate but fragile compared to hard tissues such as bone and teeth for comparison with AM records. Shapes of teeth are likely to be recorded by dental plaster models or x-ray radiographs at medical hospitals and dental clinics when the subject is alive. Very often, the police will contact dental clinics to check for possible matching dental records. In this case, they will first use suitably found teeth or jaw bones. Shapes of individual teeth and bones are useful when there is an existing reference since teeth are more hardy and stable. PM identification requires use of biometric characteristics that resist early decay of body tissues. Statistics show that 20% of the 9/11 victims, identified in the first year, were manually identified using dental records [4]. Moreover, 75% of Tsunami victims in Thailand were similarly identified using dental records, compared to 0.5% identified using DNA [5]. Furthermore, dental identification combined with DNA identification is a powerful tool for human forensic science since dental records are also valuable sources of DNA as other parts of the body get destroyed or degraded in mass disasters Table 1.1 compares the biometric identifiers in terms of robustness to decomposition, accuracy, time and instrument requirement factors.

The above three biometric identifiers are most prevalent forensic identification methods. Other identifiers such as personal items, gender, estimated age, height, build, color of skin, scars, moles, tattoos are also valuable for identification as well as medical evidence such as previous fractures or surgery, missing organs or implants. However, we must be aware that visual identification is one of the least reliable forms of identification and can be fraught with error. For example, facial and other characteristics can change due to trauma, swelling, fragmentation, and decomposition;

hair colour, skin colour, and other physical descriptors can be useful, but cannot be used alone to confirm identification when disfiguring has occurred which could lead to misidentification of the individual [6]. In such cases, most medical examiners will not attempt a visual ID since it may create significant emotional trauma to family members.

Table 1.1 Biometric identifiers comparison

	Dental	DNA	Fingerprint
Robustness	High	Mid.	Low
Accuracy	Mid.	High	High
Time	Short	Long	Short
Instrument required	Mid.	High	Mid.

1.2 Forensic Dental Identification

- Definition

Forensic dentistry or forensic odontology is the examination of dental evidence, which will be presented in the interest of justice. It represents the overlap between the dental and the legal professions [7].

- History

“It is always tempting to suggest that the history of bitemark evidence (and hence forensic dentistry) began with the eating of forbidden fruit in the Garden of Eden.” [8] The earliest documented reference was recorded during the first century. “Agrippina the Younger, fourth wife of Emperor Claudius I and the ambitious mother by a previous marriage of Nero, contracted for the death of Lollia Paulina. To ensure that the contract was accurately concluded, Agrippina had Paulina’s head brought to her. The confirmation of identification was made based on dental misalignments and other peculiarities.” [9]

- Legal and social reasons

Forensic dental identification serves several legal and social requirements. (1)The criminal investigation cannot start before the victim has been identified; (2) remarriage is not allowed in several religions unless the partner is confirmed dead; (3) confirmation of death is also required by several religions before burial; (4) an

identity is a basic premise to preserve human rights and dignity beyond life in most cultures; and (5) it helps to bring relief and proper closure to family members [7].

- Scopes

There are six areas of practice of forensic dentistry: (1) Identification of found human remains (2) Identification in mass fatalities (3) Assessment of bite mark injuries (4) Assessment of cases of abuse (child, spouse, elderly) (5) Civil cases involving malpractice (6) Age estimation. This thesis focuses on the first two areas.

- Procedure

Many people know that dental identification is to compare the PM dental remains with AM dental records to confirm identity. Those records include written notes in dental chart, 2D radiographs, 3D dental casts, etc. However, few people understand the complexities and difficulties of dental identification. Usually, after human remains are found and reported, police will initiate a request for dental identification. Often personal items, such as a wallet or driving licence, may be found and thus help to corroborate the AM records. Geographical location and circumstantial evidence could also enable tentative identification. Currently, dental identification relies on a systematic dental chart prepared by forensic experts and manual radiograph comparison, which often take very long time before correct identity establishment. Tooth features include characteristics of teeth (e.g., tooth present or absent, dental pathology and restorations, crown and root morphology) recorded in dental charts. If AM dental record is available, tentative identity is established depending on the number of matches in the dental chart. Four conclusions can be drawn [10]:

- *Positive identification*: the AM and PM data match in sufficient details, and are from the same individual.
- *Possible identification*: the AM and PM data have consistent features but identity not established positively.
- *Insufficient evidence*: The available information is insufficient to form the basis for a conclusion.
- *Exclusion*: the AM and PM data are obviously inconsistent.

If no AM dental record is available and no other possible ways of identification, PM dental profiling is carried out to limit the population search space. A PM profile will indicate age, ancestry background, sex and occupation, dietary habits, habitual behaviours and occasionally on dental or systemic diseases [7]. Forensic

dentists will assist forensic anthropologists to trace evidences under such circumstances.

- **Dental Radiograph**

Dental radiograph, also known as dental X-ray, is one of the major available sources for dental graph identification at present. It plays an important role in forensic dental identification. There are three types of dental radiographs as shown in Figure 1.2: bitewing, periapical and panoramic.

Bitewing

Bitewing radiographs are taken during most routine dental check-ups and are useful for revealing cavities in the teeth. The bitewing view is taken to visualize the posterior teeth, usually the molars and premolars. The name bitewing refers to a little tab of paper or plastic situated in the centre of the X-ray film, which when bitten on, allows the film to hover so that it captures an even amount of maxillary and mandibular information. It is shown in Figure 1.2 (a).

Periapical

The periapical view could be taken of both anterior and posterior teeth. The objective is to capture the tip of the root on the film. This is often helpful in determining the cause of pain in a specific tooth, because it allows a dentist to visualize the tooth as well as the surrounding bone in their entirety as shown in Figure 1.2 (b). One difference between periapical and bitewing radiographs is the imaging setup. For bitewing radiographs, the film is parallel to the teeth and the X-ray beam is perpendicular to both the teeth and the film. In contrast, periapical radiographs do not require that the film be parallel to the teeth. In some cases, the film and the teeth are deliberately set not to be parallel so that the whole tooth can be imaged on a small radiograph film.

Panoramic

Panoramic films are extraoral films, in which the film is exposed outside the patient's mouth. Panoramic X-rays give a broad overview of the entire dentition (the development of teeth and their arrangement in the mouth). They provide information

not only about the teeth, but also the upper and lower jawbones, sinuses, and other hard and soft tissues in the head and neck as shown in Figure 1.2 (c).

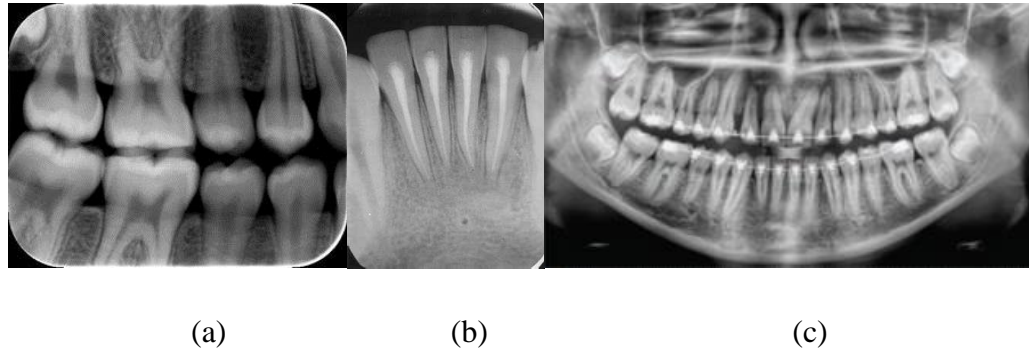


Figure 1.2 Three types of dental radiographs: (a) A bitewing radiograph (b) a periapical radiograph (c) a panoramic radiograph [11]

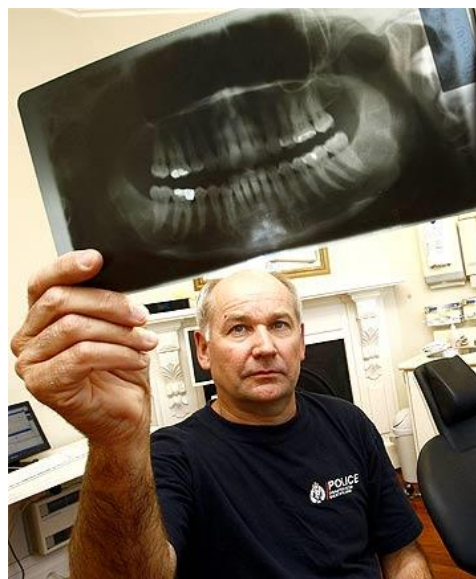


Figure 1.3 Forensic dentist Dave Antunovic of New Plymouth in the police uniform identifying bodies for the Christchurch coroner [12]

An individual's dentition is defined by the number of teeth present, the orientation of the teeth, and dental restorations. Figure 1.3 shows forensic dentist Dave Antunovic is identifying bodies for the Christchurch coroner using dental radiographs.

1.3 Research Gaps and Problem Statement

As mentioned above, it is extremely difficult to build a dental chart automatically as every tooth condition has to be examined and recorded before identification, which is currently done by forensic experts manually. Identification efficiency is quite low. For this reason, since the last three decades, computer-aided identification is receiving more and more attention. There are software systems like Computer-Assisted Post Mortem Identification (CAPMI) [13], WinID [14] and Disaster And Victim Identification (DAVID) [15] based on text-automated search, where the matched images (x-ray radiographs) are examined and verified manually. A prototype of radiograph-based Automated Dental Identification System(ADIS) [16-37] has been developed for a web-based application [38].

However, the automated radiograph-based dental identification approach could not accurately identify blurred radiographs and radiographs obtained with different imaging angles. Since dental radiographs are 2D projections of the 3D shapes, changes in the imaging angle can result in significant variation in the 2D images that cannot be accounted for without 3D information of the teeth [34] as shown in Figure 1.4. Chen et al. [26] reported that 14 of the 25 subjects in their database could not be identified due to poor image quality, variation of the dental structure and insufficient number of AM images. When taking radiographic images of jaw fragments, care must be taken that the beam and film orientation (i.e., imaging angles) be the same as would be expected on a living subject. Otherwise, the teeth will be wrongly identified under incorrect film-orienting.

In addition, user interaction was needed when the results went wrong during the preprocessing steps, therefore, making it a less automatic process.

Furthermore, sample size and the types of radiographs used in existing study were limited, most of which are bitewing images. The identification with missing teeth case was still a hurdle to the 2D identification methodologies and has not been extensively explored. Single tooth identification is a big challenge in this domain.

As there is a trend in extending 2D identification scheme to 3D scheme because of emerging and available 3D scanning/imaging systems, this thesis targets at 3D identification methodology development that can potentially overcome the

aforementioned limitations imposed by the 2D radiographs. Further details and a comprehensive review of the current identification method, methodology, algorithms, and systems will be presented in next chapter.



Figure 1.4 An example of mismatched X-ray tooth contours due to imaging angle change [34]

1.4 Research Objectives and Scopes

The primary objective of this thesis is to develop computer-based 3D identification approaches that overcome key hurdles in 2D identification. The hurdles include inaccurate tooth contour extraction from blurred radiographs and incorrect matching due to differences in imaging angles. Partial identification and single tooth identification will be investigated. This 3D Automatic Dental Identification Scheme (3D-ADIS) is targeted for applications in cases of Missing and Unidentified Persons (MUP) and cases of Mass Disaster Victims (MDV). The Identification Flow Diagram of the proposed 3D-ADIS is shown in Figure 1.5. There are two phases. In the enrolment phase, a feature database will be prepared by suitable extraction of features of models in the digital model repository. In the identification phase, given a PM dental record x , a list of matches, x_1, x_2, \dots , in order of best matches, retrieved from archived AM records is made available for final determination by a forensic expert.

3D-ADIS Identification Overview Flow Diagram

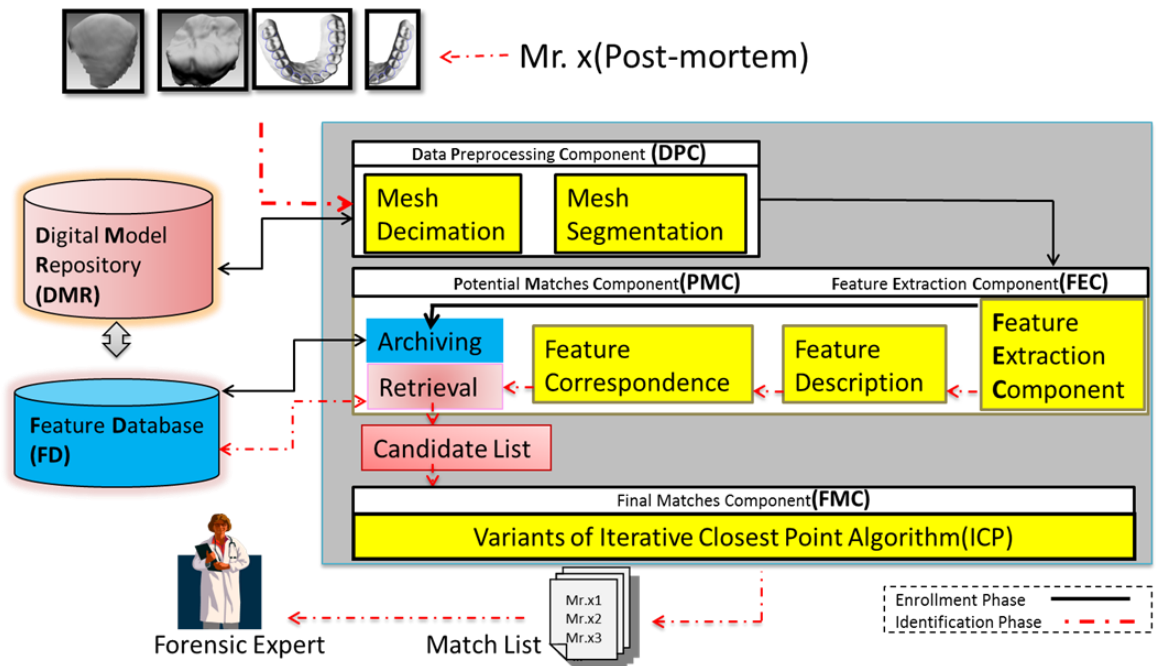


Figure 1.5 3D-ADIS identification overview flow diagram

3D-ADIS involves investigation and development of solutions to several challenging problems in 3D digital image processing that are imposed by the nature of dental surface models: segmentation, classification, feature extraction, and image matching. As shown in Figure 1.5, 3D-ADIS consists of the following components.

Data Preprocessing Component (DPC) This component provides digitized dental models. The digitized models are scanned and reconstructed dense mesh models. The preprocessing component involves mesh decimation and segmentation.

Feature Extraction Component (FEC) This component archives different features extracted for dental models and registration scheme. Features include but not limited to curvature, perceptually salient points, dental arches, frequency domain characteristics.

Potential Matches Component (PMC) This component involves suitable correspondence algorithms to use the extracted features to quickly obtain potentially good initial matches for the Final Matches Component.

Final Matches Component (FMC) This component computes the final matching and provides the ranked (in order of best match) candidate list.

Digital Model Repository (DMR) This stores the digitized dental models that serve as the AM models.

Feature Database (FD) This stores the feature suitably extracted from the DMR.

The FEC, PMC and FMC are key components in 3D-ADIS.

Figure 1.6 shows the scenarios and the three major parts of this research. There are two scenarios in forensic dental identification: teeth are found with jaws and teeth are found with highly partial jaws or without jaws. Point-based and arch-based identification techniques are developed for the teeth-with-jaw scenario and the single tooth identification is developed for the without-jaw and highly-partial-jaw scenario.

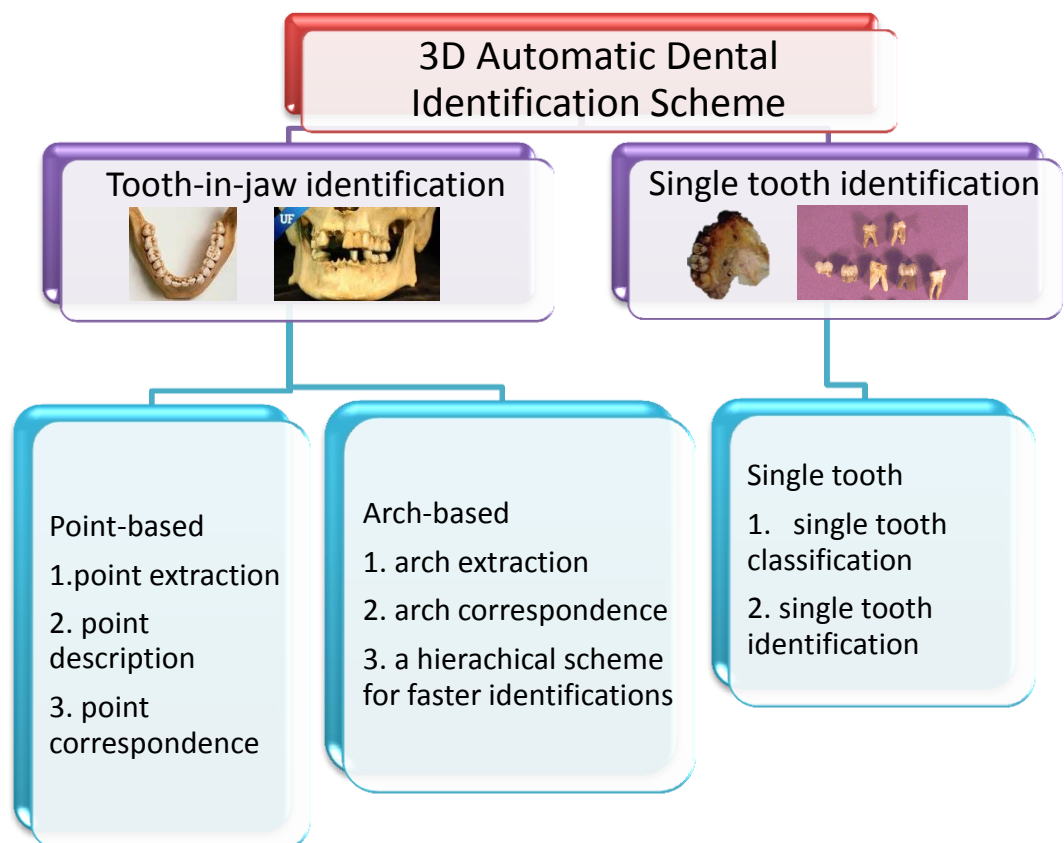


Figure 1.6 Scenarios and scopes of study

1.5 Research Significance

This research aims to overcome problems in traditional dental chart identification and 2D radiograph-based automated dental identification, and provide a faster and more robust computer-facilitated identification process to facilitate expert investigation. More specifically, this study is significant for several reasons:

- It could provide new vision into forensic dental identification as this is the first attempt at 3D dental identification through a systematic and comprehensive investigation.
- It could contribute to a better understanding of the differences of 3D anatomic dental features among individuals. It could shed light on the validity of using those 3D anatomic dental features in identification.
- It may provide the identification system guidelines, structures and database for other research work in 3D dental identification.

1.6 Thesis Structure

Chapter 2 provides a comprehensive literature survey of 2D dental identification scheme as well as the 3D identification trend.

Chapter 3 presents the point-based matching and identification techniques for 3D dental identification and key issues such as point feature extraction and correspondence in 3D dental identification

Chapter 4 introduces another useful dental feature in identification, the dental arch and arch-based matching and identification techniques. Arch feature extraction and correspondence techniques are developed. In order to promote the identification efficiency, a hierarchical ranking identification scheme which eliminates a large number of imposter matches is developed to speed up identification process.

Chapter 5 examines discriminative characteristics regarding four types of human teeth: incisor, canine, premolar and molar. Eigenteeth features are extracted and classified to deal with the challenging single tooth identification problem.

Chapter 6 concludes the thesis with suggestions for future work.

Chapter 2 Literature Review

As the primary objective of this thesis is to develop 3D dental model matching and identification techniques for dental identification that overcome key hurdles in those based on 2D radiographs, the focus in chapter 2 is on a comprehensive survey of techniques in 2D dental identification scheme.

2.1 Comparative Dental Identification Using Dental Chart

The first step of traditional dental identification is to prepare a dental chart, fill up detailed written descriptions, and retrieve radiographs of the found PM dental record. Figure 2.1 shows an example of a dental chart which records the examination date, site, and tooth characteristics. After a PM chart is obtained, it is used to compare and match with archived AM charts by a forensic expert or trained personnel.

B.C. CORONERS' SERVICE
DENTAL IDENTIFICATION FORM

CORNER Case No. 99-129-0008

INVESTIGATING CORNER S. Bellavia

LOCATION Bat Hardy

CORONERS FORENSIC UNIT CASE # 98-123

POLICE FILE NO. 98-3317

POLICE AGENCY Crime Art Hardy

POLICE INVESTIGATOR Pst. H. Gillman

DATE: 04 December 1998

EXAMINATION SITE Vancouver City Hospital

AUTOPSY No. _____

HOSPITAL _____

PATHOLOGIST _____

CIRCUMSTANCES OF EXAMINATION Mutilated remains found on Nov 09, 98 in the rear of Chevy Blt, Bat Hardy, B.C. Tentative I.D.

01 Aug 19 --- R-D-E

	A21	A	A20	Fx	Fx	Fx	K22	Fx	Fx	Fx	Fx	Fx	Fx	Fx	Fx	X	X
UPPER RIGHT																	
	46	47	46	46	44	43	42	41		31	32	33	34	35	36	37	38
LOWER RIGHT																	
	A25	A25	Fx	Fx	Fx	Fx	Fx	Fx	Fx	Fx	Fx	Fx	A25				X
	1P	2L															2P

CODE: Shade all restorations on Chart. Outline Prosthetic Appliances.
Circle the appropriate description

Follow Code:

A. Amalgam	T.C. Temporary Crown	DN. Root Treatment	X. Missing
C. Composite	G.C. Gold Crown	BR. Bridge Work (Bracket & shield)	PX. Pseudoanatomically missing
G. Gold	P.C. Porcelain Crown	PR. Partial Denture (Bracket & Shield)	NR. Not Recovered
SE. Resene Sealant	PMH. Porcelain / Metal Crown		
TE. Temporary Filling	SC. Stainless Steel Crown		

1. Mottled Enamel	8. Erosion	15. Retained Occlusal Tooth	22. Congenitally Absent
2. Enamel Hypoplasia	9. Fractured Enamel	16. Unusual Restorations	23. Fractured apical root(s)
3. Discoloration	10. Rotation	17. Unusual Appliances	24. Buccal restoration complete
4. Staining	11. Malpositioned Teeth	18. Core Formation	
5. Calculus	12. Malocclusion	19. Post	
6. Abrasion	13. Unerupted Teeth	20. Pin	
7. Attraction	14. Supernumerary Teeth	21. Cavity	25. _____

Post mortem dental x-ray ☒ Yes ☐ No

Photos ☐ Yes ☐ No

Study Models ☐ Yes ☐ No

Jaws Reconstructed ☐ Yes ☐ No

Description: Unrecoverable

Remarks: Circular deposits gross, root most mouth edges,
likely to have "peg-shaped" #22. Fractured apical root(s).

Figure 2.1 An example of PM dental chart [7]

2.2 Dental Identification Using Computer-aided Software

It has been recommended that any incident involving a number greater than 50 victims would benefit from computer-assisted identification [39]. Statistics show that

identifying the 2,749 victims of 9/11 disaster took around 40 months [40]. The number of Asian tsunami victims identified during the first 9 months was only 2,200 out of 190,000, which only constituted 1.16% of the total number of victims. It is also estimated that there are over 100,000 unsolved missing unidentified person (MUP) cases in the National Crime Information Center (NCIC), and 60% of these have remained unsolved for 90 days or longer. Recent disasters have led to greater attention to automatic methods of human identification. Dental information includes the dental charts and dental radiographs shown previously in Figure 1.2. There are computer-aided software systems such as CAPMI [13], WinID [14] and DAVID [15]. In these systems, dental codes are searched and matched automatically but the dental radiographs are manually compared. These systems still involve a much manual intervention.

CAPMI

Computer Assisted Post Mortem Identification (CAPMI) system was initiated in 1983 by the US Army Institute of Dental Research (USAIDR) with its aim to improve the efficiency of forensic scientists. CAPMI produces ranked lists. Both non-dental and dental characteristics are incorporated in the comparison. CAPMI is a sorting tool, not an identification system, which is efficient and meaningful only when handling large numbers of cases. The list guides forensic odontologists to the most probable AM matches to the PM records, so that they can rapidly proceed with a positive identification by comparison of radiographs [13]. Friedman et. al. studied the dental characteristics of 7030 soldiers. Based on 363 simulations, they found that in 90% of the cases with two or more characteristics CAPMI gets a hit at the top of the candidate list, and that in 96% of the cases CAPMI gets a hit within the top 4 candidates [41].

WinID

WinID [14] is a similar dental computer system that matches missing persons to the unidentified human remains using dental characteristics. Information about restored dental surfaces, physical descriptors, and pathological and anthropologic findings can be entered into the WinID database. The WinID dental codes are extensions of the CAPMI. WinID provides a visual representation of the dental codes in the form of a dental chart. Figure 2.2 shows an example of a dental identification using WinID3. In

Figure 2.2(a), ID#, dead body found date, estimated age, post mortem condition, type of case, etc. are recorded and typed into the WinID system. Figure 2.2(b) shows some recorded identifiers of the body, including gender, height, weight, hair colour, eye colour and blood type. Figure 2.2 (c) shows the dental characteristics of the body and radiographs input into system. For example, 'X' means a missing tooth mark. Letters 'O', 'F', 'D', 'M', and 'L' represent 'occlusal', 'frontal', 'distal', 'mesial', and 'lingual' respectively, which are different surfaces of a single tooth. These marks are used to record tooth fillings on each particular surface. Once the data are prepared, a candidate list consisting of similar records will be retrieved by a best-matches search as shown in Figure 2.2(d). Then manual examination on radiographs will be carried on by forensic experts.

Both CAMPI and WinID use the same comparison algorithm and are equally capable of ranking possible identifications. However, only WinID is capable of generating a ranked list of non-dental identifier matches as well as a list of most restoration hits. WinID is also capable of displaying radiographs, which is very useful features of WinID over CAPMI as shown in Figure 2.2(e). The user can easily switch between English, French, German, Italian, Portuguese and Spanish language.

Post Record ID#: 101 13/6/2013				
Name	Identifiers	Dental	Comments	Graphic
ID#:	101	NCIC#:	97-48544	
Originating agency:	ADAMS CO.	Originating agency#:	97-45	
MedExam/Cor#:	ADAMS CO, IL	MedExam/Cor#:	97-45	
Date Body Found:	2/4/1997	EstAge	40 to	
Body Parts Not Recovered:	G			
Post Mortem Condition:	Fire, Burning			
Disposition:	Active			
Linked Graphic:	p101.gif			Add Graphic
Type of Case:	Accident			

Filter | Record 2 | Change Record with Arrows

(a)

Post Record ID#: 101 13/6/2013

Name	Identifiers	Dental	Comments	Graphic
Post				
Sex:	Male	Race:	White	
Height:	70 177cm		in cm	Fill in second number to specify a range for height or weight.
Weight:	150 68kg	to	lb kg	
HairColor:	Blond	EyeColor:	Brown	BloodType: A+
User Designated Fields / Site Specific Fields				
Entered by:		P1:		G1:
Date:		P2:		G2:
Time:		P3:		G3:
A1:		P4:		G4:
A2:		P5:		G5:

Filter Record 2 Change Record with Arrows

(b)

Post Record ID#: 101 13/6/2013

Name	Identifiers	Dental	Comments	Graphic																																																
Click on Tooth Number to Add or Edit Dental Codes																																																				
<table border="1"> <tr> <td>18</td><td>17</td><td>16</td><td>15</td><td>14</td><td>13</td><td>12</td><td>11</td> <td>21</td><td>22</td><td>23</td><td>24</td><td>25</td><td>26</td><td>27</td><td>28</td> <td>38</td><td>37</td><td>36</td><td>35</td><td>34</td><td>33</td><td>32</td><td>31</td> <td>41</td><td>42</td><td>43</td><td>44</td><td>45</td><td>46</td><td>47</td><td>48</td> </tr> </table>					18	17	16	15	14	13	12	11	21	22	23	24	25	26	27	28	38	37	36	35	34	33	32	31	41	42	43	44	45	46	47	48																
18	17	16	15	14	13	12	11	21	22	23	24	25	26	27	28	38	37	36	35	34	33	32	31	41	42	43	44	45	46	47	48																					
18 /	21 /	38 MOF	41 /	...																																																
17 OD	22 /	37 MOD	42 /	...																																																
16 /	23 /	36 X	43 /	...																																																
15 /	24 OD	35 X	44 /	...																																																
14 /	25 MOD	34 /	45 X	...																																																
13 /	26 MD	33 /	46 X	...																																																
12 /	27 /	32 /	47 X	...																																																
11 /	28 /	31 /	48 OF	...																																																
				<input type="checkbox"/> Mark all Upper as Virgin <input type="checkbox"/> Mark all Lower as Virgin <input type="checkbox"/> Mark all Upper as Missing <input type="checkbox"/> Mark all Lower as Missing <input type="checkbox"/> Mark all Upper as Denture <input type="checkbox"/> Mark all Lower as Denture <input type="checkbox"/> Mark all Upper as No Info <input type="checkbox"/> Mark all Lower as No Info																																																
<table border="1"> <tr> <td>18</td><td>17</td><td>16</td><td>15</td><td>14</td><td>13</td><td>12</td><td>11</td> <td>21</td><td>22</td><td>23</td><td>24</td><td>25</td><td>26</td><td>27</td><td>28</td> </tr> <tr> <td>48</td><td>47</td><td>46</td><td>45</td><td>44</td><td>43</td><td>42</td><td>41</td> <td>31</td><td>32</td><td>33</td><td>34</td><td>35</td><td>36</td><td>37</td><td>38</td> </tr> <tr> <td><input type="checkbox"/></td><td><input checked="" type="checkbox"/></td><td><input checked="" type="checkbox"/></td><td><input checked="" type="checkbox"/></td><td><input type="checkbox"/></td><td><input type="checkbox"/></td><td><input type="checkbox"/></td><td><input type="checkbox"/></td> <td><input type="checkbox"/></td><td><input type="checkbox"/></td><td><input type="checkbox"/></td><td><input type="checkbox"/></td><td><input checked="" type="checkbox"/></td><td><input checked="" type="checkbox"/></td><td><input checked="" type="checkbox"/></td><td><input type="checkbox"/></td> </tr> </table>					18	17	16	15	14	13	12	11	21	22	23	24	25	26	27	28	48	47	46	45	44	43	42	41	31	32	33	34	35	36	37	38	<input type="checkbox"/>	<input checked="" type="checkbox"/>	<input checked="" type="checkbox"/>	<input checked="" type="checkbox"/>	<input type="checkbox"/>	<input type="checkbox"/>	<input type="checkbox"/>	<input type="checkbox"/>	<input type="checkbox"/>	<input type="checkbox"/>	<input type="checkbox"/>	<input type="checkbox"/>	<input checked="" type="checkbox"/>	<input checked="" type="checkbox"/>	<input checked="" type="checkbox"/>	<input type="checkbox"/>
18	17	16	15	14	13	12	11	21	22	23	24	25	26	27	28																																					
48	47	46	45	44	43	42	41	31	32	33	34	35	36	37	38																																					
<input type="checkbox"/>	<input checked="" type="checkbox"/>	<input checked="" type="checkbox"/>	<input checked="" type="checkbox"/>	<input type="checkbox"/>	<input type="checkbox"/>	<input type="checkbox"/>	<input type="checkbox"/>	<input type="checkbox"/>	<input type="checkbox"/>	<input type="checkbox"/>	<input type="checkbox"/>	<input checked="" type="checkbox"/>	<input checked="" type="checkbox"/>	<input checked="" type="checkbox"/>	<input type="checkbox"/>																																					

Filter Record 2 Change Record with Arrows

(c)

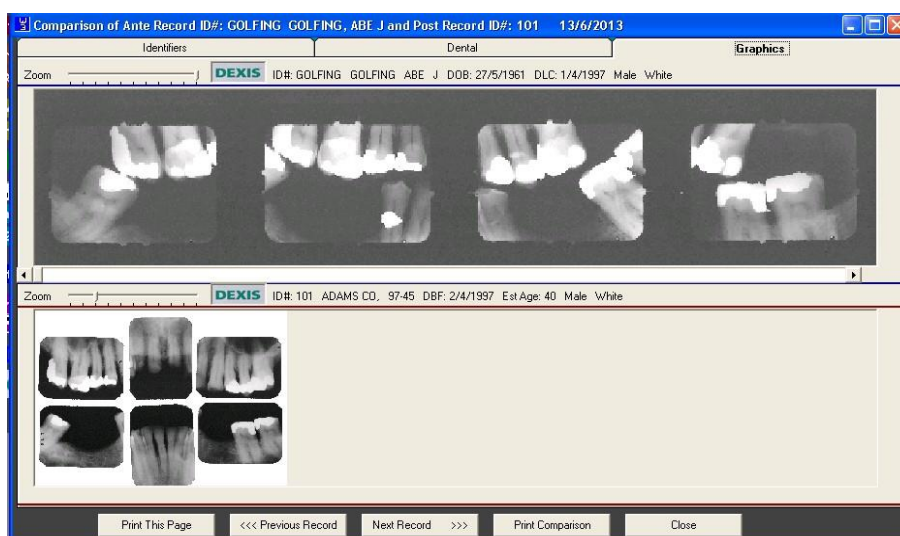
Best Matches to Post Record ID#: 101 13/6/2013

Rank	ID#	Hits	Miss	Possible	No-Info
1	GOLFING	9	0	3	20
2	EATON	5	7	0	20
3	FOX	2	1	9	20
4	BAKER	2	3	7	20
4	NEEDMAN	2	3	7	20
5	ALLISON	2	4	6	20
6	DONALDSON	1	2	9	20

Number of Rankings to be Displayed: 25 50 100 All

AnteMortem Records: No Filter

(d)



(e)

Figure 2.2 An example of a dental chart produced by WinID[14]

DAVID

In 1997 the Victorian Institute of Forensic Medicine (VIFM) Australia initialized an internally supported but unfunded pilot computer system development project. This system is for the storage, retrieval and tentative matching of the dental records. It combined the skills of the VIFM Information Technology systems manager (VW), an experienced odontologist (JGC) and an expert database designer (JC) [15]. The interface of DAVID is shown in Figure 2.3. The columns are the state of the AM tooth and the rows are the state of the PM tooth. The values are shown the cumulative score for the matching process. Later, some new features have been integrated into “DAVID web”. It enables the contrast and brightness adjustment of photographs, radiographs and to reveal features of interest.

MATCH MATRIX FOR DVI

PM MClosed / AM MOpen 10 match matrix1

PM/AM	Sound	Damaged	MOpen	MClosed	Crown	Bridge	Denture	Unknown	Fill	Root	Uneru
Sound	100	-1000	-1000	-1000	-1000	-1000	-1000	0	-100	-1000	100
Damaged	100	10	-1000	-1000	10	10	-1000	0	10	-1000	10
MOpen	10	10	0	-1000	10	10	-1000	0	10	10	10
MClosed	10	10	10	100	10	100	100	0	10	10	10
Crown	10	10	-1000	-1000	100	10	-1000	0	10	10	10
Bridge	10	10	10	10	10	100	10	0	10	10	10
Denture	10	10	10	100	10	10	100	0	10	10	10
Unknown	10	10	10	10	10	10	10	10	10	10	10
Fill	10	10	-1000	-1000	0	0	-1000	0	100	-100	10
Root	10	10	-1000	-1000	10	10	0	0	10	10	10
Unerupt	-1000	-1000	-1000	10	-1000	-1000	-1000	0	-1000	-1000	100

Deciduous Match 10

Deciduous MisMatch Penalty -1000

Filling Surface Match 10

Filling Surface Mismatch Penalty -100

PRINT SAVE EXIT

Figure 2.3 Match matrix for DVI[15]

2.3 A Radiograph-based Automated Dental Identification System (ADIS)

In 1997, the Criminal Justice Information Services Division (CJIS) of the FBI created a dental task force (DTF) whose goal is to improve the utilization and effectiveness of the National Crime Information Center's (NCIC) Missing and Unidentified Persons (MUP) files. The CJIS of the FBI includes in its strategic plan the creation of an Automated Dental Identification System (ADIS), with similar goals and objectives to its Automated Fingerprint Identification System (AFIS) but using dental/teeth characteristics instead of fingerprints [20]. Research teams from West Virginia University (WVU), Michigan State University (MSU), and University of Miami (UM) are developing a research prototype of ADIS. ADIS aims to speed up the PM identification process. The benefit of ADIS will surpass saving millions of dollars to also include psychological benefits of families of missing persons when knowing the disposition of their loved ones without having to wait extended period of time [17]. ADIS uses state-of-the-art techniques from multi-disciplines that include but not limited to digital image processing, pattern recognition, soft-computing and internet technology [16]. A comprehensive literature review regarding technologies in ADIS system is presented and compared here. The architectural design of ADIS research

prototype is discussed in further detail in [16, 19]. The ADIS system structure is shown in Figure 2.4.

- The Potential Matches Search (PMS) component (Coarse-grained matching in Figure 2.4) manages the archiving, searching and retrieval of dental records in order to produce a candidate list of matches. This component is developed by the research teams at MSU and UM and is primarily responsible for archiving and retrieval of dental records based on high-level dental features. These features include the number/position of teeth and shape properties of teeth among other features. The implementation of this component requires techniques for: dental film classification [19, 23]; teeth segmentation [19, 26], [16, 22] and [24]; extraction of teeth contour [19, 22, 26], and feature indexing [23].
- The Image Comparison (IC) component registers and compares two sets of dental records and is used during the search process. The desirable features of this stage are speed and accuracy. This component is developed by the research team at WVU and is responsible for low-level comparison of the radiographs of a subject case against those of candidate reference cases. Realization of this component follows a pyramidal architecture for image matching [16, 19], and [35]. Image comparison is carried out in the following steps: preprocessing of images, where enhancement, segmentation and alignment are achieved to correct for possible geometric and/or intensity transformations [16, 19, 24] and [35]; decision making, where low-level features are extracted from corresponding regions in the subject and the reference radiographs and used as basis for computing a probability of match between the subject record and a reference record [19] and [35].
- The Digital Image Repository (DIR) this is the image and feature database component and is being developed by WVU and UM [16].

Given a PM dental record, a short list of archived AM records will be retrieved which have a high similarity with that given PM record. With reference to ADIS shown in Figure 2.4, high-level dental features are firstly, used to generate a candidate list by the PMS component, then IC matching, where dental X-ray images of the subject PM record and the candidate list are examined to produce a ranked short match list. Finally, the short match list is

presented to a forensic expert to examine the radiographs of the PM subject against those in the short match list. Furthermore, to integrate internet sources, enable remote access and collaboration, a Web-ADIS was developed in 2007 [38].

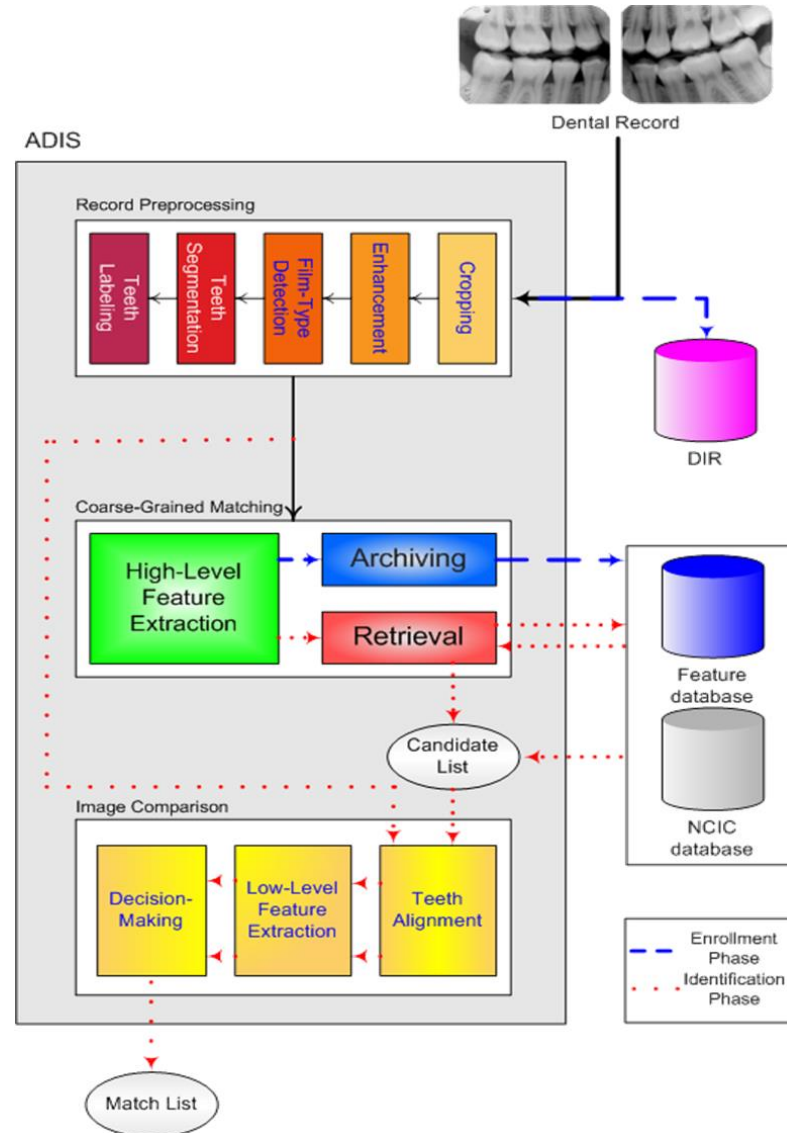


Figure 2.4 Systematic structures of ADIS [42]

The approaches, advantages, disadvantages and performances are summarized, compared and analysed in the major four steps of 2D automated dental identification scheme: image segmentation, feature extraction, teeth classification (Atlas registration) and matching as shown in Figure 2.5.

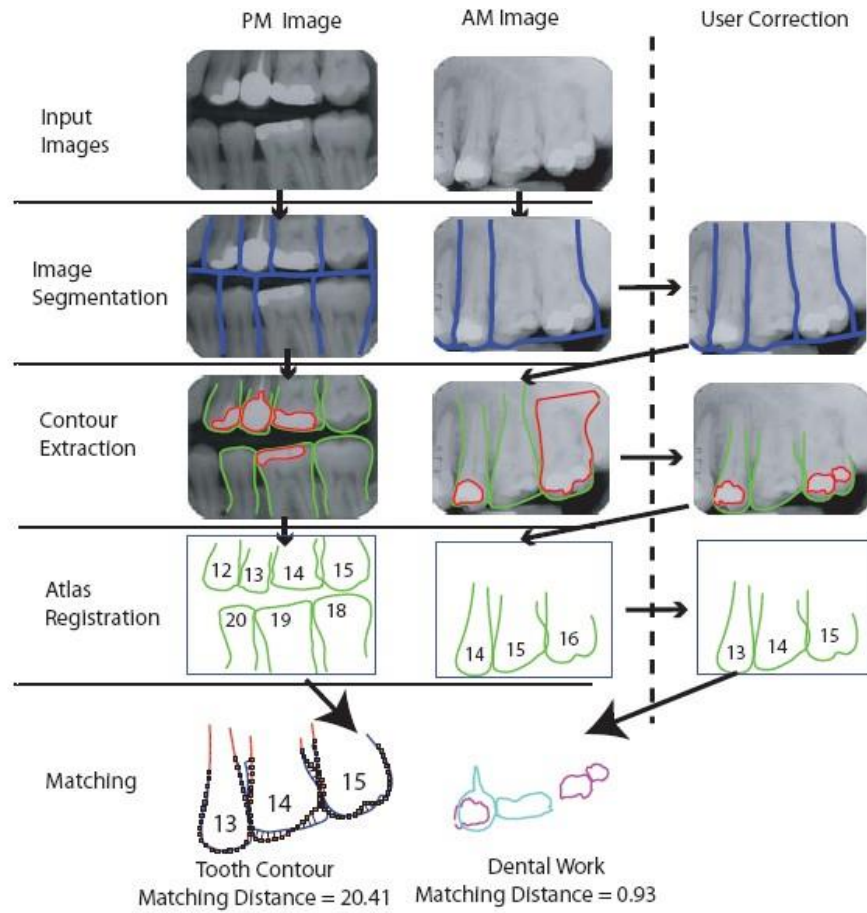


Figure 2.5 Main components in ADIS and identification with user interaction [34]

2.3.1 Image Segmentation

With the development of medical imaging techniques, image segmentation in 2D and 3D domains has received extensive attention in the last decade. Some recent research results show the variety of computer aided techniques in medical image segmentation. Li et al. [43] proposed a graph-theoretic approach for optimal surface segmentation in volumetric images. Jorge et al. [44] integrated information obtained from texture segmentation methods with boundary information and embedded that in a region growing strategy for brain tomographic image segmentation. Chen et al. [45] developed a level set method based on the Bayesian risk classification error which is robust for various types of medical images. Han et al. [46] proposed a coarse-to-fine strategy for hand radiograph segmentation. The watershed transform is first applied to get metaphyseal regions, then noise removal, labeling, ellipse region fitting are performed to find the epiphyseal regions of interest. An active contour model

approach based on gradient vector flow (GVF) is used to get the fine level segmentation [46]. Tu et al. [47] proposed an auto-context learning algorithm for high level vision tasks and 3D brain image segmentation, which integrates low-level context information by fusing a large number of low-level appearance features with context and implicit shape information. The reported performance is higher than the state-of-the-art algorithms at that time and has the potential usage for structured prediction problems.

Presently, most of the dental identification techniques are developed based on processing 2D x-rays radiographs. By matching the extracted tooth contours between an AM image and a PM image, a person's identity is obtained. In dental identification, segmentation is often concerned with segmentation of a full jaw region (e.g., panoramic radiographs) with full set of teeth or partial jaw region (bitewing or periapical radiographs) focusing on individual tooth, isolating each tooth from the background, the jaw bones, the soft tissues and the neighbouring teeth. In order to extract the tooth contour, image segmentation is inevitable and it is crucial to the exact tooth contour extraction which would affect the final matching accuracy. However, most of the segmentation techniques are affected by different types of noise embedded in images due to poor lighting or low resolution. Several X-ray image segmentation approaches have been proposed in the last decade. Several researchers contributed to dental radiograph segmentation. Jain and Chen [22] used Y-axis projection histogram to segment the upper teeth and the lower teeth in bitewing and panoramic dental images by detecting the gap valley. An intensity integral projection was applied to isolate each tooth from its neighbouring teeth by detecting the gap between them. However, their approach has to be manually intervened to specify an initial valley gap. Chen reported that by using the fast marching methods [48], the correct rate segmentation of the 611 x-ray radiographs was 61.1% . 38.9% of the images were of incorrect segmentation line between upper and lower teeth, under segmentation, over segmentation, or improper segmentation requiring manual corrections [34]. Nomir et al. [29] introduced a fully automated 4-step segmentation strategy. They first applied iterative thresholding to divide the image into teeth region and background region. Then the adaptive threshold was used to increase the accuracy and remove teeth interference. Next, horizontal integral projection is presented to separate the upper and lower jaw. Finally, vertical integral projection was applied to

isolate individual teeth. Nomir and Abdel-Mottaleb [25] also introduced another fully automatic segmentation technique to improve the image contrast by utilizing mathematical morphology, and later window-based adaptive threshold and integral projection applied to segment the teeth and separate the upper and lower jaw. Said et al. [24] reported that segmentation accuracy was improved by applying a morphological filtering combined with 2D wavelet transform method. Later Said et al. [32] presented a technique to improve segmentation performance by using grayscale contrast stretching transformation beside a fully automated segmentation approach based on mathematical morphology. Table 2.1 lists research dealing with dental x-ray image segmentation and feature extraction, including the approaches, accuracy, advantages and disadvantages.

Table 2.1 Tooth segmentation algorithm comparison

Author /year /reference	Approach	No. /types of images	Reported accuracy	Advantages	Disadvantages
Jain et al.[21]2004	histogram integral projection	130 bitewing	failure rate 2.61%	simple and easy to implement	semi-automated cannot handle poor quality images
Nomir et al.[29]2005	iterative and adaptive thresholding , integral projection	117 bitewing	failure rate 11.18%	fully automated Adaptive thresholding improves iterative thresholding	cannot handle poor quality images(eg. teeth at the borders)
Zhou et al.[25]2005	morphology , adaptive threshold, integral projection	123 Bitewing	failure rate 3.47 %	fully automated	the database is small

Said et al.[32]2006	grayscale contrast stretching transformation morphology	two sets of 500 bitewing 130 periapical	failure rate 1.27%	fully automated High accuracy	difficult to deal with poor quality images
Said et al.[31]2006	1) convolution filtering using point spread function (PSF) 2) connected components labeling	500 bitewing	failure rate 1.141%	fully automated low failure rate and high optimality	partly correspondence failure because of background noise and mismatching
Chen et al.[34]2007	fast marching	611 in total Bitewing Periapical panoramic	accuracy 61.1% without user correction	all types of dental radiographs	semi-automated difficult to cannot handle poor quality images

2.3.2 Feature Extraction

The feature extraction in dental identification concerns the extraction of the crown and root contours of teeth as well as dental restoration contours. Chen et al. [21] proposed a semi-automatic contour extraction method. Crown centre of the rectangular bounding box was manually specified for each tooth. Then the crown and the root of a tooth are divided by drawing a line through the crown centre. In addition, Chen et al. [18] presented a dynamic energy term for directional snake to discriminate boundaries of adjacent teeth combined with an active contour model algorithm [49]. Shah et al. [33] investigated that active contour models based on edges were driven by the gradient of the image intensities. However, the gradient between the teeth and the background was not prominent because there were bone and soft tissue regions. Therefore, accurate tooth contours could not be extracted. Furthermore, snake-based schemes utilize parametric representation of the contour which often fail to evolve in noisy conditions and there is a possibility that it fails to split and merge when local minima are presented [50]. They used an active contour without edges to extract

tooth contours in noisy condition. The comparison of the above methods is listed in Table 2.2.

Table 2.2 Tooth contour extraction algorithm comparison

Author /year /reference	Approach	No. /types of images	Reported accuracy	Advantages	Disadvantages
Chen et al.[21]2004	Bayes rule	130 bitewing images	not available	simple	semi-automated
Chen et al.[18]2004	dynamic energy gradient vector flow and active contour models	130 bitewing images	not available	improved based on[21]	not accurate cannot deal with local minima
Zhou et al.[25]2005	active contour adaptive threshold	123 Bitewing	not available	fully automated	cannot deal with overlapping teeth
Shah et al.[33]2006	active contour without edges	340 teeth represented in images 10 AM and 10 PM records (60 images)	perfect contour extraction: 58.10% Perfect crown contour extraction: 12.83%	very fast, 0.16 second per tooth Robust against noise Contour is tight and smooth	part of neighbouring tooth sometimes also included erroneously in the segmentation

2.3.3 Tooth Classification

The human dental atlas is a model describing the shapes of teeth and their relative positions. A complete dental structure of an adult contains 32 teeth, 16 in each jaw. Every single tooth has a specific index (1-32) in the dental atlas. For an automatic dental identification system, the tooth classification is important because it helps to decrease the search space by limiting the comparison of the teeth which have the same index number in the dental atlas.

Although not much effort has been put into tooth classification due to its complexity and difficulty, there are some pioneering contributions in 2D dental identification scheme. Mahoor and Abdel-Mottaleb [16] proposed a method to obtain the indices of teeth in bitewing images by using Bayesian classification. Two kinds of Fourier descriptors are compared to select the best for teeth classification. Two major limitations of their method are: (1) only molars and premolars are classified and numbered; (2) missing teeth case has not been considered, i.e., only jaws with complete set of teeth considered. Jain and Chen [27] proposed a two-stage registration method. The first stage is to classify the teeth into three types: molar, bicuspid and incisor by applying support vector machine techniques to the Fourier descriptors of contours and other tooth features. In the second stage they use a Hidden Markov Model (HMM) as an underlying representation of the dental atlas to handle the problem of missing teeth and the three types of dental images. However, error occurs when identifying short sequence dental images which contain only 3 or 4 teeth and error also occurs when distances between neighbouring teeth are not representatives of the training data in dealing with missing teeth case. More recently, Lin et al. [51] presented a binary linear support vector machine technique to distinguish molars and premolars by using the skew-adjusted relative length/width ratios of both teeth and pulps and crown sizes as features. A numbering scheme which combines a missing teeth detection algorithm is also proposed. However, the images they used are only bitewing images which only contain molars and premolars. Table 2.3 lists research dealing with tooth classification and outlines the key features, advantages and disadvantages:

Table 2.3 Tooth classification algorithm comparison

Author /year /reference	Feature	Approach	No. /types of images	Reported accuracy	Advantages	Disadvantages
Abdel-Mottaleb et al.[16] 2003	two Fourier descriptor s of teeth contours	bayesian classificatio n	50 bitewing containing 220 molar and 180 premolar	72%- 95.5%	ability to correct misclassificatio n	missing teeth not considered only bitewing images
Jain et al.[27]2005	Fourier descriptor of teeth contours	SVM HMM	25 people 1772 tooth contours	82.9% upper teeth 93.8% lower teeth	three types of dental images fusion score of different features	errors occur when there are few teeth and when outliers appear in test data
Nassar et al.[52] 2008	eigenteeth	least square error classifier PCA String matching	507 bitewing and periapical images	87%	Fast; four teeth types classification;	Need tedious view normalization and validation
Lin et al. [51] 2010	length/wid th ratios of both teeth and pulps and crown sizes	binary linear SVM smith- waterman algorithm	47 bitewing images with 369 teeth in total	Classificati on 95.1% numbering 98.0%	Higher accuracy	cannot deal with high similarity teeth sequences; inconsistency of jaw arrangement; overlapped teeth

2.3.4 Matching

Registration and retrieval is the process of transforming an image of an object and measuring its resemblance either to another image of the same object, or to an image of another object. In dental identification, the extracted tooth contours with the same indices are compared by calculating the differences according to the convergence of

an optimal transformation or a measure of closeness to an optimal similarity metric. Nassar et al. [30] used a multi-resolution genetic algorithm to align the dental image by utilizing the location and orientation of the edge points. But they assumed that affine transformations sufficed to restore geometric discrepancies between two images of which the tested validity must be within a variation of 18 degrees. In addition, the testing images are 52 pairs of single tooth. The correction of misalignments is time-consuming. Nomir et al.[53] present two matching techniques. The first technique represents high curvature points on the tooth contour using signature vectors, and then the signature vector distances are calculated. The second method uses hierarchical chamfer distance transformation to reduce the searching space and accordingly the retrieval time is reduced. They compare the results and show that the hierarchical chamfer distance outperforms the signature vectors. Furthermore, the results are fused both at the matching level and the decision level to improve the performance. A separate decision is made for each matcher. These decisions are then fused into a final vote at the decision level or stage[53]. The matching accuracy is 80% and 84% respectively. And they test their methods only on 162 AM and 50 PM bitewing images, not including the panoramic and periapical images. Later, they investigated another matching technique [53], representing each tooth by the smallest of features extracted using the forcefield energy function and Fourier descriptors. They fuse results of the above three matching algorithms at matching level and decision level by using the Bayesian framework method to improve the overall performance. Nassar et al. [35] presented the use of learnable inherent dental image features for tooth-to-tooth image comparisons and the probabilistic models of class-conditional densities. An adaptive strategic search technique combined with back propagation to tackle with tooth-to-tooth binary classification problem is also proposed. The experimental results show that the matching accuracy exceeds 80% with low false rejection rate. They show potential robustness of their method that it is capable of dealing alignment imperfections within $\pm 5\%$ of scaling and $\pm 5^\circ$ of rotation. However, the selection of ROI is carried out manually. In addition, this is a tooth-to-tooth matching scheme in which the useful information of teeth arrangement is not used. Furthermore, the panoramic dental images are not included. Omaira and Abdel-Mottaleb [54] introduced a modified hierarchical chamfer distance algorithm with multi-representation of teeth contours.

The search space, computational load and the time complexity are significantly reduced. And this algorithm outperforms their previous one in [29]. Table 2.4 lists research projects dealing with image matching and outlines the key features, advantages and disadvantages:

Table 2.4 Tooth matching algorithm comparison

Author /year /reference	Feature	Approach	No. /types of images	Reported accuracy	Advantages	Disadvantages
Jain et al.[21] 2004	Tooth contours	Euclidean distance of tooth contour Affine Transformations	38 PM 130 AM images Bitewing Periapical	65.8% for the rank 1	Easy and simple	Small database, cannot deal with poor image quality; partly visible tooth ; high similarity between different individuals
Nomir et al.[29]2005	Signature vector for salient points on tooth contours	Euclidean distance of tooth contour Affine Transformations	Bitewing 43PM 117AM	First rank 76% teeth 74.4% images	Automatic in every step	Only bitewing images. Failure due to poor image quality
Chen et al.[26]2005	Tooth and dental work contours	Euclidean distance of tooth contours area-based metric to align dental work ;contours	166PM 235AM	First rank 72%	Fusion matching scheme	The accuracy is not high enough.
Nassar [30]2006	location and orientation information of edge points	Multi-Resolution Genetic Algorithm (MR-GA) Affine Transformations	52 single teeth-pair images	Algorithm converge s in 85% cases	capable to fully correct misalignments of up to 18 degrees within two minutes	excessive misalignments decrease accuracy

Banumathi et al. [55]2007	Tooth contour	Affine transformation	15PM 30AM bitewing periapical	70%	Morphological contour detection is better than the Gaussian contour detection and semiautomated contour detection	Low accuracy No panoramic images
Nomir et al.[36] 2007	Tooth contour and pixels within the tooth area	Fourier descriptor for tooth contour; force energy function for tooth area	50 PM 162 AM bitewing	86%	Higher accuracy. Improvement in dealing with poor quality images when representing tooth by only the contour information	A small database
Nomir et al.[37] 2007	Curvature of contour points; Tooth distance map (DT)	Root mean squares of signature Root mean squares of the distance maps	162 AM 50 PM	Signature vectors Technique: 80% Hierarchical Technique: 84%	The hierarchical technique decreases the searching space and reduces time Fusion to improve performance	Accuracy is not high enough; bitewing images only
Nassar et al.[35]2007	Convolution value of the ROI Class-	Nonlinear filter discrete convolution Bayesian classification	2000 pairs of single tooth	80%	capable of dealing small alignment imperfections	Manual selection of ROI; Week in dealing with different

	conditional densities	Back propagation dynamic-range uni-variation of variables	Bitewing Periapical			views
Nomir et al.[53] 2008	Curvature of contour points;	Root mean squares of signature vectors	187 AM 50 PM bitewing	Signature vectors 80%	Fused biometric system has higher accuracy	Tested only on bitewing dental images
	Tooth distance map (DT)	Root mean squares of the distance maps		Hierarchical 84%		Segmentation requires good quality radiographs
	forcefield energy function and fourier descriptors of tooth contours	Euclidean distance of feature vectors fusion at the matching, decision, and matcher level		Force field and FD 86%		Contour misclassification
Nomir et al.[54] 2008	Multi-resolution teeth contours's hierarchical chamfer distance	Multi-resolution representation of teeth contours; Hierarchical chamfer; Majority voting;	187 AM 50 PM bitewing	84%	Decreased search spaced; less computational load; less time complexity	Problems in matching low quality images; partial appeared teeth;

2.5 Dental Identification Trend

With the successful identification scheme developed in 3D face recognition and 3D ear recognition [56, 57], there is a trend towards using 3D techniques. Nowadays, the acquisition of 3D models has been made easier and fast due to the fast emerging real-time scanning and 3D reconstruction technologies. In addition, there are dental research works in assisting 3D reconstruction of teeth from CT images [58] and 3D automatic tooth segmentation [59] for dental identification. However, these works remain in the preprocessing stage, i.e., preparing the data for 3D dental identification.

None of the aforementioned efforts has investigated the complete 3D dental identification process. This research aims to develop an automated 3D dental identification scheme with suitable identification methodologies and algorithms for retrieving matching digitized 3D dental casts as for 2D dental identification.

2.6 Summary

Chapter 2 provides a comprehensive literature survey of 2D dental identification schemes - from the dental chart identification to software-assisted identification, and also a prototype of automated dental identification based on x-ray radiographs. The approaches, advantages, disadvantages and performances are summarized, compared and analysed in the major four steps of computer-assisted 2D dental identification schemes: image segmentation, feature extraction, teeth classification and matching. The 3D identification trend is also presented to further elaborate the research gaps in dental identification.

Chapter 3 Point-based Matching and Identification

3.1 Introduction

Chapter 3 presents the development of a point-based matching approach. The point-based matching and identification approach is a pose invariant dental identification (PIDI) technique involving algorithms for feature extraction, description and correspondence on digitized dental casts. 60 PM samples and 200 AM samples are used in experiments. Different shape descriptors (saliency, Gaussian curvature, integral volume) are proposed and compared with regard to pose invariant characteristics.

A performance index used in the evaluation of the approach is the identification accuracy based on the correctly identified PM samples relative to the total number of PM samples tested. Matched AM samples are ranked, whereby rank-1 match using the evaluated technique indicates that the AM sample from the database has been identified to be the most likely match to the PM sample being identified. If it is rank-2 matched, it means that it is the next likely match, and likewise for subsequent ranking.

PC with two Duo Core CPUs with a clock speed of 2.33 GHz and 1.96GB RAM is used throughout the tests for consistent computational time comparison. Unit of matching errors (alignment errors) in this thesis is millimeter (mm).

3.2 System Approach Overview

An overview of the point-based approach is shown in Figure 3.1. For every PM digitized dental model, it will retrieve from an AM database of 200 digitized dental models to find the closest match. The input is the digitized dental cast and the output is a ranked list of matched models. The digitized model is first decimated and segmented before feature point detection, description and correspondence. Finally the ranked list will be presented to forensic experts for further identity confirmation. Manual segmentation and auto segmentation are compared regarding the identification accuracy. Three shape descriptors are proposed and compared according to their pose invariant characteristics.

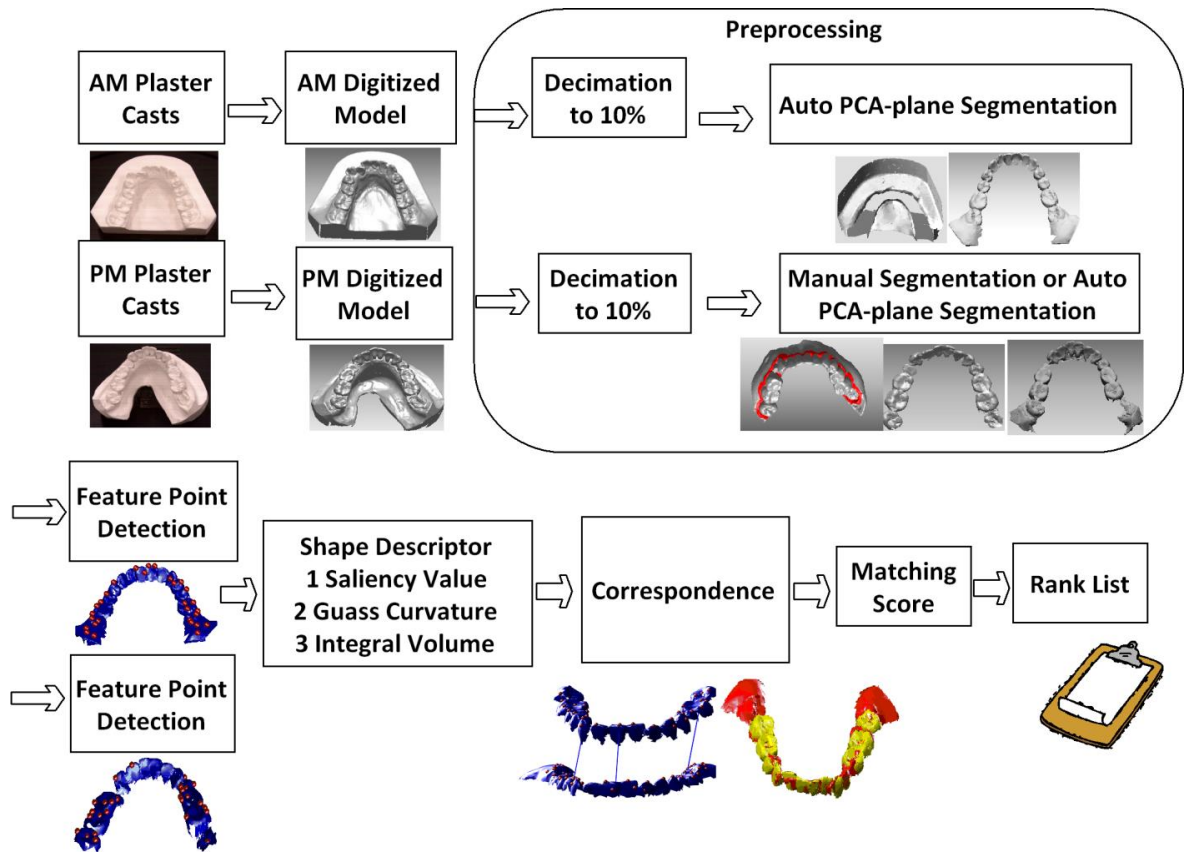


Figure 3.1 An overview of the point-based approach

3.3 Algorithm Overview

The three main components in pose invariant dental identification (PIDI) technique are feature extraction, shape descriptor definition and correspondence. Table 3.1 shows the main steps. The details are elaborated in the following sections.

Table 3.1 Main steps of pose invariant dental identification (PIDI) technique

<p>Input: 60 PM surface model and 200 AM surface model</p> <p>Output: 60 ranked lists with each having 200 ranks</p> <p>Steps:</p> <p>1) Feature Extraction</p> <ol style="list-style-type: none"> 1. Compute bounding boxes of one PM sample and one AM sample as shown in Figure 3.4 (a) 2. Define the neighborhood points x_j of point v_i as $N(v_i, \sigma)$ which are points in Euclidean distance σ using v_i as the center point as shown in Figure 3.4(b) 3. Apply the six scales of Gaussian filter as shown in Figure 3.4 (c) 4. Compute the Difference-of-Gaussian (DoG) at each scale 5. Search for the vertices within distance $2\sigma_6$ to the boundary vertices and set the saliency of all these vertices to zero 6. Normalize the saliency value 7. Set the saliency value to zero if it is not larger than the saliency of certain value of its neighboring vertices 8. Add the saliency map at all six scales 9. Extract a vertex as a feature point whose saliency value is a local maximum and larger than certain value of the global maximum <p>2) Shape Descriptor Definition</p> <ol style="list-style-type: none"> 10. Use the computed saliency value in step 1-9 to compare with the Gaussian curvature descriptor and integral volume descriptor in pose variation experiment V. (Figure3.5) <p>3) Correspondence</p> <ol style="list-style-type: none"> 11. For any feature point p in the PM sample, we choose a set of correspondence points (q_1, \dots, q_n) in AM sample according to a threshold value $C(p) - C(q) < 0.1 \cdot C(p)$, $C(p)$, $C(q)$ denote the saliency value/Gaussian curvature/integral volume value at point p and q respectively 12. For each pair of feature points (p_i, p_j) in the PM sample, choose any $q_i \in C(p_i)$, $q_j \in C(p_j)$ and set the point pair (q_i, q_j) which minimizes the distance root mean squared (dRMS) error as the associated correspondence pair and sort in order of ascending dRMS error 13. Add another point, and repeat step 12 to form correspondence tri-pairs. The tri-pair which minimize cRMS error is taken as the best tri-pair correspondence. 14. Fine correspondence using ICP algorithm 15. Repeat step 1-14 for matching the same PM sample to another AM sample in the AM database until finishing all of them. Sort the matching error 16. Match another PM sample to all the AM samples by repeating step 1-15

3.4 Data Preparation

The data samples used in this study are mandibular dental plasters obtained from National University Hospital. They are adult dentitions. These samples have multi-race characteristics in Asian groups, belonging to the Chinese, Indian, and Malay ethnic groups.

AM sample acquisition

The AM set comprises 200 digitized plaster samples of the mandibular teeth. These plaster samples are scanned by one investigator (X1) with the Minolta VIVID 900 Surface Laser Scanner (Konica-Minolta Corporation, Osaka, Japan) for acquisition of the surfaces of the plaster samples. The scanning resolution is 0.02mm. The age range of the 200 AM samples is 12 to 35 years. The mean age is 23.6 ± 5.4 comprising 111 males and 89 females.

PM sample acquisition

The PM set consists of 60 digitized plaster samples of the mandibular teeth. There are two groups: 50 genuine and 10 imposter samples. These 60 samples were obtained independently by another investigator at another time (X2). These 60 samples were scanned with the same Minolta VIVID 900 surface laser scanner and then categorized into four groups. The age range of the 60 PM sample is 12 to 34 years. The mean age is 21.4 ± 4.2 years comprising 24 males and 36 females.

Figure 3.15 shows the digitization process. The dental plaster is placed on a rotating table facing the scanner. 6 angles (0 60 120 180 240 300) are used to obtain 6 scanned surfaces, which are then registered and pieced together to form a complete surface of digitized dental plaster. There are two categories of differences between the PM and AM dental records. One category is the non-deformable changes in locations and shapes of the teeth (e.g., missing tooth crowns or entire tooth, disruption of anatomical location of teeth and damage to bony features etc. as shown in Figure 3.2 (c)). The other category belongs to those with changes during the preparation of the PM records (e.g., noises occurred during the preparation as shown in Figure 3.2 (d)) and the orientations and appearances are different as shown in corresponding AM/PM sample pairs in Figure 3.2 (e)). This is to consider those samples prepared by different

investigators (such as by X1 and X2) at different time where the initial orientation and the mesh topology are not necessarily the same. The pose invariant dental identification approach aims to be able to handle the two aforementioned kinds of differences between the AM and PM samples. The detailed differences are shown in Figure 3.2. There are four groups of PM samples.

Group one: This group consists of seven complete samples as shown in Figure 3.2 (a). The first row shows the manually segmented PM samples and the second row shows the auto-segmented PM samples. This group of samples is to be tested in an increased AM sample database which comprises 200 AM samples. The identification accuracy will be compared in Experiment I described below.

Group two: This group consists of 10 Imposter PM samples as shown in Figure 3.2 (b) which do not have corresponding AM samples in the AM database. These are used to compare with the genuine match results to find a threshold for imposter sample detection in Experiment II.

Group three: This group consists of 11 genuine PM samples with missing teeth and missing tooth crowns as shown in Figure 3.2 (c).

PM8-one incisor, one canine and one molar were missing;

PM9-left half teeth were lost;

PM10-four incisors were lost;

PM11-two molars were missing;

PM12-three molars and two incisors were lost;

PM13- only five molars left;

PM14- four molars were lost;

PM15- one molar and one lateral incisor were lost;

PM16-one molar and one canine were missing;

PM17- right half teeth were lost;

PM18-two molars and two canines were missing.

Partial samples are commonly found after disasters. Each of the 11 partial PM samples is anatomically unique in the number and position of missing teeth as well as symmetry of the lower dental jaw to represent a range of anatomic variations for matching. The 11 manually segmented PM samples are shown in the top two rows and the auto-segmented PM samples are shown in the lower two rows.

Group four: Figure 3.2 (d) shows two examples of noisy samples used in this group. Noise occurred during the scanning process. 32 out of 50 PM samples were found having noises. Comparing the noisy PM samples to their AM samples, the individual tooth shapes in PM samples are severely corrupted which can render visual matching difficult. This group aims to show the robustness of the proposed approach in the presence of significant noise. Figure 3.2 (d) shows the orientation, appearance and topology differences of the genuine samples.

Preprocessing

To facilitate efficient and accurate matching of corresponding AM and PM surface images, preprocessing of the digital images is required to reduce the size of the images and to eliminate unnecessary data such as the bottom part of a dental plaster. Preprocessing is a two-step process which involves the decimation and segmentation of the PM samples and AM samples. There are three operations in preprocessing: 1) decimation to 10% of the original points for all the AM and PM samples; 2) manual segmentation and auto PCA-plane segmentation for 60 PM samples; 3) auto PCA-plane segmentation for 200 AM samples.

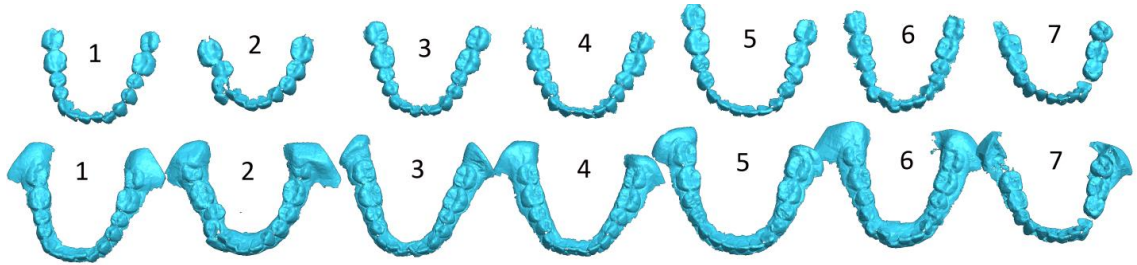
1) Decimation The method of decimation reported by Schroeder et al. [60] is applied to the scanned digital surfaces. The size of each digitized sample is 14~30MB, comprising of 340k~400k triangles and so is decimated to 10% to achieve higher computational speed. Every surface image is decimated by 90% to achieve higher computational speed while preserving as accurately as possible the important original topology and geometry of shapes. Only 10% of the original mesh is used for

identification. It aims to show that competitive identification accuracy can be achieved by using the developed 3D identification scheme at a large-scale decimation level. All the samples shown in Figure 3.2 are decimated samples.

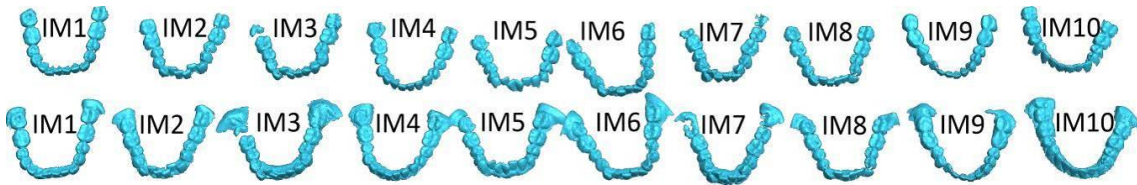
2) Manual Segmentation After decimation, segmentation of the 60 PM surface mesh images is carried out manually using the software RAPIDFORM 2006 (INUS Technology, Seoul, South Korea) to delineate the shapes of the crowns of the mandibular teeth at the level of the gingival margins. Segmentation is the most tedious and time-consuming step both in 3D and 2D dental biometrics. For a large database, automatic segmentation is required. Moreover, segmentation for a sample taken from a dry skull is different from that for a living subject. The reasons have been described in details in [61]. The crowns are delineated based on a presumption of a healthy gingival margin level across the tooth crowns as shown in Figure 3.3 (b) the dot line indicates. These delineated crown shapes from the PM sample are the rigid non-deformable elements that are used for matching with the AM samples.

3) Auto Segmentation Kondo et al. [62] proposed a semi-automatic tooth segmentation method. However, an initialization is needed to calculate the range image and four reference points need to be manually specified by users at the beginning. Kronfeld et al. [63] presented a highly automatic segmentation method for segmentation of teeth from the mesh model by applying an active contour algorithm. However, they reported that manual adjustment is still needed when the initial snakes are not appropriately located at the transition between teeth and gum, and also manual corrections of some parameters are inevitable. Both methods fail where the boundary between tooth and gum is very smooth and where the teeth are overlapping with each other. Instead of single-tooth segmentation, an automatic processing method is proposed for a large database to eliminate the bottom part of the plaster which does not contain tooth information. The Principal Component Analysis (PCA)-plane passing through the centroid of the plaster is first calculated. The dental plaster is then segmented by its PCA-plane into the crown part and bottom part as illustrated in Figure 3.3 (d-f). It costs 15 seconds on average per sample in the MATLAB programming environment (version R2007a The MathWorks, Inc., running on a PC with two Duo Core CPUs with a clock speed of 2.33 GHz and 1.96GB RAM), including sample import and export time. As compared with the manually segmented

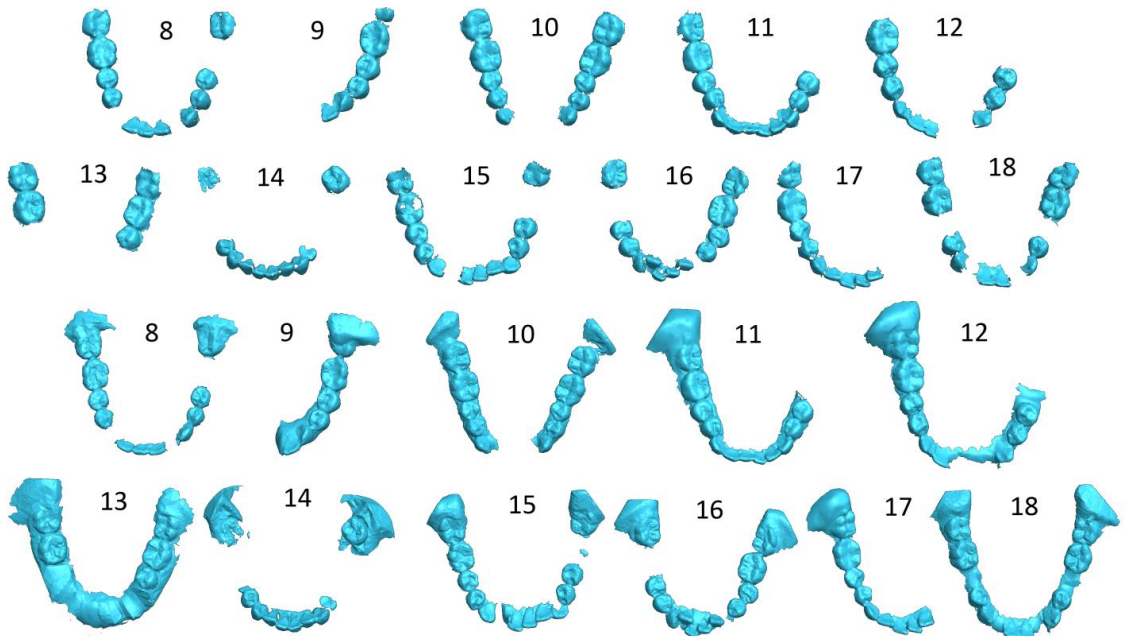
samples, a portion of tooth gum and dental plaster is still attached to the mesh as it is shown in Figure 3.2 (a-c) bottom row. Detail descriptions of Figure 3.2 are shown below.



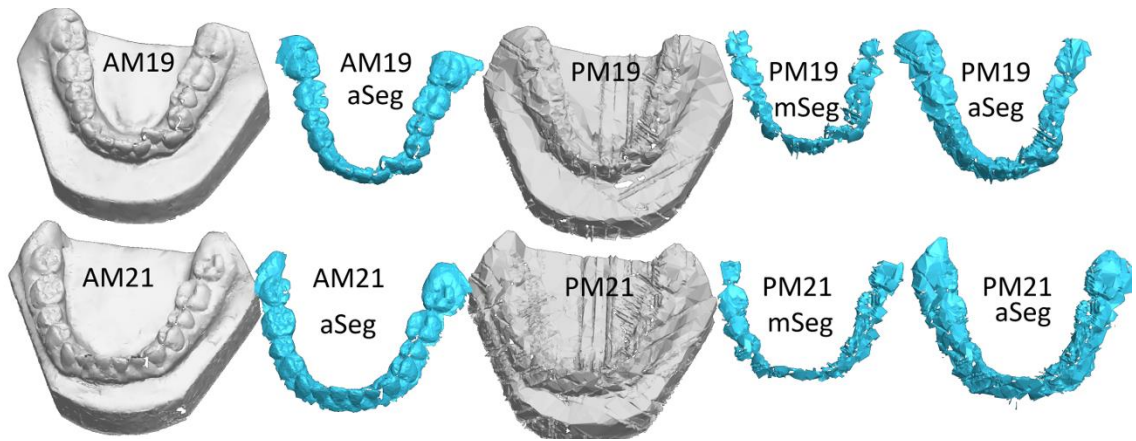
(a) Top row: manual segmented seven complete PM samples; bottom row: auto segmented seven complete PM samples



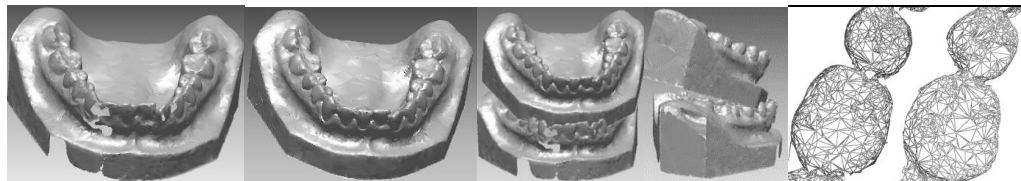
(b) Top row: manual segmented 10 imposter PM samples; bottom row: auto segmented 10 imposter PM samples



(c) Top two rows: manual segmented 11 partial samples; bottom two rows: auto segmented 11 partial samples



(d) Top row left to right: decimated sample AM19; auto segmented sample AM19; decimated sample PM19; manual segmented sample PM19; auto segmented sample PM19; bottom row left to right: decimated sample AM21; auto segmented sample AM21; decimated sample PM21; manual segmented sample PM21; auto segmented sample PM21



(e) Difference in genuine samples in two scans(left to right): AM sample; PM sample; front view of different initial positions of AM and PM samples; side view of different initial positions of AM and PM samples; mesh topology difference

Figure 3.2 Sample illustration

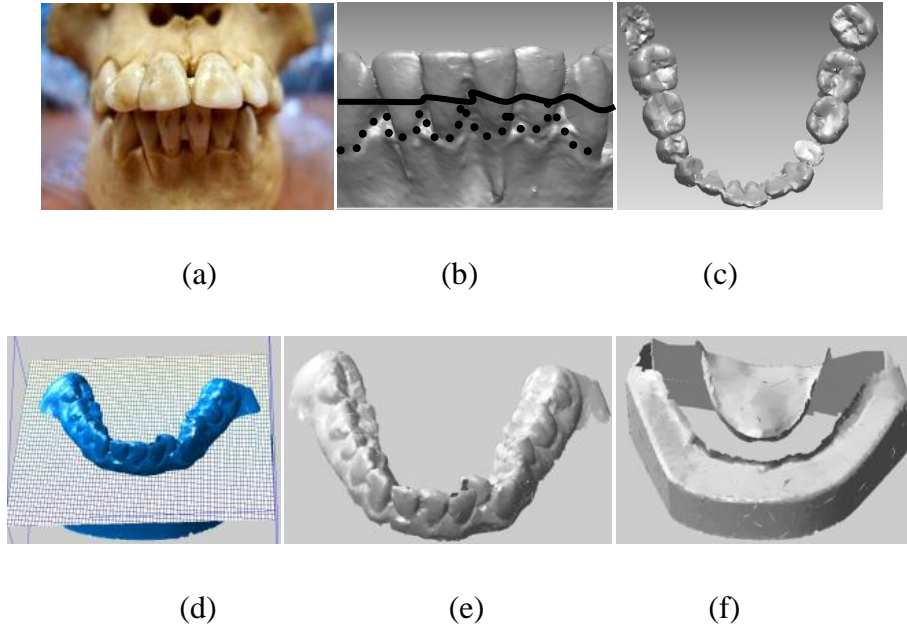


Figure 3.3 Manual segmentation of a human skull (a) a human skull (b) the expected detected interstices (solid line) and the interstices obtained by minima curvature rule (dash line) (c) a set of manual segmented mandibular teeth of a human skull (d) PCA-plane (e) segmented tooth crown (f) bottom part of a dental plaster

3.5 Dental Feature Point Extraction

The feature extracted in this study is geometric invariant and visually salient feature point [64, 65]. A multi-scale feature extraction algorithm is presented to extract these feature points on digitized dental surfaces. Steps for feature point extraction list below.

a. *Gaussian multi-scale representation*

The first step is to compute the bounding box to define a neighbourhood for each vertex v on the dental surface. $\sigma_i \in \{1\epsilon, 2\epsilon, 3\epsilon, 4\epsilon, 5\epsilon, 6\epsilon\}$, where ϵ is 0.3% of the length of the diagonal of the bounding box of the dental surface as shown in Figure3.4(a). For each vertex v , the neighbourhood $N(v, \sigma)$ is point x_i within distance σ as shown in Figure3.4(b). Equation

$$N(v, \sigma) = \{x \mid \|x - v\| < \sigma, x : \text{vertex}\} \quad (3.1)$$

is used for calculating the neighbourhood points. Six Gaussian filters are applied on the dental surface. A representation of the surface model $G(v, \sigma)$ was computed using equation

$$G(v, \sigma) = \frac{\sum_{x_i \in N(v, 2\sigma)} x_i \cdot \exp\left[-\|x_i - v\|^2 / (2\sigma^2)\right]}{\sum_{x_i \in N(v, 2\sigma)} \exp\left[-\|x_i - v\|^2 / (2\sigma^2)\right]}. \quad (3.2)$$

b. *Saliency computation*

The second step of feature extraction is the mesh saliency of the dental surface. Difference-of-Gaussian (*DoG*) for each vertex v is defined:

$$DoG(v) = G(v, \sigma_i) - G(v, k\sigma_i) \quad (3.3)$$

as the difference between its Gaussian representation at scale (σ_i) and scale $(k\sigma_i)$. The constant factor k is set 2. In order to extract the small number visually distinct feature points, each saliency map is normalized using the non-linear suppression operator S proposed by Itti et al [66]. To observe the difference of the Gaussian filters on the dental surface, one molar is shown in Figure 3.4(c).

c. *Boundary removal*

The third step is to remove the feature points on the boundary of the dental surface. The dental surface is not a closed surface after segmentation. The multi-scale representation is Gaussian average of the neighbourhood points, the boundary points are possibly detected as feature points since they have only one side neighbourhood points. Those false feature points are redundant information for correspondence. Therefore, in order to remove the boundary effect, the following algorithm is applied: 1) search for the boundary vertices which have neighbourhood points on one side 2) search for the vertices within distance $2\sigma_6$ to the boundary points 3) set the saliency of all these vertices to zero

As shown in Figure 3.13(a), boundary points are detected as feature points by the existing work [64, 65]. Usually, more feature points require more computational time in finding correspondence. The number of extracted points and the total time in matching genuine samples and imposter samples are compared in [61]. It is about six

times faster using feature point detection algorithm in this work in matching one PM sample to its genuine AM sample.

d. *Feature point extraction*

The fourth step is to suppress more points and extract the most visually distinct points. The saliency value of a point at each scale is set to zero unless it is larger than the saliency of 85% of its neighbouring vertices. The saliency value at all six scales are added up followed by a normalization process. Finally, a vertex whose saliency value is a local maximum and larger than 60% of the global maximum is detected as a feature point.

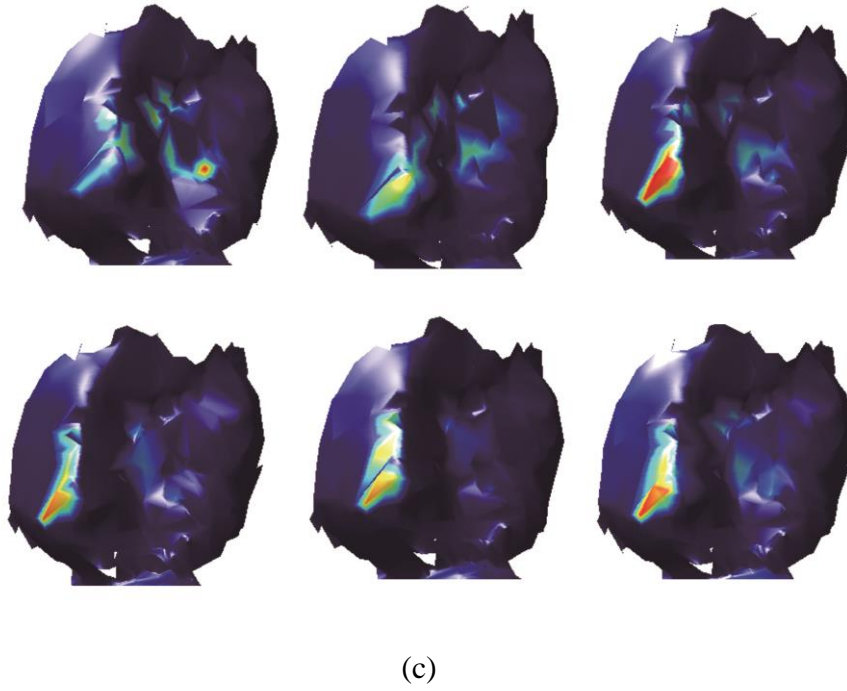
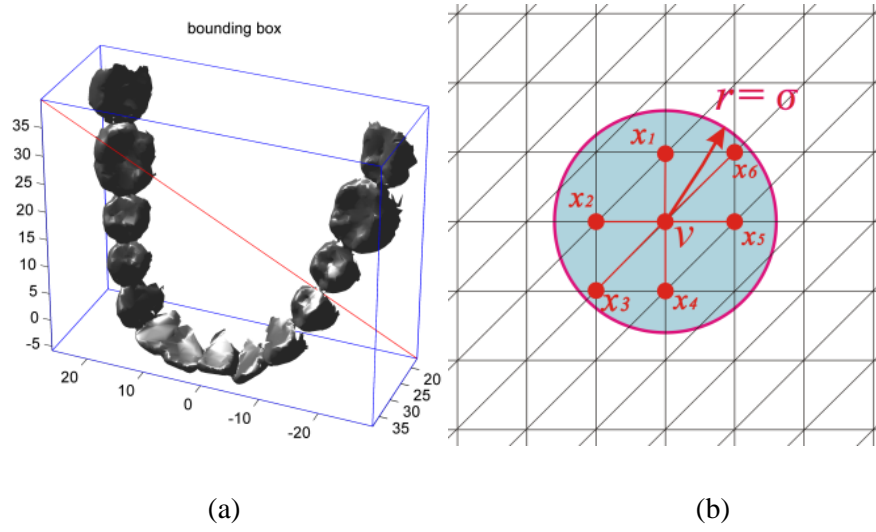


Figure 3.4 Bounding box and diagonal length of a dental surface (b) neighbourhood determination using a query ball for vertex v (c) 6 differently Gaussian-filtered models of a molar from the dental arch

3.6 Point Feature Descriptions

After feature extraction, a shape descriptor needs to be assigned to each feature point for correspondence in the matching stage. The descriptor determination is important since different descriptors exhibit different correspondence capabilities. In this study,

the performance of three descriptors is compared: the saliency value, the Gauss curvature, and the integral volume.

Option 1 Saliency value descriptor

The feature points are extracted based on their saliency values in the last section. The saliency value could also be used to determine the degree of correspondence as shown in Figure 3.5 (a).

Option 2 Gaussian curvature descriptor

Curvature is often used in 3D mesh processing because it is one of the geometric invariant characteristics of mesh model. The Gaussian curvature is computed using the method in [67]. Gaussian curvature map on dental surface is shown in Figure 3.5 (b)

Option 3 Integral volume descriptor

Integral volume at point p is defined as the intersection volume of a ball of radius r centered at point p with the interior of the surface model as shown in Figure 3.5(c). The integral volume can be computed using techniques based on convolution of the occupancy voxel grid [68]. However, in their study, only models with distinct features in the benchmark database were tested, for example, dragon model with sharp claws and tail tips, the bunny model with ear tips, the David head model with an obvious nose tip, which are quite different from the dental surfaces taken from the real humans and have highly irregular shapes. In this study, a method based on the mean curvature estimation [69] is adopted and simplified to compute the integral volume.

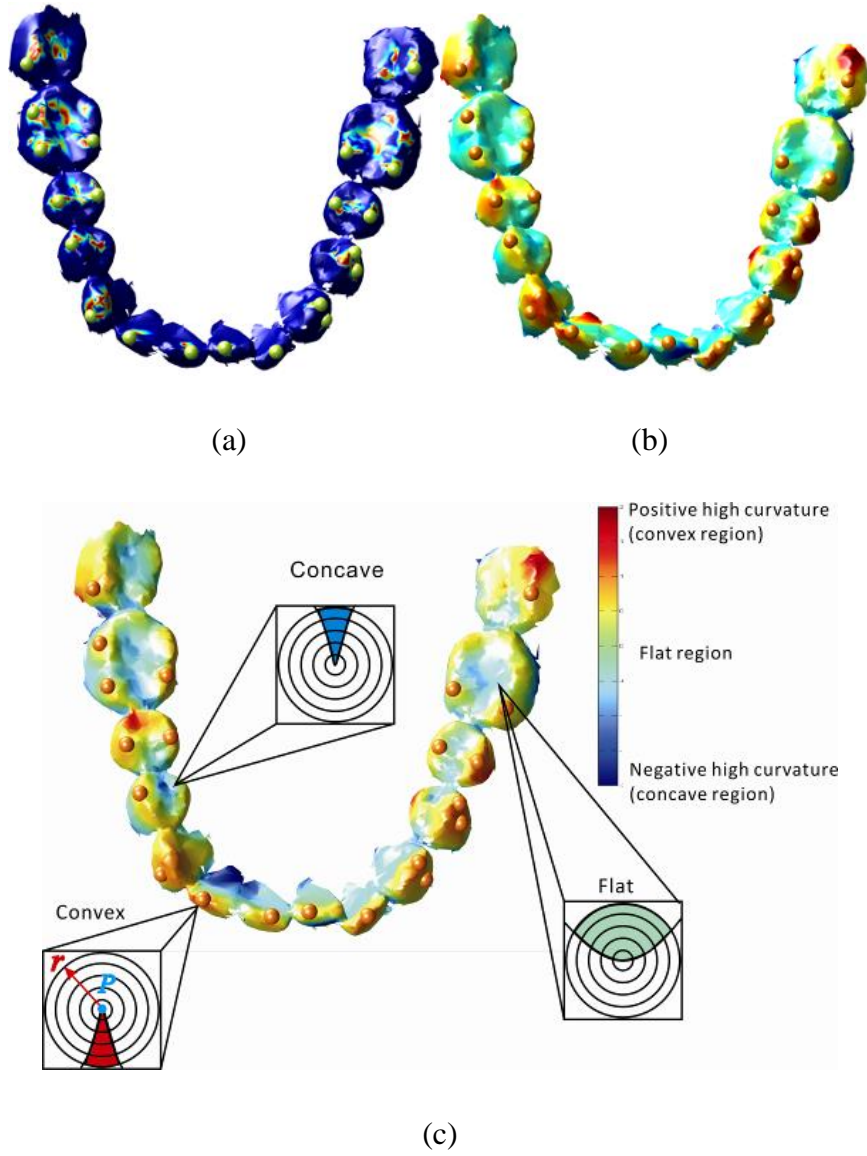


Figure 3.5 (a) Saliency descriptor (b) Gaussian curvature descriptor(c) Integral volume descriptor

The integral volume descriptor at vertex p associated with the local mean curvature could be computed using equation (3.4) [68] as

$$V_r(p) = \frac{2\pi}{3}r^3 - \frac{\pi H_{(p)}}{4}r^4 + O(r^5) \quad (3.4)$$

Where $H_{(p)}$ is the local mean curvature at vertex p and r is the radius of the ball. The first term is the half volume of the ball, while the second term involves the mean curvature H at vertex p . In this study, the integral volume descriptor is normalized by

the volume of a ball $\frac{4}{3}\pi r^3$ to form equation (3.5). Therefore, it becomes the ratio between the volume of the intersection and the volume of the entire ball. Thus its value is within range $[0, 1]$.

$$V_r(p) = \frac{1}{2} - \frac{3}{16} H_{(p)} \cdot r + O(r^2) \quad (3.5)$$

To estimate the mean curvature, equation (3.6), (3.7) and (3.8) are used.

$$H(v_i) = \frac{\frac{1}{4} \sum_{j=1}^{ne} \|v_j - v_i\| \gamma_j}{\frac{1}{3} A} \quad (3.6)$$

where γ_j is the angle between the normal of the two faces adjacent to edge (v_i, v_j) as shown in Figure 3.6. ne is the number of edges adjacent to v_i . A is the sum of the faces area around v_i .

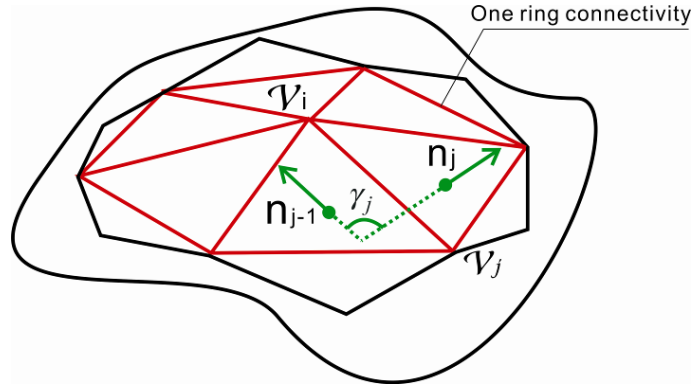


Figure 3.6 One ring connectivity for mean curvature estimation

$$w_{ij} = e^{\frac{-g_{ij}}{g_{i, \max}}} \quad (3.7)$$

where w_{ij} in equation (3.7) is a weighted factor between the centre vertex v_i and neighbour v_j and g_{ij} is the Euclidian distance between v_i and v_j . $g_{i, \max}$ is the max Euclidian distance from vertex v_i to the other vertices in a query ball as shown in Figure 3.4(b).

$$H(v_i) = \sum_{j=1}^n w_{ij} \cdot H(v_j) \quad (3.8)$$

where n is the number of neighbour vertices which is searched by the query ball as shown in Figure 3.4(b).

3.7 Coarse-to-fine Matching

Let P' and Q' be the feature points extracted from the PM dental surface and the AM dental surface respectively. For each feature point $p_i \in P'$ and $q_i \in Q'$, the respective descriptor values (saliency, Gaussian curvature, integral volume) $S(p_i)$ and $S(q_i)$ are calculated. The following steps are for finding three feature points both in PM and AM samples with similar values and similar relative positions in Euclidean space for correspondence.

- For any feature point $p \in P'$, select the salient point q as potential correspondence if $|S(p) - S(q)| < \varepsilon$, where ε is threshold value and set to be 0.1 from tests. Therefore, a set of potential correspondences for each feature point are determined and designated as $(C(p_1), \dots, C(p_n))$.
- For each pair of feature points (p_i, p_j) , choose any $q_i \in C(p_i)$, $q_j \in C(p_j)$ and set the point pair (q_i, q_j) which minimizes the distance root mean squared (dRMS) error defined in equation

$$dRMS^2(P', Q') = \frac{1}{n^2} \sum_{i=1}^n \sum_{j=1}^n (\|p_i - p_j\| - \|q_i - q_j\|)^2 \quad (3.9)$$

as the associated correspondence pair, resulting in a set $E2$ of two-point correspondences. $\|\cdot\|$ denotes the Euclidian distance of these two feature points. $E2$ is then sorted in order of ascending dRMS error. Any $e \in E2$ whose dRMS error is larger than threshold ε_{dRMS} is discarded.

- For each two-point correspondence $e \in E2$, add another potential correspondence pair (p_k, q_k) which minimizes the dRMS error. In this way, a set $E3$ of triplet-point correspondence is formed. $E3$ is then sorted in order of ascending dRMS error. Any $e \in E3$ whose dRMS error is larger than a threshold ε_{dRMS} is discarded.

- For each triplet-point correspondence in E3, a rotation and translation matrix can be obtained by Singular Value Decomposition (SVD) method and the corresponding coordinate root mean square (cRMS) error is then computed using equation

$$cRMS^2(P, Q) = \min_{R, t} \frac{1}{n} \sum_{i=1}^n \|Rp_i + t - q_i\|^2. \quad (3.10)$$

Finally, E3 is sorted in order of *cRMS* error.

The first triplet-point correspondence in E3 corresponding to minimal *cRMS* error is taken as the best triplet-point correspondence. With the estimated initial position by feature points correspondence, the fine comparisons are achieved by utilizing iterative closest point (ICP) algorithm which was first developed by Besl and Mckay [70], Chen and Medioni [71]. ICP is an algorithm for minimizing the difference between two point clouds. It is simple and is commonly applied in real-time for 2D/3D surface reconstruction, robot localization and optimal path planning. The following thresholds are specified in the experiments. The maximum number of iterations is 30, the minimum error change is smaller than 1e-12 and the minimum coordinate change is smaller than 1e-12 between iterations. When one of the above mentioned thresholds is met, the algorithm stops and it is considered to have converged. The differences of genuine sample identification and imposter sample identification are shown in Figure 3.7. The comparison shows that genuine samples require less iterations and the final matching error is much smaller.

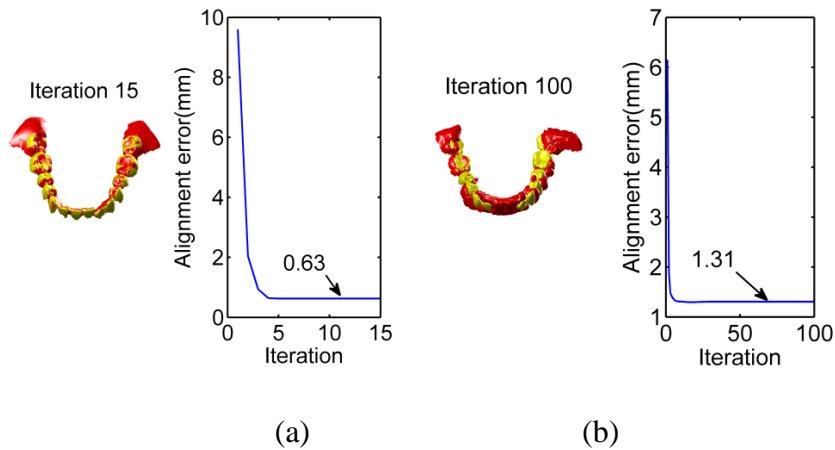


Figure 3.7 Differences in genuine sample identification and imposter sample identification (a) genuine sample (b) imposter samples.

3.8 Experiments and Discussion

Experiment I Complete Sample Identification

In Experiment I, seven samples shown in Figure 3.2(a) are tested with 100 AM samples and 200 AM samples. The comparison is shown in Table 3.2 and Table 3.3. The first four ranks of the average errors are compared in Table 3.4. The average error is calculated as the arithmetic mean error of the correctly matched results at each rank. Comparing Table 3.2 and Table 3.3, all the samples achieve rank-1 accuracy by using this work in contrast with that only 5 out of 7 achieving rank-1 accuracy by using existing algorithm ICP alone. Rank of sample PM2 and PM3 slightly decreases using ICP due to the fact that increasing the sample size may lead to inclusion of more dentitions that are similar and thus lead to more mismatches; however, this work is more robust to AM sample size increase as every correct match is still retrieved at rank-1 after AM sample size increase.

The rank-1 identification accuracy of auto-segmented complete PM samples in this work is 100% by dividing the number of correct matches at rank-1 by the total number of PM sample, which is $7/7 \times 100\% = 100\%$. This accuracy is to be compared with results in Chapter 4.

It can be concluded from Table 3.4 that much lower rank-1 error is achieved by using this work compared to that using ICP. If the error change ratio is defined as the quotient of three successive ranks, for example, $\mu_{12/23}$ and $\mu_{23/34}$ are used to denote the error change ratio between rank1-2 and rank3-4 in matching manually segmented sample using this work, then $\mu_{12/23} = (0.924 - 0.522) / (0.935 - 0.924) = 36.5$, in contrast with $\mu_{23/34} = (0.935 - 0.924) / (0.954 - 0.935) = 0.59$. The rank1-2 slope is bigger using this work both for manually and auto segmented samples, thus this work is more discriminative to differentiate the genuine sample from the rest in the database by comparing the error change ratio. The error change rate of genuine manually segmented sample $e = \mu_{12/23} / \mu_{23/34} = 61.9$ ($36.5 / 0.59$) by using this work. The comparison is shown in Figure3.8.

Table 3.2 Identification of 7 genuine PM complete samples from 200 AM samples

	PM	1	2	3	4	5	6	7
Manually	ICP	1	1	1	1	1	1	1
Segmented	This	1	1	1	1	1	1	1
Rank	Work							
Auto	ICP	1	9	3	1	1	1	1
Segmented	This	1	1	1	1	1	1	1
Rank	Work							

Table 3.3 Identification of 7 genuine PM complete samples from 100 AM samples

	PM	1	2	3	4	5	6	7
Manually	ICP	1	1	1	1	1	1	1
Segmented	This	1	1	1	1	1	1	1
Rank	Work							
Auto	ICP	1	3	2	1	1	1	1
Segmented	This	1	1	1	1	1	1	1
Rank	Work							

Table 3.4 Genuine matching error at first four ranks (7PM vs 200AM)

		Rank1	Rank2	Rank3	Rank4
Manually	ICP	0.710	0.972	1.028	1.038
Segmented	This Work	0.522	0.924	0.935	0.954
Auto	ICP	0.992	1.130	1.180	1.215
Segmented	This Work	0.646	1.084	1.103	1.140

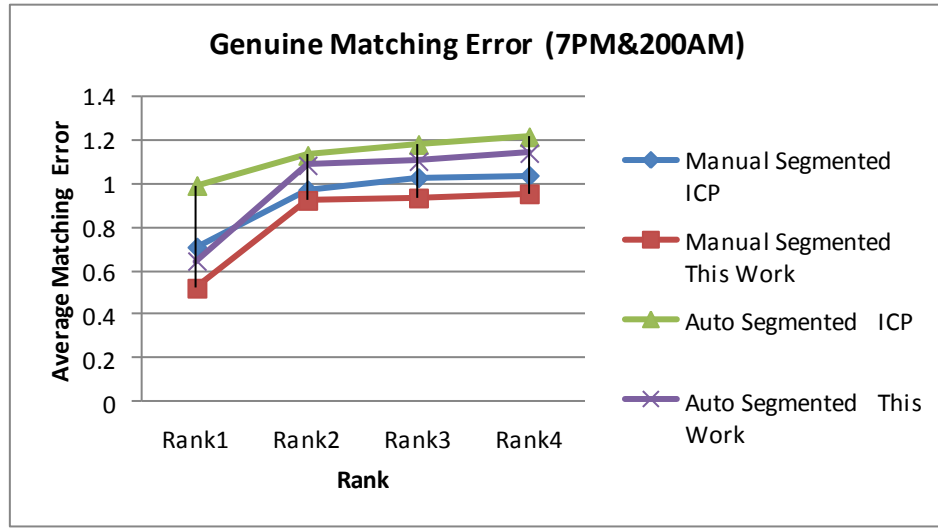


Figure 3.8 Matching error comparison of genuine samples at first four ranks

Experiment II Imposter Sample Identification

Consider an actual situation of PM sample identification that when a jaw is found, forensic experts do not know whether it has a corresponding record in the AM database. This is often called open-set identification in biometrics. During identification, it is good if certain thresholds, trends or graphs could indicate that corresponding record of this sample is present or absent in the AM database, i.e., is a genuine or imposter sample. In most 2D radiograph literatures [25-30, 35, 36, 51-54, 72-76], imposter identification has not been well investigated. Proper thresholds have not been discussed to indicate the presence and absence of victims in AM database.

This experiment is designed to find an appropriate error threshold for the system to identify imposter samples. 10 imposter samples in Figure 3.2 (b) which do not have their corresponding AM samples in the AM database are matched against 200 AM samples. Average matching errors at first four ranks are shown in Table 3.5 and Figure 3.9. $\mu'_{12/23}$ and $\mu'_{23/34}$ are used to denote the error change ratio between rank1-2 and rank3-4 in matching manual segmented imposter sample using this work, then $\mu'_{12/23} = (0.921-0.883)/(0.937-0.921)=2.4$, in contrast with $\mu'_{23/34} = (0.937-0.921)/(0.956-0.937)=0.84$. The error change rate of imposter manually segmented sample using this work denoted as $e' = \mu'_{12/23} / \mu'_{23/34} = 2.9$ ($2.4/0.84$). We observe that there is not much difference between using ICP and this work in imposter

identification. As calculated in Experiment I, the error change rate of genuine identification is 61.9 which is much larger than the error change rate of imposter identification. Therefore, the system could distinguish imposter samples at a threshold of 0.8 according to the rank-1 error and the error change rate. 0.8 is determined by comparing the arithmetic mean rank-1 errors of genuine samples and imposter samples in Table 3.4 and Table 3.5.

Table 3.5 Imposter matching error at first four ranks (10PM&200AM)

		Rank1	Rank2	Rank3	Rank4
Manual	ICP	0.882	0.919	0.936	0.960
Segmented	This Work	0.883	0.921	0.937	0.956
Auto	ICP	1.036	1.087	1.127	1.138
Segmented	This Work	0.998	1.060	1.091	1.115

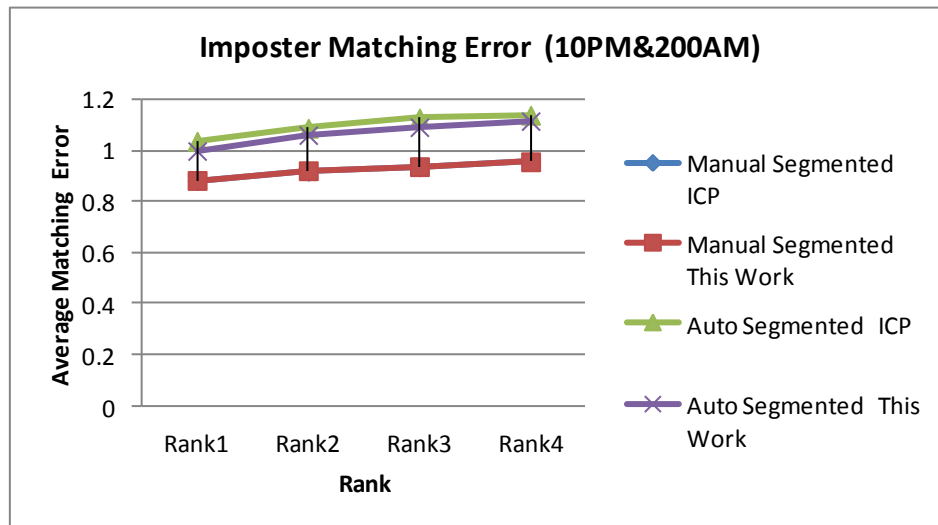


Figure 3.9 Matching error comparison of imposter samples at first four ranks

Experiment III Partial Samples Identification

In the PM samples, it is common to see that the lower jaws of victims are broken into pieces or some teeth are missing due to violence or other forces. It is more challenging to identify partial PM samples when full PM samples of teeth are not available. In the presence of missing teeth, it will be difficult for the matching

algorithm in 2D to correctly correspond the tooth sequences in AM and PM images if the missing teeth have not been properly detected. It is also reported that matching algorithm cannot properly align AM and PM radiographs if they do not contain the same number of teeth [34]. Mahoor and Abdel-Mottaleb [28] proposed Bayesian classification method using Fourier descriptors to obtain the indices of teeth in bitewing images. The classification accuracy is high, 72%~95.5% for molar and premolar classification in maxillary and mandibular jaws. However, their work deals with bitewing images, which only include two classes of teeth: molars and premolars. Furthermore, it is assumed that there are no missing molars or premolars in the images. Anil Jain et al. [27] developed a hybrid model involving the Support Vector Machine (SVM) and the Hidden Markov Model (HMM) for the representation and classification of teeth. It deals with all three types of dental radiographs (bitewing, periapical, and panoramic images) and it considers all three classes of teeth (molars, bi(cuspids), and incisors). However, the accuracy is not high. For fully automatic extraction of tooth contours, the reported rank-1 accuracy is 60.1%[34].

In this experiment, ϵ is adjusted to 0.25% of the length of the diagonal of the bounding box of the dental surface as shown in Figure 3.4(a) due to the fact that partial samples need more detailed description. The results are shown in Table 3.6. Both manual and auto segmented samples are used. Starting from the same initial orientation, correct and higher ranks are obtained by using this work compared to those of applying ICP alone. However, it is observed some samples are not perfectly matched. It is probably because sample PM9 and PM13 are the most partial ones among the eleven which only contain five teeth. Partial identification is more difficult because a correct matching cannot be guaranteed with the same ϵ value for every PM sample (ϵ determines the neighborhood size). Namely, ϵ should be adjusted according to how partial the PM sample is. If the ϵ is adjust to 0.15% of the length of the diagonal of the bounding box, sample PM9 and PM13 are correctly matched and rank-1 accuracy is achieved in both identification processes as shown in Figure 3.10 (a-g). Figure 3.10 shows some of the non-rank-1 matching results and their corresponding corrected results with different ϵ values using this work compared to those using ICP. Most of the samples are well-aligned with corrected ϵ values as shown in Figure 3.10 (c, f, h, j) except auto-segmented PM8 as shown in Figure 3.10

(l). This may due to the fact that partial auto-segmented sample is more likely to stay at local minima. The rank-1 identification accuracy of auto-segmented partial PM samples in this work is 72.7% by dividing the number of correct matches at rank-1 by the total number of PM partial sample, which is $8/11 \times 100\% = 72.7\%$. 100% identification is achieved at rank-4.

Table 3.6 Identification of 11 PM genuine partial samples from 200 AM samples

	PM	8	9	10	11	12	13	14	15	16	17	18
Manual	ICP	1	89	1	1	1	162	1	83	1	166	1
Segmented	This	1	6	1	1	1	81	1	1	1	1	1
Rank	Work											
Auto	ICP	196	1	1	3	54	12	1	1	3	148	1
Segmented	This	3	1	1	4	1	3	1	1	1	1	1
Rank	Work											

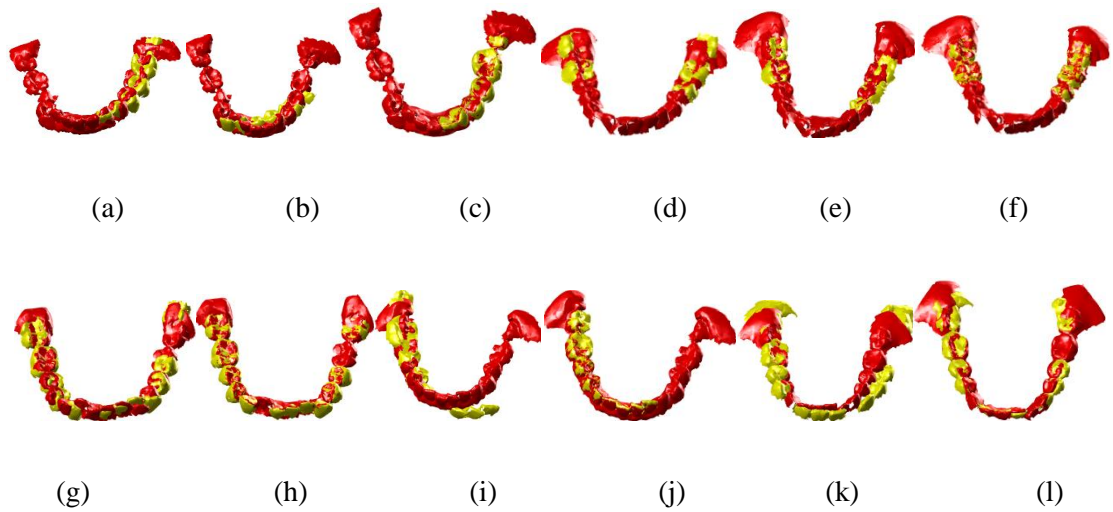


Figure 3.10 (a) manual PM9 ICP (b) manual PM9 this work $\epsilon=0.25\%$ (c) manual PM9 this work $\epsilon=0.15\%$ (d) manual PM13 ICP (e) manual PM13 this work $\epsilon=0.25\%$ (f) manual PM13 this work $\epsilon=0.15\%$ (g) manual PM15 ICP (h) manual PM15 this work $\epsilon=0.25\%$ (i) manual PM17 ICP (j) manual PM17 this work $\epsilon=0.25\%$ (k) auto PM8 ICP (l) auto PM8 this work $\epsilon=0.25\%$ and $\epsilon=0.15\%$

Experiment IV Noisy Sample Identification

Figure 3.11 shows the specific rank of each noisy sample (PM19-PM50). ‘ManN’ denotes the manual segmented noisy sample and ‘AutoN’ denotes auto segmented noisy sample. In experiment IV, ϵ is adjusted to 0.2% of the length of the diagonal of the bounding box of the dental surface as shown in Figure 3.4(a) because severe corrupted samples need much more detailed description. Figure 3.12 shows some of the non-rank-1 matching results aligned using this work comparing to those using ICP. However, samples in Figure 3.12 (c-f) almost have the same alignment error using different matching algorithms and they are equally well-aligned but they are not rank-1 samples. This is due to the segmentation differences and the noises. The PM samples have extra points and surfaces when superimposing with their corresponding AM samples as indicated in Figure 3.12 (c-f) and all these extra parts will be calculated as matching error.

The rank-1 identification accuracy of auto-segmented noisy PM samples in this work is 78.1% by dividing the number of correct matches at rank-1 by the total number of noisy PM sample, which is $25/32 \times 100\% = 78.1\%$. 100% identification is achieved at rank-30.

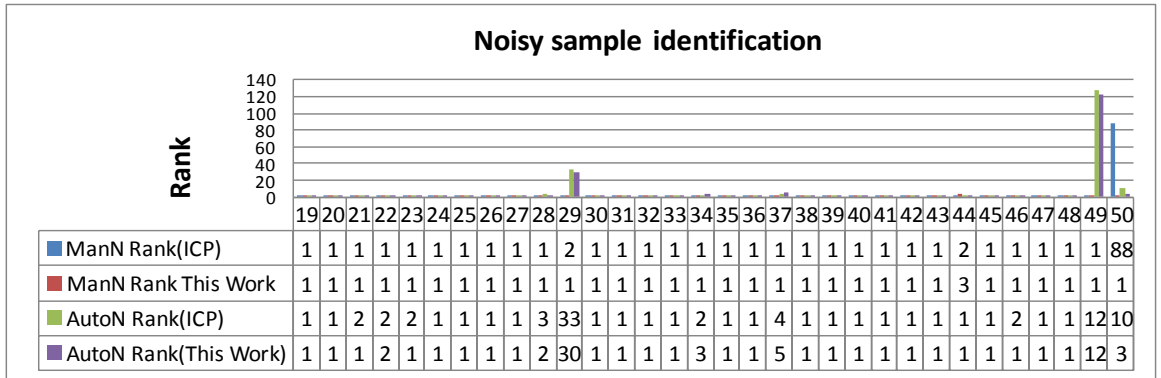


Figure 3.11 Noisy sample specific rank

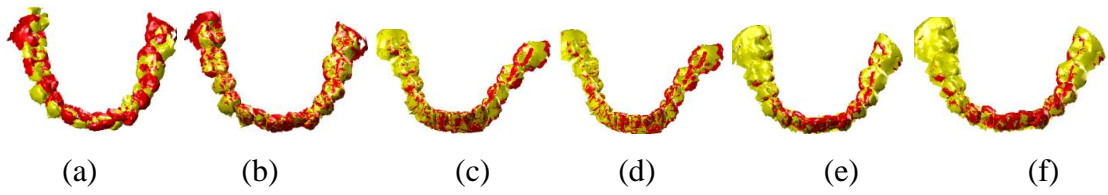


Figure 3.12 (a) manual PM50 ICP error=1.39 (b) manual PM50 this work error=0.67 (c) auto PM29 ICP error=1.08 (d) auto PM29 this work error=1.05 (e) auto PM50 ICP error=1.42 (f) auto PM50 this work error=1.24

The Cumulative Match Characteristic (CMC) Curve

Overall accuracy of 50 genuine PM samples is also calculated and compared. Cumulative Match Characteristic (CMC) curve is a standard statistical method used to evaluate the performance of the closed-set identification (A biometric task where an unidentified individual is known to be in the database and the system attempts to determine his/her identity) experiment. It plots the rank versus identification rate. Identification of 50 PM genuine samples from 200 AM samples, each sample has 200 possible ranks. The x axis represents the rank of retrieved subjects. The y axis indicates the percentage of cumulated number of correct retrievals at certain rank. The faster the CMC curve approaches one, the better the matching algorithm. The overall identification accuracy of Experiment I, III, and IV of the 50 genuine PM samples which include 7 complete sets, 11 partial sets and 32 noisy sets is compared in Figure 3.13. The manual identification verifications were carried out on the retrieved results to serve as the correct benchmark matches in Experiment I, III, and IV. The identification of manual-segmented samples using this work has the highest 94% rank-1 accuracy. With a fully automated process, the rank-1 accuracy decreases to 80%. In contrast, identifications using ICP only achieve 86% and 64% rank-1 accuracy in manual and auto process respectively.

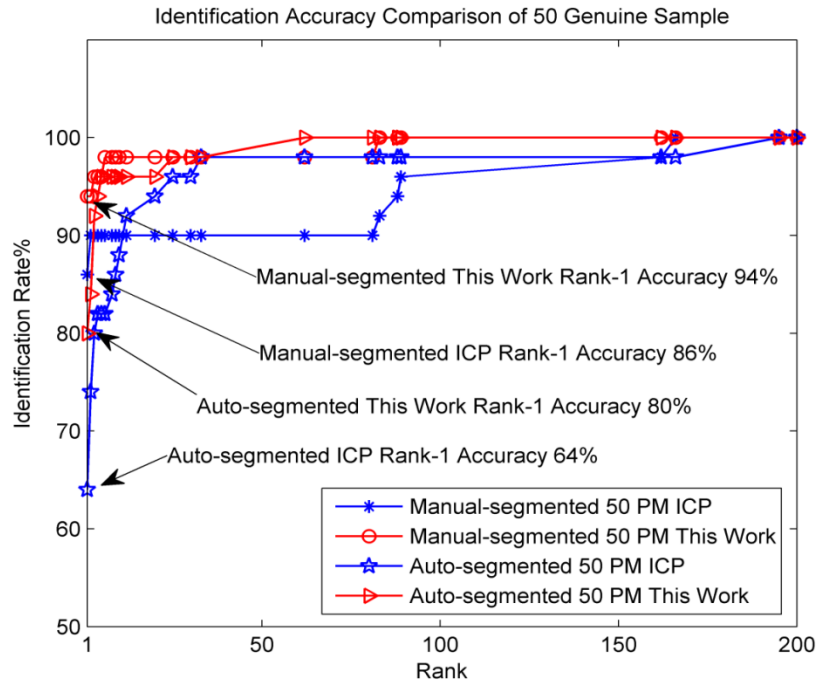


Figure 3.13 Identification accuracy comparison of 50 genuine samples

Experiment V Feature Extraction Comparison

Figure 3.14 shows the differences of feature points extracted on complete, partial and noisy dental surfaces using this work and the existing work in literature [64, 65]. More feature points usually require more computational time in finding correspondence, making this work especially more suitable for partial and noisy sets. The computational time for finding correspondence is significantly reduced (six times faster) by applying the extraction algorithm in this work. The redundant points are indicated with red circles as shown in the top row. Those redundant points could also cause mismatching sometimes.

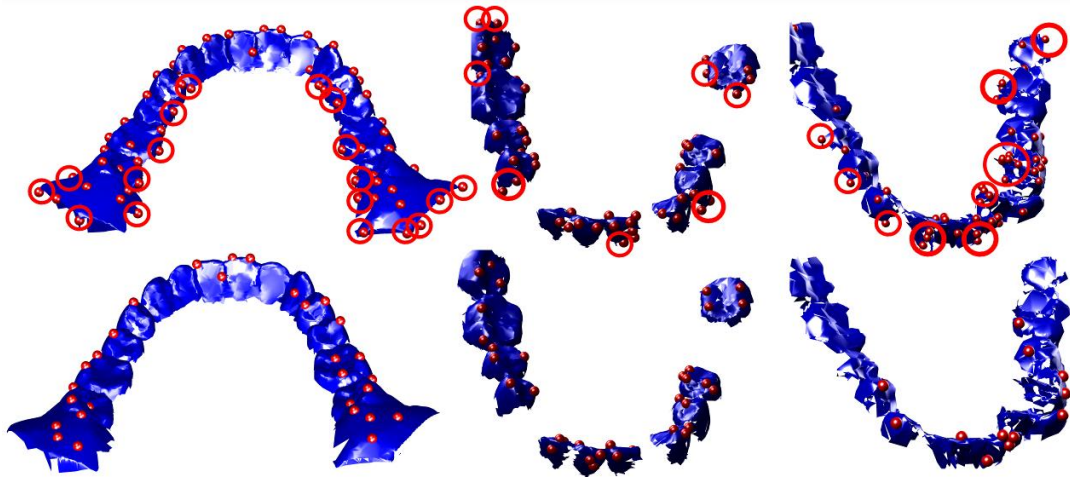


Figure 3.14 Feature points on complete, partial and noisy dental meshes (left to right): upper row existing work; lower row: this work

Experiment VI Correspondence Algorithm Comparison

In Experiment VI, the existing greedy correspondence (GC) algorithm [68] is compared with the proposed triplet correspondence (TC) algorithm. The GC algorithm first finds the best correspondences for each pair of feature points. Then it combines the pairs to form best corresponding sets of four points, and then combines fours into eights and so on. Three manual segmented samples in Figure 3.2 are selected: complete sample PM1, partial sample PM9 and noisy sample PM19. In fact, any of the complete samples and noisy samples in Figure 3.2 (a) and Figure 3.2 (d) can be used to compare, however, partial sample PM9 is selected. These three samples are compared under 30 to 180 degree rotation variations with 30 incremental degrees each time. Figure 3.15 shows the possible initial rotations during sample acquisition process. The initial orientation cannot be exactly the same during two acquisitions even if the sample is scanned by the same investigator. The dental plaster is placed on a wedge to face the scanner. Then the wedge and the plaster are placed on a rotatable disk. Thus the possible rotations of the initial orientation are about the rotation axis from 0 to 360 degree. The rotate axis is the principal axis with the smallest Eigen value calculated by principle component analysis. If the rotation axis is represented using unit vector (u, v, w) , where $u^2 + v^2 + w^2 = 1$, the rotation about this axis by the angle θ could be specified as matrix R [77], where

$$\mathbf{R} = \begin{bmatrix} u^2 + (1-u^2)\cos\theta & uv(1-\cos\theta) - w\sin\theta & uw(1-\cos\theta) + v\sin\theta \\ uv(1-\cos\theta) + w\sin\theta & v^2 + (1-v^2)\cos\theta & vw(1-\cos\theta) - u\sin\theta \\ uw(1-\cos\theta) - v\sin\theta & vw(1-\cos\theta) + u\sin\theta & w^2 + (1-w^2)\cos\theta \end{bmatrix} \quad (3.11)$$

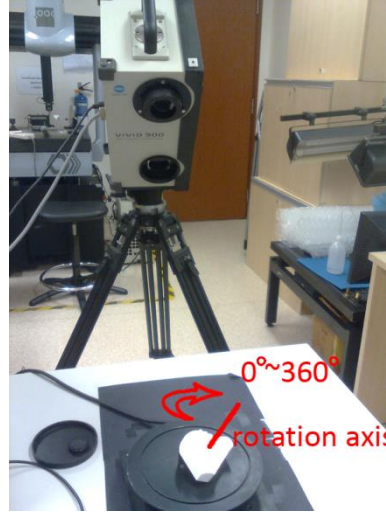


Figure 3.15 Possible initial rotations

The results are shown in Table 3.7. The left column shows the results obtained using existing method [68], and the right column shows the results obtained using the correspondence algorithm in this study. Three symbols were used to quickly index the matching results.

😊 -A smiling face means perfect matches

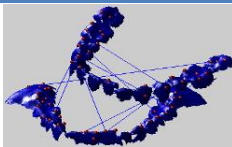

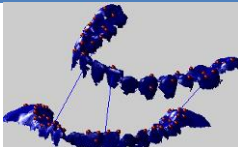



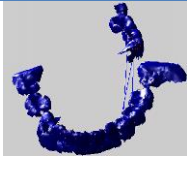
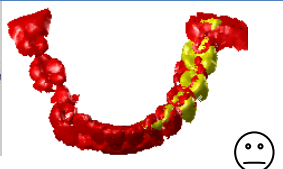
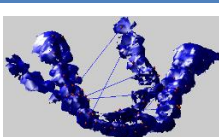
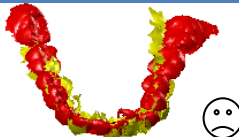
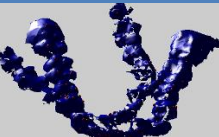
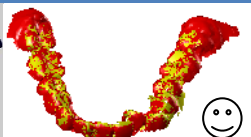
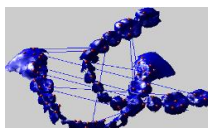

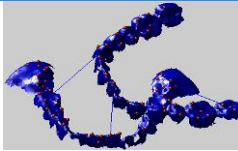

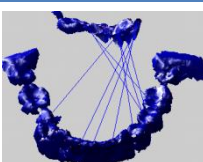

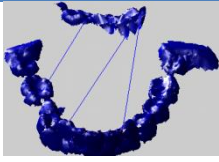

😐 -A neutral face indicates matches achieve approximately right positions but not perfect matches

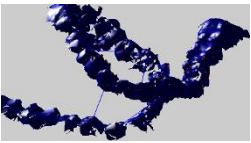

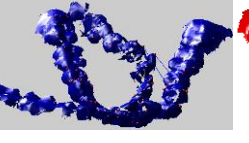

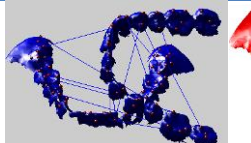

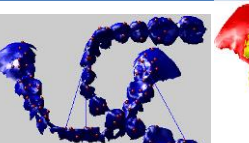

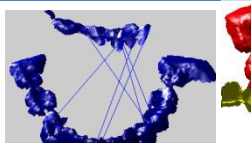

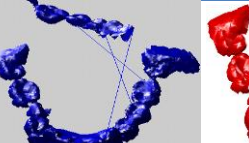

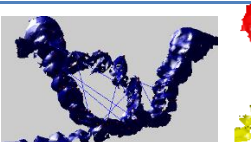

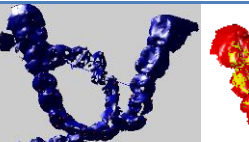
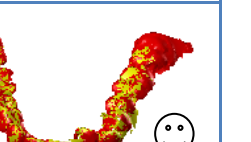
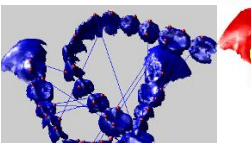

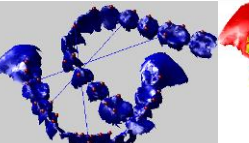

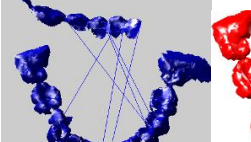

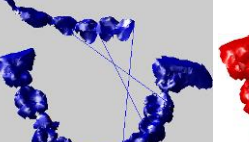

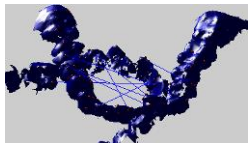

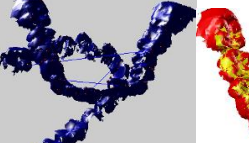

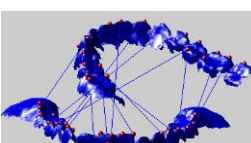

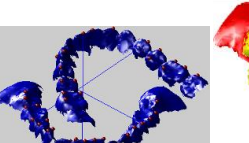



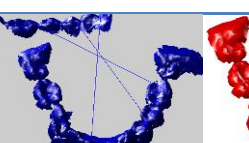

😞 -A sad face implies bad matches

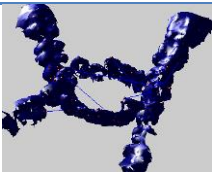
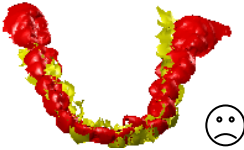
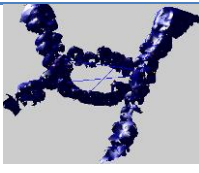

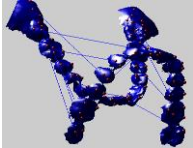

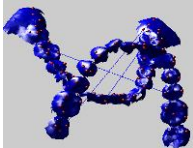

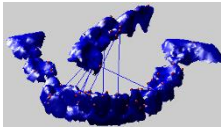

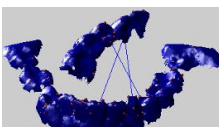

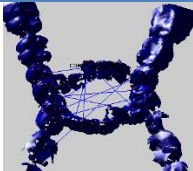

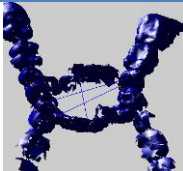

The following two conclusions could be drawn from the results shown in Table 3.7. Obviously, fewer and noisy points in samples often mean more difficulties in getting the right matches. Comparing the results in Table 3.7, correct matching is achieved for sample PM1 and PM19 in every case using the method in this work (TC) when existing method (GC) fails to correctly align these samples in most cases. This work

is also more robust in partial identification as shown in 30° and 90° rotations. The improved corresponding algorithm in this work is less sensitive to pose variations. This is because the existing method was mostly developed for closed surfaces without boundary which have significant salient features, such as the finger and nose tip of humans, the ear tip and the claw tip of animal models, but not for corresponding dental mesh with highly similar convex and concave, saddle shapes. However, failure cases are observed in matching partial PM9 under 120°, 150° and 180° rotations. It could be concluded that if the PM sample is too partial and asymmetrical, human interaction is needed or single tooth identification scheme is to be developed which will compare single PM tooth to single AM tooth.

Table 3.7 Correspondence algorithm comparison

Sample	Existing work[68]		This work	
	Rotation 30°			
PM1 complete				
PM9 partial				
PM19 noisy				
Rotation 60°				
PM1 complete				
PM9 partial				




PM19 noisy				
Rotation 90°				
PM1 complete				
PM9 partial				
PM19 noisy				
Rotation 120°				
PM1 complete				
PM9 partial				
PM19 noisy				
Rotation 150°				
PM1 complete				
PM9 partial				









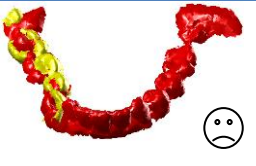












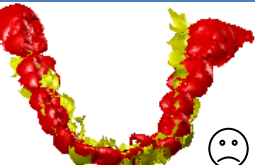


PM19 noisy				
Rotation 180°				
PM1 complete				
PM9 partial				
PM19 noisy				

Experiment VII Shape Descriptor Comparison Regarding Pose Variations

In Experiment VII, the three shape descriptors are compared regarding pose variations. The same three manual segmented samples in Experiment VI are used: complete sample PM1, partial sample PM9 and noisy sample PM19. These three samples are compared under 60 to 180 rotation variations with 60 incremental degrees each time as shown in Table 3.8. In matching complete sample PM1, saliency and Gaussian curvature descriptors have equal performance when integral volume fails in 60 ° rotation. In matching partial sample PM9, three descriptors have equal performance. In matching noisy sample PM19, saliency descriptor in this work is more robust to pose variations than the other two descriptors.

Table 3.8 Shape descriptor comparison

Sample	Shape descriptor	Rotation 60°	Rotation 120°	Rotation 180°
PM1	Saliency			

	Gaussian Curvature			
	Integral Volume			
PM9	Saliency			
	Gaussian Curvature			
	Integral Volume			
PM19	Saliency			
	Gaussian Curvature			
	Integral Volume			

3.9 Computational Time

Towards developing an automated system, not only identification accuracy should be considered but also the identification speed. As mentioned earlier, all the experiments are tested in MATLAB programming environment (version R2007a The MathWorks,

Inc., running on a PC with two Duo Core CPUs with a clock speed of 2.33 GHz and 1.96GB RAM.) Table 3.9 lists the time required in each experimental step. Time is calculated as average time in Experiment I for the samples shown in Figure 3.2 (a) lower row. For example, identifying 7 PM sample from 200 AM sample cost 18900 seconds (5.25 hours) in total. Therefore, identifying 1 PM from 200 AM would cost 2700 seconds (45 minutes) which includes time for data import, feature point extraction and matching. Time calculation is more or less the same in other Experiments (II-VII) although there are slight differences. For example, partial sample often require less time. Time unit in Table 3.9 is second. The difference between identification time and matching time is identification time includes time for data import, feature extraction and matching.

Table 3.9 Computational time in Experiment I [Unit: Second (s)]

Identifying 1 PM from 200 AM	2700 (45 minutes)
Data Import (per sample)	0.12
Point Extraction (per sample)	10.8
Matching 1 PM to 1 AM	2.53
Matching 1 PM to 200 AM	506 (8.43 minutes) (Duo Core 2.33 GHz)

Chen [34] reported that it takes 7 hours to retrieve one subject from 133 subjects (PC with a 2.99 GHz Pentium 4 processor) with 66% rank-1 accuracy, not including time for tooth contour extraction [34]. Although it is hard to compare the computational speed as different dataset and different hardware are used, the time listed in Table 3.9 is to give an intuitive feeling of the computational time of this work. As far, no benchmark dental databases are available. Table 3.9 is useful for the comparison of identification speed in Chapter 4 using the same computer system.

3.10 Summary

A point-based approach has been proposed for human 3D dental identification. The (PIDI) algorithm includes algorithms for feature extraction, feature description and correspondence. 60 PM samples and 200 ante mortem samples are used in this study. These 60 samples consist of the 7 complete genuine samples, in addition, 11 partial

genuine samples, 32 noisy genuine samples and 10 imposter samples taken from multi-ethnic Asian groups (Chinese, Indian and Malay) are also included.

The rank-1 identification accuracy of complete sample identification is 100%. The rank-1 identification accuracy of matching 11 partial PM sample is 72.7% and 78.1% for 32 noisy PM samples.

Overall accuracy of 50 genuine samples (complete, partial, and noisy) is also calculated and compared in experiments between manually segmented PM samples and auto-segmented PM samples. 94% rank-1 identification accuracy has been achieved in identification of 50 manually segmented PM samples and it decreases to 80% in identification of 50 auto-segmented PM samples. In contrast, only 86% and 64% rank-1 accuracy have been achieved respectively in the above two identifications by applying the existing iterative closet point (ICP) algorithm alone. In addition, the proposed approach is more robust to obtain the correct identities when AM sample size is increased. Furthermore, based on the sample size used in this study, a matching error threshold of 0.8 has been identified to differentiate genuine and imposter samples. Compared to the literatures, this work makes the following contributions:

1. Existing system based on 2D x-ray radiographs. Radiographs with poor contrast and exposure levels are unsuitable for identification, as it is difficult to extract tooth contours accurately with minimal geometric distortions. However, using 3D makes the identification more feasible even under large-scale decimation in noisy conditions. Samples with down to 10% of the scanned points and partial and noisy samples can be identified as demonstrated in the experiments.
2. 2D images are projections of 3D objects. Differences in the radiographs arising from different imaging angles are often significant to cause incorrect matching. The extracted tooth contour which is used as an anatomic dental feature is not an accurate description of 3D tooth profile. Once different imaging angles are applied, tooth contours of the same sample are different in profiles. In contrast, no distortion of the tooth profiles occurs as projection from 3D to 2D is not required. The problem arising from different imaging angles in 3D is what we call pose

variation problem. Results in Experiment VI and VII demonstrate the capability of the proposed method in dealing with pose variations.

3. Partial teeth identification is feasible in 3D without missing tooth detection or tooth classification.
4. More salient points are extracted using the proposed feature extraction algorithm than existing work [64, 65] thus reducing time demand for correspondence in Experiment V. The feature descriptor and the correspondence algorithm are tested to be more robust to pose variations compared to existing work [68] in Experiment VI and VII respectively.
5. The proposed approach takes 45 minutes (Duo Core CPUs with a clock speed of 2.33 GHz and 1.96GB RAM) to identify 1 PM subject from 200 subjects. Based on existing 2D approaches, it takes 7 hours (PC with a 2.99 GHz Pentium 4 processor) to identify 1 subject from 133 subjects [34].

The disadvantages of the proposed technique are acknowledged as well since presently available dental source for identification is primarily 2D radiograph. However, the reported techniques are for 3D dental image of the victim, which may not be available in every case. In addition, impressions would have to be made of the victim and 3D scanning would have to be performed, adding to the cost of the comparison technique in this study. But there is a trend towards capture and repository of 3D dental records, facilitated by availability and decreasing cost of rapid 3D scanners, such as 3Shape Dental System [78]. In a situation such as a mass disaster, where there may be hundreds of victims, it becomes feasible to also perform quick capture of dental impressions of remains. Other than text-recording of the victims' teeth status which is typically done during onsite investigation, it is more intuitive to archive and exam the 3D tooth shapes. The technique proposed could be adjunctively used with the traditional 2D dental identification method.

Chapter 4 Arch-based Matching and Identification and A Hierarchical Ranking Identification Scheme (HRIS)

Towards development of any automated scheme, the automated level, identification speed and identification accuracy are three factors should be considered and be balanced.

As the results showed in Chapter 3 that it takes 45 minutes on average to retrieve one subject from 200 subjects, to improve identification efficiency, an arch-based matching and identification approach is proposed and investigated. Dental arch extraction, arch feature description and arch matching techniques are described. A Radial Ray Algorithm (RRA) is proposed to extract dental arches. Then a Hierarchical Ranking Identification Scheme (HRIS), which combines the arch-based and point-based techniques, is proposed to speed up the retrieval of correct matches. Arch-based ranked matches serve as pre-filtered set for the more accurate point-based matching. Compared to the point-based technique alone, the HRIS is expected to improve the identification speed by excluding a large number of imposter AM samples at the arch matching level, while maintaining final identification accuracy.

In Chapter 4, only auto-segmented AM and PM are used in experiments for a fully automated hierarchical identification scheme development. Manual-segmented samples are not considered.

4.1 Introduction

The dental arch form study has been receiving increasing attention both in dental science [79-81] and engineering [62] for orthodontic applications. Dental arch is the curve formed by the cutting edges and masticating surfaces of the teeth as indicated in Figure 4.1(a). To correct malocclusions and assisting in shaping teeth and jaws, the dental arch provides important reference for dental brace (arch wire) (Figure 4.1(b)) design and customized production in orthodontic applications.

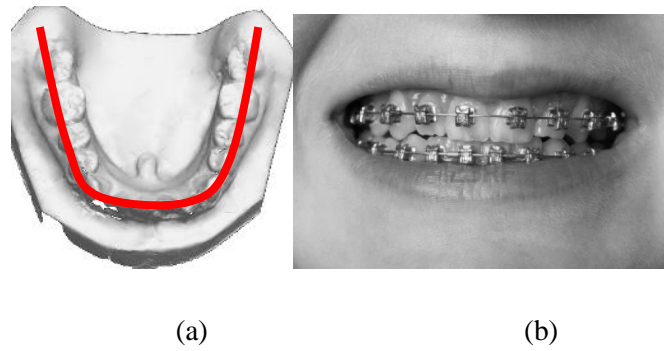


Figure 4.1 (a) Dental arch (b) Dental brace

In orthodontics, geometric morphology analyses of the dental arch form using mathematical functions such as thin-plate spline [81], beta function, natural cubic splines, polynomial equations, and Hermite cubic splines [80] under a normal occlusion assumption have been demonstrated in literatures. However, manual calibration and specification of feature points on every plaster model are required in the above mentioned studies, as illustrated in Figure 4.2, making mass extraction and fast retrieval of the dental arch infeasible. A comparison of the literature study on dental arch is presented in Table 4.1. However, most of the listed studies require full and healthy adult dentitions which include the second molars. Calibration (Figure 4.2 (a-b)) and manual specification of arch mark points (Figure 4.2 (c)) are also required. Although the arch shape is considered to be unique among individuals, the shape of dental arch is distorted in 2D radiographs, thus making it not suitable in 2D identification scheme in literatures [26, 53, 82].

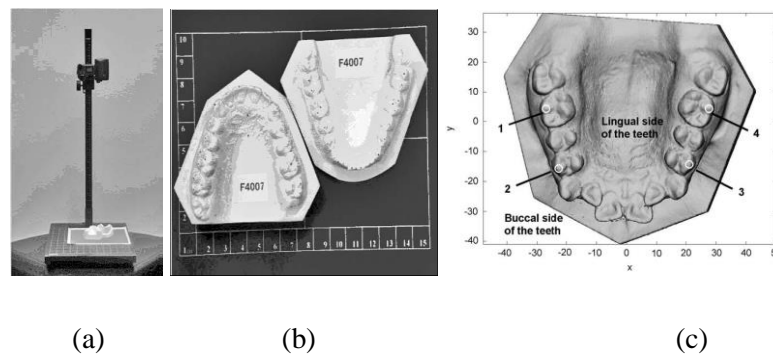


Figure 4.2 Calibration (a, b) and manual arch mark point specification (c) in literatures [62, 80]

Table 4.1 comparison of the literature study on dental arch

Year	# of Subjects	# of Arch Points	Assumptions & Requirements	Aims	Conclusions
1993 [83]	90	14	sound dentitions ideal natural occlusion manual arch mark point specification calibration	size and shape differences in sexual dimorphism	No difference in shape, male arches are slightly bigger
2004 [62]	34	Many Ridge points	manual 4 reference point specification calibration	3D tooth crown segmentation in dental casts	Algorithm is robust and accurate
2005 [81]	50	14	adult dentition ideal natural occlusion manual arch mark point specification calibration	Identification of the mean configuration of the clinical arch	No sexual dimorphism
2008 [80]	40	5 & 7	Normal occlusion manual arch mark point specification calibration	mathematical analysis of dental arch curvature	Fourth-order polynomial function may be used as a guide to fabricate customized arch wires

4.2 System Approach Overview

An overview of the Hierarchical Ranking Identification framework is shown in Figure 4.3. For every PM digitized dental model, it will also retrieve from an AM database which consists of 200 digitized dental models to find the closest match: dental arch matching first and then point matching to the top 10%, 20%, 50% ranks in arch-ranked List. The same pre-processing has been applied to new PM samples. They were first decimated and auto-segmented before arch detection and correspondence. There are two major steps in arch matching, as shown in Figure 4.3: the dental arch

extraction and correspondence. The details are elaborated in the following sections. A Radial Ray Algorithm (RRA) is proposed to automatically extract dental arch with the following features:

- It is fully automatic and fast;
- No need for manual specification of the occlusal plane and reference points;
- No need for pre-alignment and calibration of samples;
- Easy implementation;

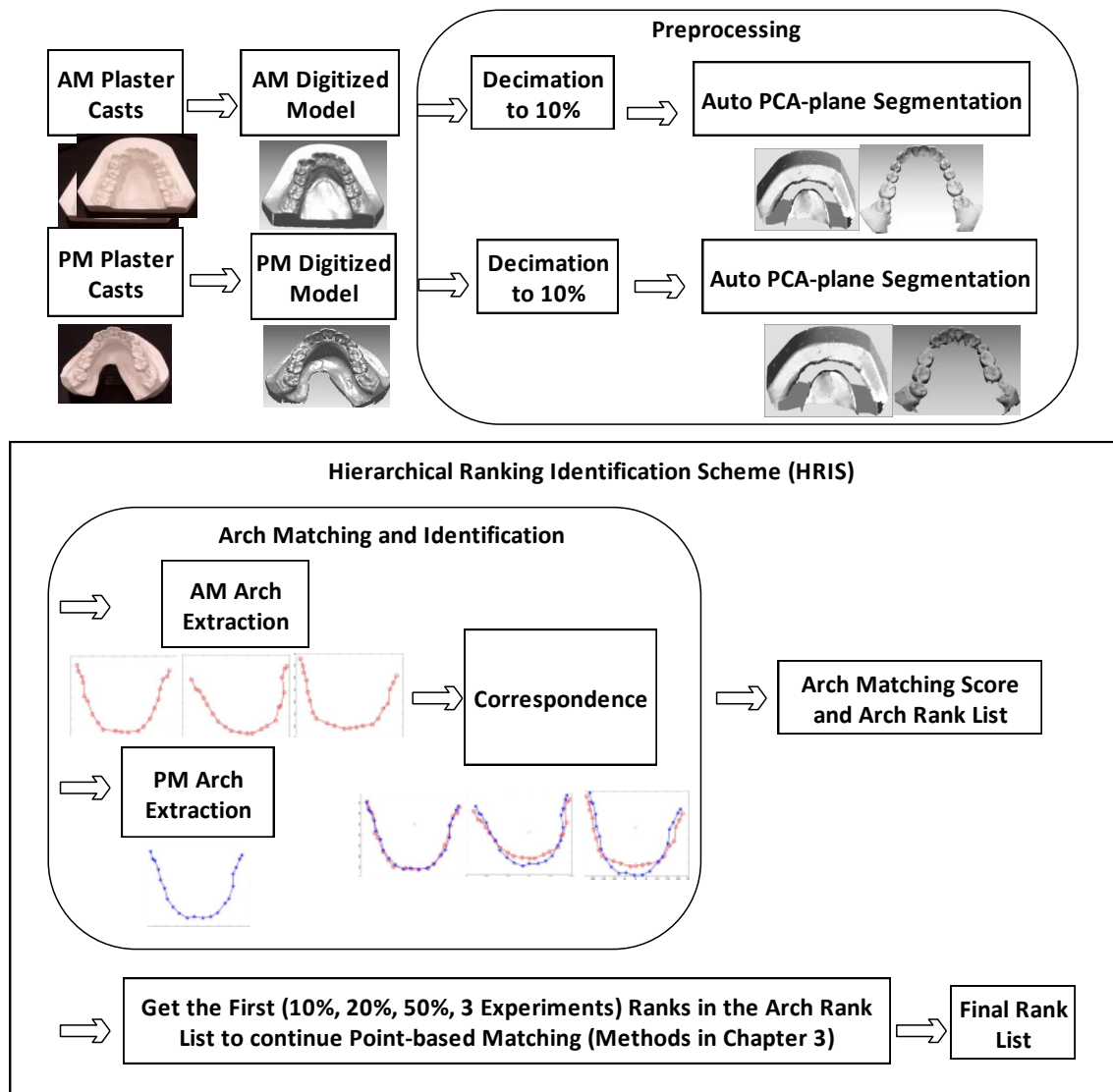


Figure 4.3 An overview of Arch-based Identification and A Hierarchical Ranking Identification Scheme

4.3 Algorithm Overview

The two main components of arch-based matching and identification framework are arch extraction and correspondence. Table 4.2 shows the main steps of the Radial Ray Algorithm (RRA) and the Hierarchical Ranking Identification Scheme (HRIS). The details are elaborated in the following sections.

Table 4.2 Main steps of Radial Ray Algorithm (RRA) and the Hierarchical Ranking Identification Scheme (HRIS)

Input: 81 PM surface model and 200 AM surface model

Output: 81 rank lists with each has 20, 40 or 100 ranks by using T10, T20, T50 respectively

Steps:

Radial Ray Algorithm (RRA)

- Arch Extraction
 - 1) PCA Alignment of principal axes x, y, z to the Euclidian coordinate X, Y, Z for both PM and AM samples (Figure4.5)
 - 2) Boundary points computation for both AM and PM samples (Figure4.7(a))
 - 3) Arch opening direction constraint (Figure4.7(b-c))
 - 4) Extract middle points of boundary points by RRA (Figure4.8)
- Arch Feature Description
 - 5) Starting from the middle extracted points, 10 points on each side are used to describe arch feature. So the total number of points 21 is specified (Figure4.10)
- Arch matching
 - 6) Flip effect constraint: flip extracted PM samples about Y axis (Figure4.11)
 - 7) Match both original and flipped PM arches to 200 AM arches by calculating rotation and translation using 21 points (Figure4.12)

The outcome is 81 arch rank lists with each having 200 ranks. (Table 4.3)

Hierarchical Ranking Identification Scheme (HRIS)

- 8) Get the first 10% (T10), 20% (T20) and 50% (T50) ranks in the arch rank lists to continue more detailed point-matching as demonstrated in Table 4.3 using methods in Table 3.1
- The outcome of using T10 threshold is 81 rank lists with each having 20 ranks
 The outcome of using T20 threshold is 81 rank lists with each having 40 ranks
 The outcome of using T50 threshold is 81 rank lists with each having 100 ranks

4.4 Data Preparation

AM samples

The same 200 ante-mortem samples are used, comprising complete mandibular teeth that have been decimated and auto-segmented.

PM samples

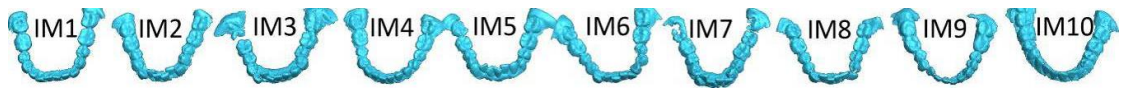
The PM samples consist of 81 mandibular teeth as shown in Figure 4.4. The samples have been pre-processed and divided into five groups as shown in Figure 4.4 (a-e) respectively.



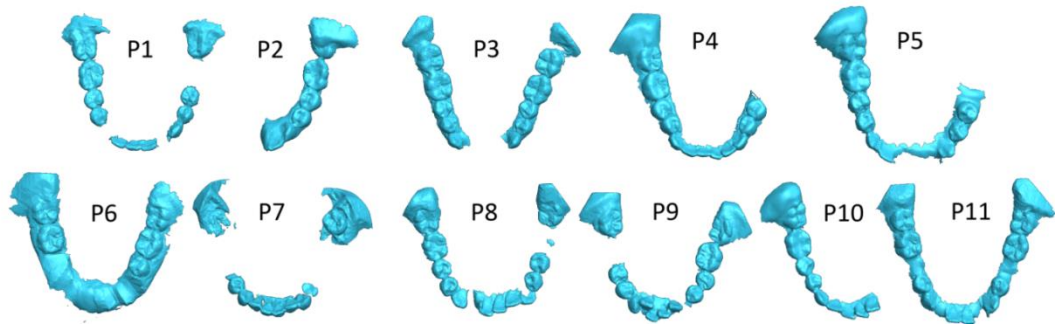
- (a) the 11 simulated PM samples (S1-S11) taken exactly from AM samples, a subset of AM samples which have the same orientation, same number of points and the same mesh topology with their AM samples. This group of samples is to test the feasibility of dental arch identification and to show inner-personal difference of dental arches.



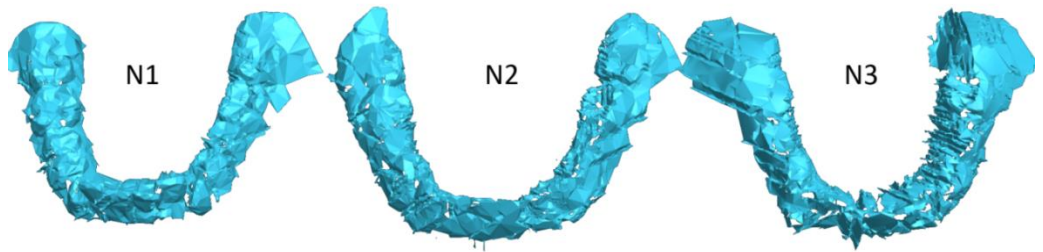
- (b) the same 7 complete samples used in Chapter 3 with addition of four new complete samples (C8-C11).



- (c) the same 10 imposter samples (IM1-IM10) in Chapter 3.



(d) the same 11 partial samples (P1-P11) used in Chapter 3.



(e) 3 of 38 noisy samples (N1-N3) with distorted individual tooth shapes that are not easily recognized even visually.

Figure 4.4 Sample illustration

4.5 Dental Arch Extraction

As a dental sample could have any initial orientation, its orientation should be properly aligned with that of matching sample. In Chapter 3, the alignment is realized by matching pose invariant feature points. In this chapter, Principal Component Analysis (PCA) alignment is used to achieve fast alignment before arch extraction. The following steps are implemented for dental arch extraction.

PCA Alignment

Compute the rotation matrix using PCA as shown in Figure 4.5 and align principal axis x , y , z to the respective Euclidian coordinate X , Y , Z . Considering only rotation around the third principal axis, which is the most possible rotation during data preparation as illustrated in Figure 3.15, there are two possible results after PCA alignment as shown in Figure 4.6 (a-b). The x and y rotations are so small and are usually neglected. Principal axes do not have positive or negative directional property. To make it more robust, if x and y rotations are also considered, there are other two

possibilities as shown in Figure 4.6 (c-d). The blue models with their bounding boxes show the different initial orientations and the grey models show results after PCA alignment. The four possibilities are:

- dental arch opening pointing towards positive Y and teeth surface pointing towards positive Z in Figure 4.6 (a)
- dental arch opening pointing towards negative Y and teeth surface pointing towards positive Z in Figure 4.6 (b);
- dental arch opening pointing towards positive Y and teeth surface pointing towards negative Z in Figure 4.6 (c)
- dental arch opening pointing towards negative Y and teeth surface pointing towards negative Z in Figure 4.6 (d)

It is interesting to find that the first principal axis is always aligned with x axis which is perpendicular to the Sagittal plane; second principal axis y is perpendicular to the Coronal plane; and the third principal axis z is perpendicular to the Transverse plane. The three planes are defined for human body anatomically as shown in Figure 4.7. As there are four possible orientations after PCA alignment, two constraints (I and II) will be added in order to achieve correct and consistent alignment to the Euclidian coordinates X, Y, Z before arch extraction.

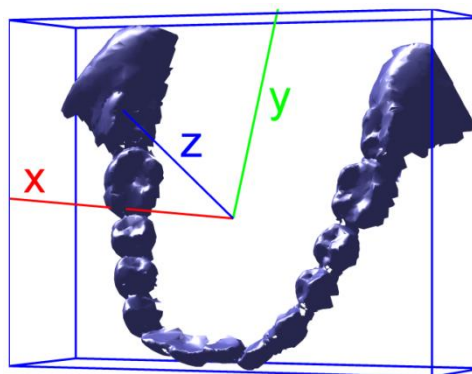


Figure 4.5 Principal axes

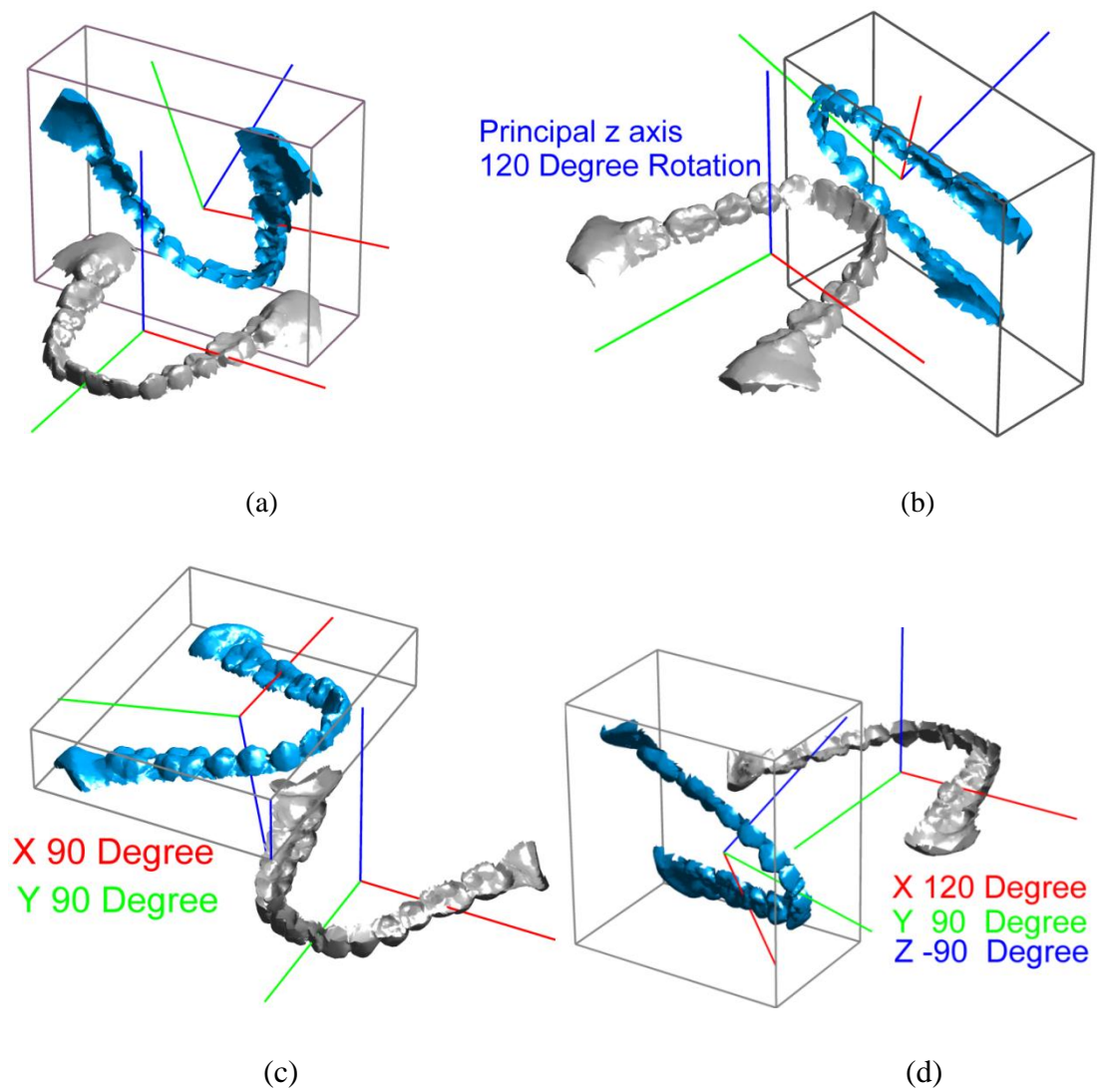


Figure 4.6 Four possible results after PCA alignment

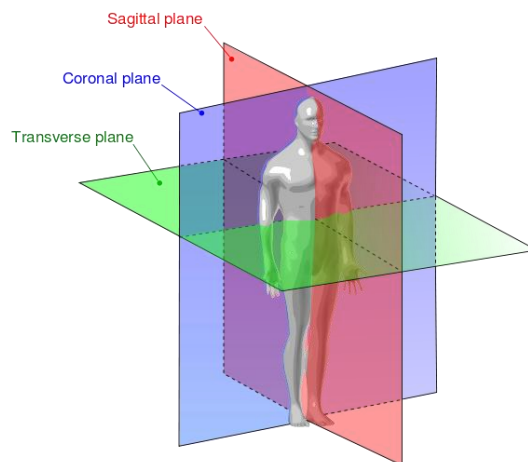


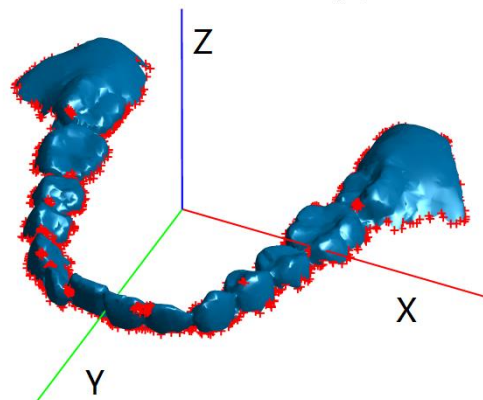
Figure 4.7 Anatomical planes of human body

Constraint 1: arch opening direction constraint

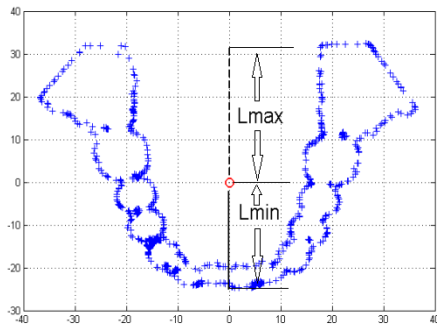
As shown in Figure 4.6 (a-d), the dental arch opening direction is either positive Y or negative Y. To get correct and consistent alignment, the following constraint is applied to get positive Y alignment.

- 1) Compute the boundary points of the mesh model and project them onto the x-y plane as shown in Figure 4.8 (a)
- 2) The centroid is the origin of the projected boundary points as shown in Figure 4.8 (b-c) and the centroid is found to be close to the anterior teeth. Let L_{max} denotes the length from the centroid to maximum Y value of boundary points (dash line)
 L_{min} denotes the length from the centroid to minimum Y value of boundary points (solid line)
- 3) If $L_{max} < L_{min}$ (L_{max} is shorter than L_{min}) as shown in Figure 4.8(c), flip boundary points about X axis on X-Y plane. This may create a flipped dental arch about Y axis. This flipped effect will be discussed later. It will be eliminated by adding another constraint (constraint 2).

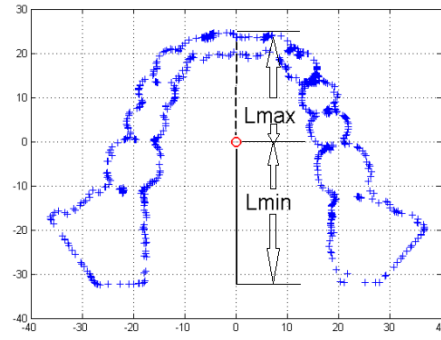
Aligned model with its boundary points



(a)



(b)



(c)

Figure 4.8 Boundary points on X-Y plane

Arch Extraction

The arch extraction method is based on the middle points (black circles in Figure 4.8) extraction of boundary points (blue '+' marks in Figure 4.9). The following steps are implemented.

- 1) Specify point B according to centroid A as shown in Figure 4.9.

L_{AB} is defined as the length between point B and the centroid A. L_{AB} is 70% of the total length L ($L_{max} + L_{min}$ in Figure 4.8(b)) of projected points along Y axis. Point B should have a higher Y value than Y maximum of boundary points to guarantee that one radial ray (black lines emitted from B) only intersect with either left jaw teeth boundary or right jaw teeth boundary. The middle points will be placed in between the longest intersection ray and the shortest ray in each sub-divided area as shown in Figure 4.9. Also B should not have a much higher Y value than Y maximum of boundary points since that will not yield descriptive enough arch shape. We observed that the use of 70% is the most suitable value for all the samples.

- 2) Start from positive X axis, divide the space into 50 sub-areas from 0 to 180 degree

The number 50 is also determined from observations. As reviewed in Table 4.1, literatures used 5, 7, 14 points to interpolate a curve to describe the arch shape. Figure 4.10 upper row shows that if we use the same number of points,

the shapes are not smooth enough to describe real arch shapes. For easy implementation and accurate arch description, no interpolation will be implemented as enough arch points could be computed to describe exact arch shape. It is true that more points will give more details of arch shape but it should not be over described. As the lower row middle and right figures show that when dividing 55 and 60 sub-areas, over described effect will appear. In each sub-area, the middle points will be placed in between the longest intersection ray and the shortest ray in each sub-divided area as shown in Figure 4.10. The middle ray length is calculated as the average length of these two.

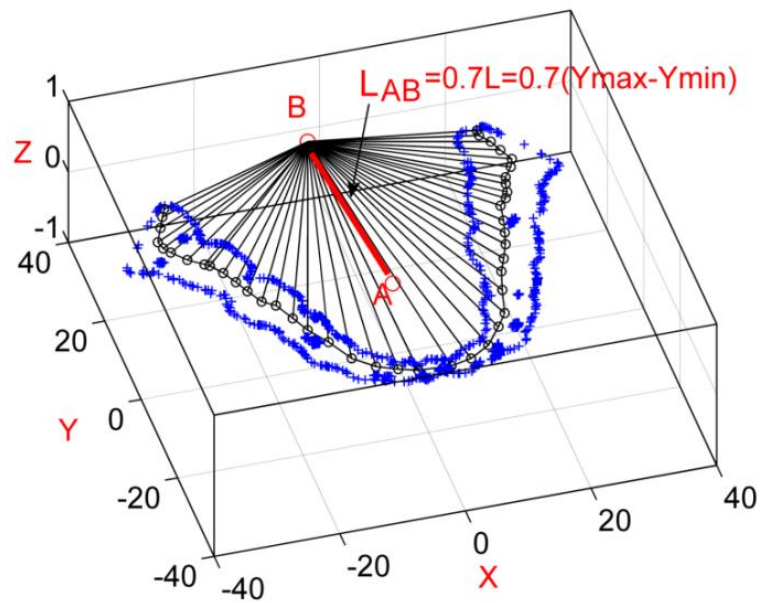


Figure 4.9 Dental arch extraction

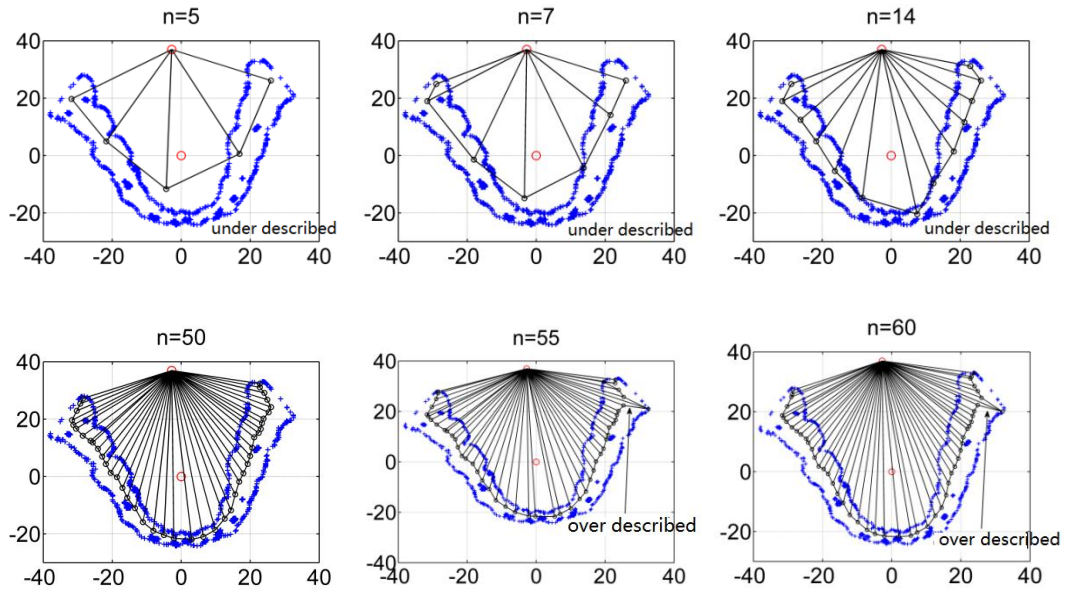


Figure 4.10 Under described (upper row) and over described (lower middle and right) dental arches

4.5 Arch Feature Description

As stated in previous arch extraction section, no interpolation is implemented for extracted points since enough arch points could be computed to describe exact arch shape. When fourth-order polynomial function [80] is used to interpolate the extract points, over fitting often occurs as more points (40+ points) are used to describe the dental arch in this work compared to literatures (14 points).

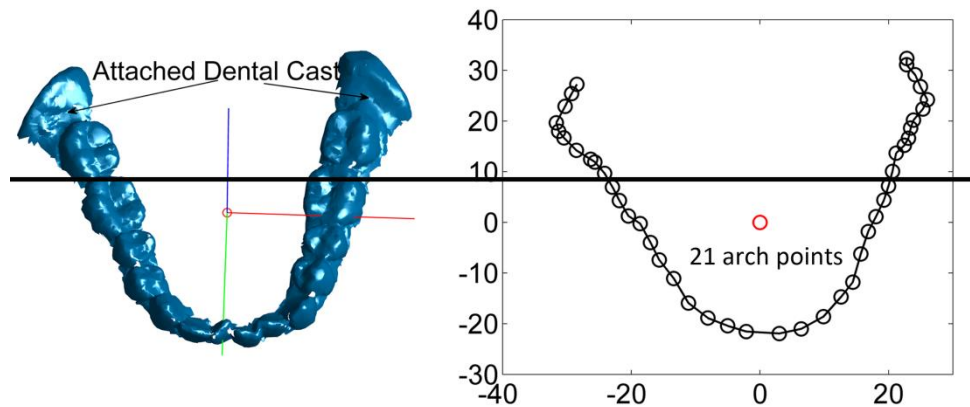


Figure 4.11 Extracted anterior dentition arch

As can be seen in Figure 4.11, parts of dental cast in the auto-segmented sample can be seen attached to the pre-processed sample. Starting from the middle

extracted points, 10 points on each side are used during matching. The suitable number of points specified is 21 from observations. As shown in Figure 4.11, the attached dental cast should be excluded, but there is no obvious boundary to separate the last molar to the attached casts. The 21 specified points include anterior teeth (incisors and canines), premolars and the first molar. All the arch points below the black line are used in identification. From samples tested, 21 points have been found to generally cover most of the anterior teeth while eliminating the attached dental cast at the posterior teeth, such as the one shown in Figure 4.11. There will be variation from samples to samples, but the 21 points will provide adequate allowance to ensure the extracted anterior teeth having the attached dental cast removed. Kieser et al. [84] indicated that anterior dentition are in fact unique. All anterior teeth are included.

4.6 Dental Arch Matching

Constraint 2: flip effect constraint

As shown in Figure 4.6, there are four possible results after PCA alignment. By adding Constraint 1- arch opening direction constraint, two possibilities are excluded and leaving with either the case shown in Figure 4.6(a) or Figure 4.6(c). However, the teeth may also flip about Y axis (left jaw teeth and right jaw teeth flip with each other) after PCA alignment. And as mentioned in Constraint 1 step 3) that if $L_{max} < L_{min}$ as shown in Figure 4.8(c), boundary points are mirrored about X axis on X-Y plane which also create a flipped dental arch about Y axis. To offset the flip effect, the extracted points are matched first, and then the flipped points are matched again. The points with smaller matching error will be taken as the correct match.

The following two steps are implemented to match the dental arch.

- 1) Calculate AM and PM dental arches and flip the PM dental arch as Figure 4.12 shows.

AM arch---red line with circle 'o' marker

PM arch---blue line with star '*' maker

Flipped PM arch--- green line with addition '+' maker

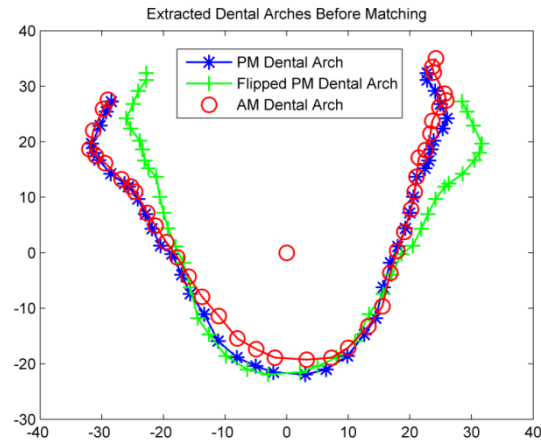


Figure 4.12 PM dental arch, flipped PM dental arch and AM dental Arch before matching

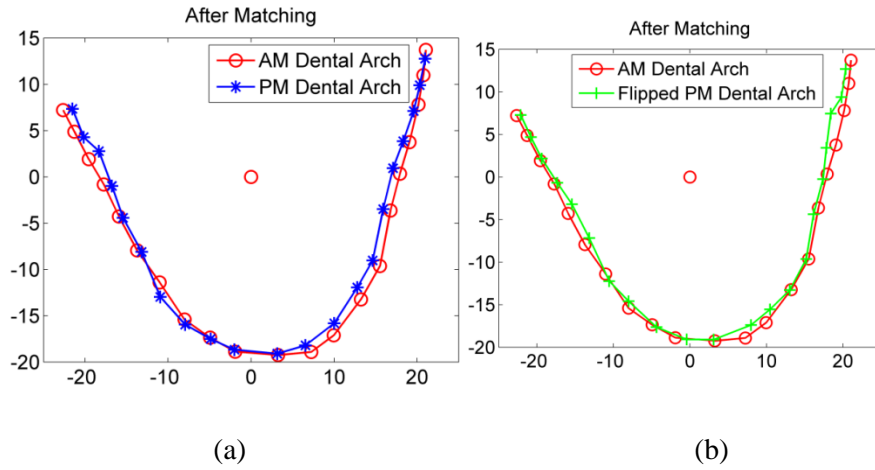


Figure 4.13 (a) AM and PM arch matching (b) AM and flipped PM arch matching

- 2) Calculate the rotation matrix using 21 points, align the extracted dental arch then calculate the point-to-point Euclidian distance. The mean distance is the matching error. Figure 4.14(a) shows the matching error (0.9109) between AM and PM arches and Figure 4.14(b) shows the matching error (0.9459) of AM and flipped PM arches. Those two errors do not have much difference since the jaw teeth has good symmetrical structure. Those two errors do not have much difference (< 1.0 error value as found for genuine matching from samples studied) as the jaw teeth in this case has good symmetrical structure. Other samples' matching errors

may have much larger difference. The smaller error (0.9109) is used to rank dental arch matching results.

- 3) Repeat the above process until all 200 AM samples have been matched and sort the matching errors in ascending order. The outcome is a ranked list which contains 200 ranks as shown in Table 4.3. Figure 4.14 shows some examples of the matching error difference when matching genuine sample and imposter samples. As it is shown in Figure 4.14, the genuine matching usually has smaller error.

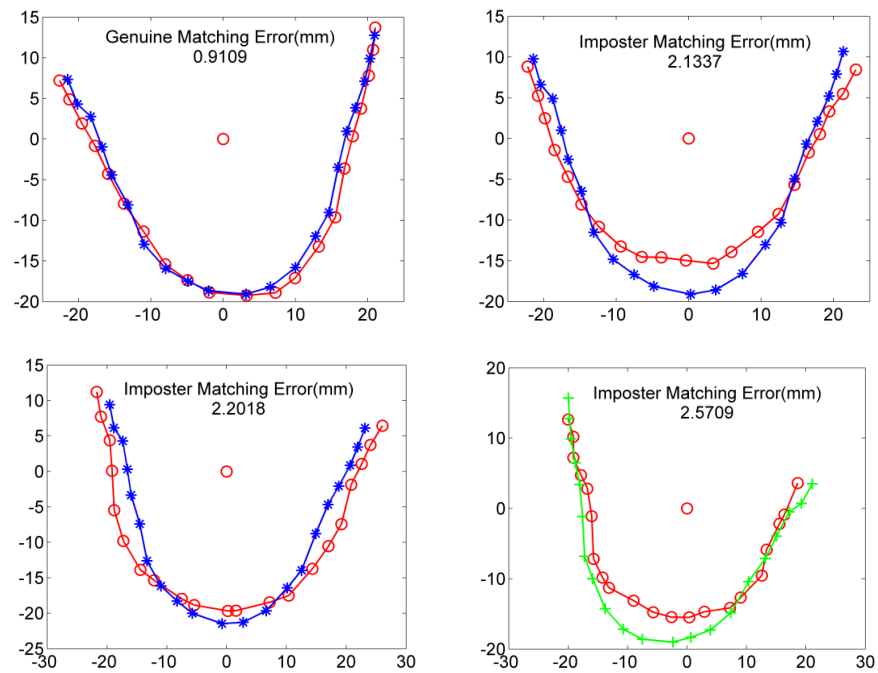


Figure 4.14 Difference of genuine arch matching error (top left) and imposter arch matching error (the other three)

4.7 Demonstration of the Hierarchical Ranking Identification Scheme

Table 4.3 1-200 arch rank list

Arch	1	...	20(<u>T10</u>)	...	40(<u>T20</u>)	...	100(<u>T50</u>)	...	200
Rank									
AM	AM30	...	AM28	...	AM72	...	AM66	...	AM156
Index									

The outcome is a ranked list which contains 200 ranks with matching error in ascending order as shown in Table 4.3. The AM sample with smallest matching error is considered to be the correct match for a PM sample and will be ranked top as rank-1. For example, for the ranked list shown in Table 4.3, most likely this PM sample has the same identity with AM30. However,

- 1) dental arch is a two dimensional feature extracted from 3D samples, it may not be accurate enough;
- 2) Also due to the variation in the data preparation procedures, PM arch and AM arch from the same person may not be exactly the same.

As it is believed that 2D arch feature matching has certain level of accuracy but is not as accurate as the point-based 3D matching. It saves time by choosing top ranks in the arch-ranked list for point-based matching instead of the entire 200 AM samples. For this, a proper threshold is needed. In this study, three thresholds are chosen: 10% ranks ($T_{10}=200*10\%=20$), 20% ranks ($T_{20}=200*20\%=40$), and 50% ranks ($T_{50}=200*50\%=100$). These three thresholds are tested for genuine PM samples in Figure 4.4 (b, d, e). For example, if the unidentified sample is PM1, as it is shown in Table 4.4, the top row of the arch matching outcome, **Arch Rank** indicates 1-200 ranks with the smallest error rank the top; **AM Index** indicates the corresponding AM sample index at each rank. Next, if threshold T10 is defined, only the first 20 ranks will be matched against in a detailed level by applying the point-based approach mentioned in Chapter 3. This will exclude 90% of the AM samples, thus saving 90% of time for point extraction and matching. The same apply for threshold T20 and T50.

4.8 Experiments and Discussion

Experiment I Feasibility of Dental Arch Identification

This experiment aims to show the feasibility of using dental arch as an identification feature. Samples in Figure 4.4(a) which have the same orientation and same mesh topology with their corresponding AM samples are tested in Experiment I. Through matching the 11 completed simulated PM samples (which is an exact subset of the AM samples), inner-personal difference of arch feature are investigated. Table 4.4 and Figure 4.15 show the matching results. Since the PM samples are selected samples of the AM samples, it excludes errors which could happen during data preparation, such

as different initial orientations, different mesh topology and different segmentation results due to different preparations at different times. Without the aforementioned errors, the results manifest that arch feature is a significantly discriminative feature with all simulated samples correctly identified at Rank 1. There is no need to carry out next level of detailed matching. In Figure 4.15, when comparing errors of rank 1 and rank 2 to the rest of the gradually increasing matching errors, it shows that genuine samples with matching errors close to 0, are highly differentiable from the rest of the imposter samples whose averaged matching errors hit above 1.

Table 4.4 Arch identification of 11 simulated PM complete samples to 200 AM samples

PM	1	2	3	4	5	6	7	8	9	10	11
Arch	1	1	1	1	1	1	1	1	1	1	1
Rank											

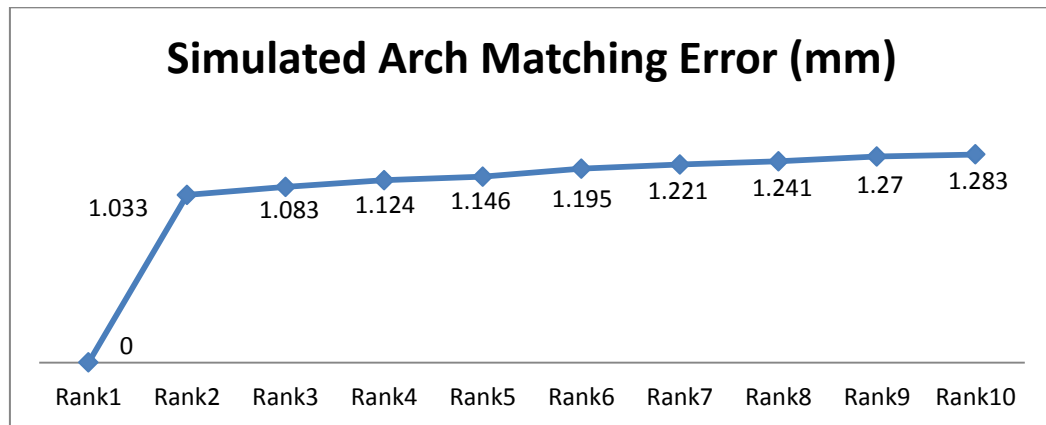


Figure 4.15 Simulated arch averaged matching errors at the first 10 ranks

Experiment II Complete Samples Identification Using HRIS

As mentioned in Experiment I, there are inevitable differences during data preparation that have to be considered, such as different initial orientations, different mesh topology and different segmentations. The difference has been illustrated in Figure 3.2(f)-differences of PM and AM samples. As the number of points and mesh topology is different, the samples prepared by PCA segmentation and PCA alignment are also different. Figure 4.16 shows the differences. The AM and PM samples belonging to the same person have not been perfectly aligned with each other after

PCA alignment due to the above mentioned difference. Thus the arch matching has relatively larger error (1.1263) as shown in Figure 4.16(b-c) compared to that in Figure 4.13(a) whose PM and AM samples are better aligned. This can be seen in only three PM samples in Table 4.5 being identified at rank 1 by applying arch matching alone.

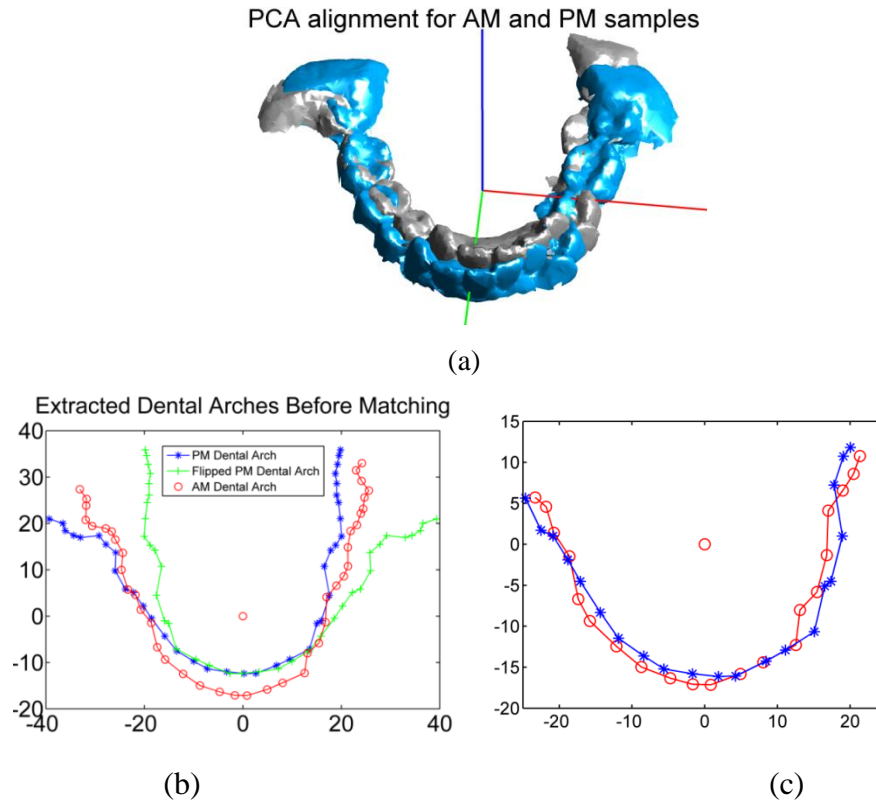


Figure 4.16 An example of samples are not identified at rank-1 after arch matching (a) PCA alignment of AM and PM samples (b) extracted arches before matching (c) arches after matching

Table 4.5 shows the identification results taking the errors into consideration. The Arch rank indicates matching results by matching dental arch alone. The following three Final rank rows show the final results by applying the proposed Hierarchical Ranking Identification scheme. The last column indicates final identification accuracy at each threshold. As it is shown in Table 4.5, only three samples are successfully identified at rank-1 after arch matching, but at rank 31, all 11 PM samples are identified. Therefore, we could indicate that top 15.5% ranked list (31/200) achieves 100% accuracy at arch matching level. Top 1% arch matching

accuracy is 54.5% (6/11); Top 2% arch matching accuracy is 63.6% (7/11); top 8% arch matching accuracy is 81.8% and top 10% arch matching accuracy is 90.9%.

In next level of point matching, top 10% accuracy also achieves 90.9%. Since threshold is set to T10, only the first 20 AM samples will be matched against. The arch rank of PM11 is 31, so its corresponding AM sample is not included in the point matching level. Thus, it could not be successfully identified at top 10% accuracy with threshold T10. However, the top 20% accuracy achieves 100% and top 50% accuracy also achieves 100%. This indicates that the complete dental sample has highly discriminative identification characteristics.

Table 4.5 Arch identification of 11 simulated PM complete samples to 200 AM samples

Complete PM	1	2	3	4	5	6	7	8	9	10	11	
Arch rank	1	2	15	2	2	20	3	1	7	1	31	
T10	1	1	1	1	1	1	1	1	1	1	NA	90.9% accuracy
T20	1	1	1	1	1	1	1	1	1	1	1	100% accuracy
T50	1	1	1	1	1	1	1	1	1	1	1	100% accuracy

To compare with the arch matching errors of the simulated PM samples in Figure 4.15, the average arch matching errors of PM sample PM1 PM8 and PM11 are used since other PM samples are not successfully identified at rank 1. The arch matching error is illustrated as the blue line with diamond markers as shown in Figure 4.17. The other three lines indicate the averaged final point-matching errors of 11 PM samples at different thresholds. Figure 4.17 shows errors at the first 10 ranks.

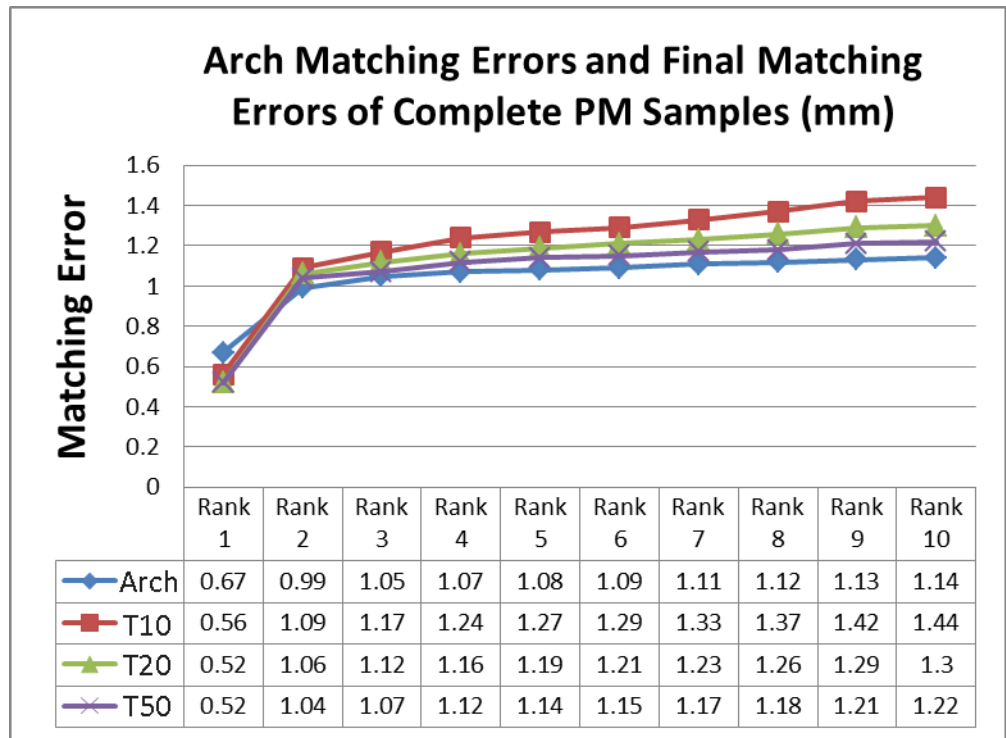


Figure 4.17 Arch matching errors and final matching errors of complete PM samples

Firstly, if we compare the blue lines in Figure 4.15 and Figure 4.17, rank 1 and rank 2 difference is decreased as data preparation difference is excluded in Experiment I, which is the ideal case. However, if data preparation difference is considered, the rank1-rank2 difference is still much bigger than that of any other two consecutive ranks in Experiment II as shown in Figure 4.17.

Secondly, the other three final matching error lines for T10, T20 and T50 thresholds follow the same trend in that rank1-rank2 difference is much bigger than that of any other two consecutive ranks. And the results in Figure 4.17 are also consistent with what have been discovered in Chapter 3 with most imposter matching error larger than 0.8 in Figure 3.8. The rank2 final matching error is all above 1 in Figure 4.17. In addition, at a particular rank, the error decreases as more AM samples included in the matching which is also consistent with what has been compared between Table 3.2 and Table 3.3. This indicates that when more AM samples are used in identification, more likely there are more similar samples to that particular PM sample. Threshold 0.8 has been found for the 200 AM samples. More AM samples could be used for future validation.

To compare with Chapter 3, the same 7 complete samples (1-7 samples in Table 4.5) achieved 100% rank-1 identification accuracy with a more than 6 times improved identification speed using HRIS.

Experiment III Imposter Sample Identification Using HRIS

Samples used in imposter sample identification are shown in Figure 4.4(c) which is the same set of samples as shown in Figure 3.2(b). These chosen PM samples do not have corresponding AM samples in the AM database.

As what has been investigated in Experiment II in Chapter 3, a threshold of final matching error of 0.8 appears to be suitable to distinguish the genuine PM sample identification and imposter PM sample identification, based on the 200 AM samples and the tested imposter PM samples used. In Chapter 4, imposter sample identification experiment is design to investigate the arch threshold for the two groups and as well verify the matching error threshold. The results are shown in Figure 4.18.

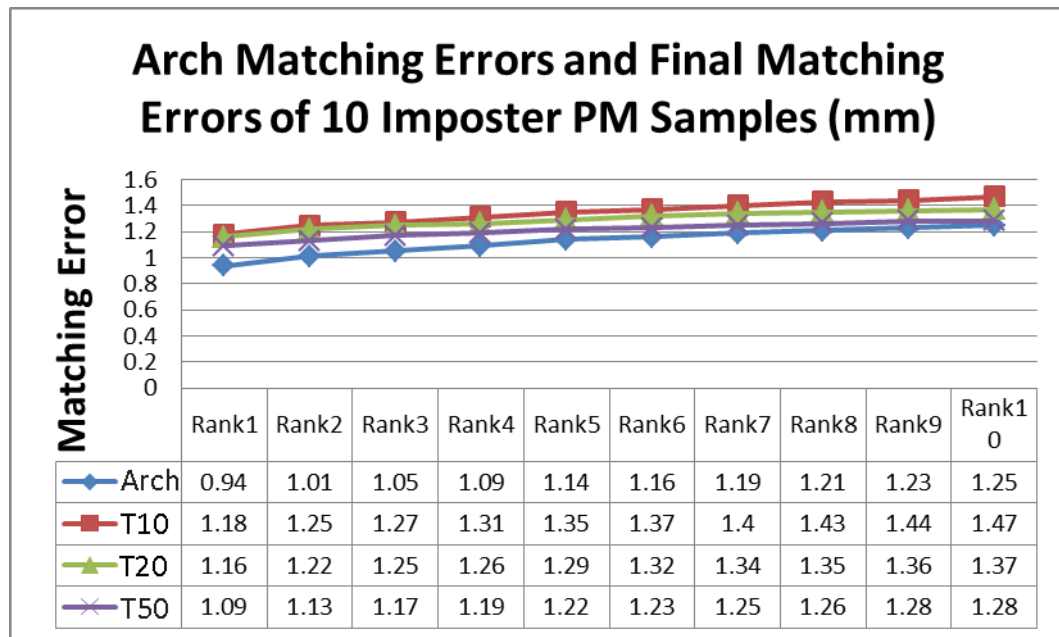


Figure 4.18 Arch matching errors and final matching errors of 10 imposter PM samples

Firstly, comparing Figure 4.17 (genuine) and Figure 4.18 (imposter), the most obvious difference is the difference between rank-1 and rank-2 errors. All of the four error lines are gradually increasing from rank1 to rank10. There is no obvious

difference between rank1-rank2 error and any other two consecutive ranks in imposter identification.

Secondly, the rank1 errors are all below 0.8 in Figure 4.17 in contrast with those above 0.8 in Figure 4.18. In addition, at a particular rank, the error decreases as more AM samples are included in the matching. When more AM samples are used in identification, more likely there are more similar samples to that particular PM sample. Threshold 0.8 has been found for using 200 AM samples. More AM samples could be used for future validation.

Experiment IV Partial Sample Identification Using HRIS

Samples used in partial sample identification are shown in Figure 4.4(d). These samples are designed to the ability of the HRIS to identify partial samples. The results are shown in Table 4.6. The last column indicates the final identification accuracy at each threshold.

The top 10% ranked list achieved is only 27.3% accuracy; top 20% ranked list achieved 45.5% accuracy and top 50% ranked list achieved 72.7% accuracy. This indicates that with half of the AM database is filtered after arch matching, 72.7% accuracy can be obtained. The rank-1 identification accuracy of matching 11 partial PM sample is 54.5% when half of the AM database is filtered.

It is observed that partial samples that have higher arch rank (P1, P8, P11) often have less number of missing teeth and better left-jaw-and-right-jaw symmetry than those having lower ranks (P2, P3, P4, P5, P6, P7, P9, P10). Figure 4.19 shows the dental arches of partial samples P1, P8, P11 which are identified to be within the top 10%. Even with some teeth missing, extracted dental arch looks crooked in Figure 4.19 (a); however, relatively high rank is still obtained if a sample has less number of missing teeth and better left-jaw-and-right-jaw symmetry.

Table 4.6 Identification of 11 PM partial samples from 200 AM samples (HRIS)

Partial PM	P1	P2	P3	P4	P5	P6	P7	P8	P9	P10	P11	
Arch rank	7	74	34	34	124	96	124	1	94	152	12	
T10	2	NA	NA	NA	NA	NA	NA	1	NA	NA	1	27.3%
T20	2	NA	1	1	NA	NA	NA	1	NA	NA	1	45.5%
T50	3	1	1	1	NA	3	NA	1	1	NA	1	72.7%

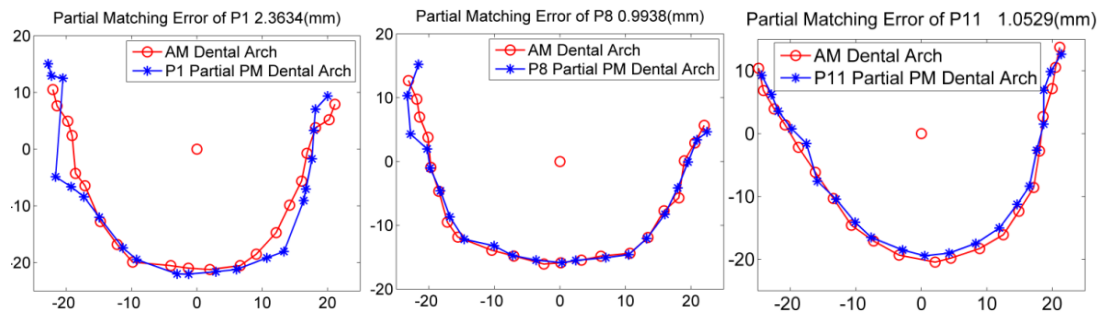


Figure 4.19 Dental arches of top 10% identified partial samples

Experiment V Noisy Sample Identification Using HRIS

The number of noisy samples has been increased from 32 to 38. A few examples of noisy samples are shown both in Figure 3.2 (d) and Figure 4.4 (e). Experiment IV in Chapter 3 and this experiment show that when a single tooth shape in the jaw has been severely distorted, it is still identifiable as long as the sample keeps its arch curve. Table 4.7 and Table 4.8 show the results of noisy sample identification using HRIS. ‘NA’ denotes rank ‘not available’ at certain threshold.

The top 10% ranked list achieves 39.5% accuracy; top 20% ranked list achieves 55.3% accuracy and top 50% ranked list achieves 73.7% accuracy. This indicates that if half of the AM database is filtered after arch matching, 73.7% accuracy can be obtained.

To compare with noisy sample identification accuracy in Chapter 3, the rank-1 identification accuracy of matching 32 noisy PM samples (The first 32 samples in Table 4.7 and Table 4.8) is 59.4%.

Table 4.7 Identification of noisy samples (1-19) from 200 AM samples (HRIS)

Noisy PM	1	2	3	4	5	6	7	8	9	10	11	12	13	14	15	16	17	18	19
Arch rank	3	9	1	7	2	8	119	26	53	2	129	30	7	107	166	142	162	3	1
T10	1	1	1	1	1	1	NA	NA	NA	1	NA	NA	1	NA	NA	NA	NA	1	2
T20	1	1	1	1	1	1	NA	1	NA	1	NA	1	1	NA	NA	NA	NA	1	2
T20	1	1	1	1	1	1	NA	1	NA	1	NA	1	1	NA	NA	NA	NA	1	2

Table 4.8 Identification of noisy samples (20-38) from 200 AM samples (HRIS)

Noisy	2	2	2	2	2	2	26	2	2	2	3	3	3	3	3	3	3	3	3
PM	0	1	2	3	4	5		7	8	9	0	1	2	3	4	5	6	7	8
Arch	3	1	3	1	9	2	115	7	3	1	1	7	8	7	2	1	1	4	7
rank		3	4	0		7		7	4	2	9	2	2	6	2	0	4	4	2
				2						8						2			
T10	1	1	N	N	3	N	NA	N	N	N	1	N	N	N	N	1	N	N	N
			A	A		A		A	A	A	6	A	A	A	A		A	A	A
T20	1	1	1	N	3	1	NA	N	3	N	3	N	N	N	1	1	N	N	N
				A				A	7	A	2	A	A	A			A	A	A
T50	1	1	1	N	6	1	NA	1	9	N	8	1	1	7	1	2	N	1	1
				A					4	A	0			6			A		

The Cumulative Match Characteristic (CMC) Curve

Overall accuracy of 60 genuine PM samples is also calculated. As what has been evaluated after Experiment IV in Chapter 3, CMC curve (red line with triangle marker) is shown in Figure 4.20. There are 60 genuine samples which consist of 11 complete samples in Figure 4.4 (b), 11 partial samples in Figure 4.4 (d) and 38 noisy samples in Figure 4.4 (e). For each threshold, CMC curve is shown in Figure 4.20.

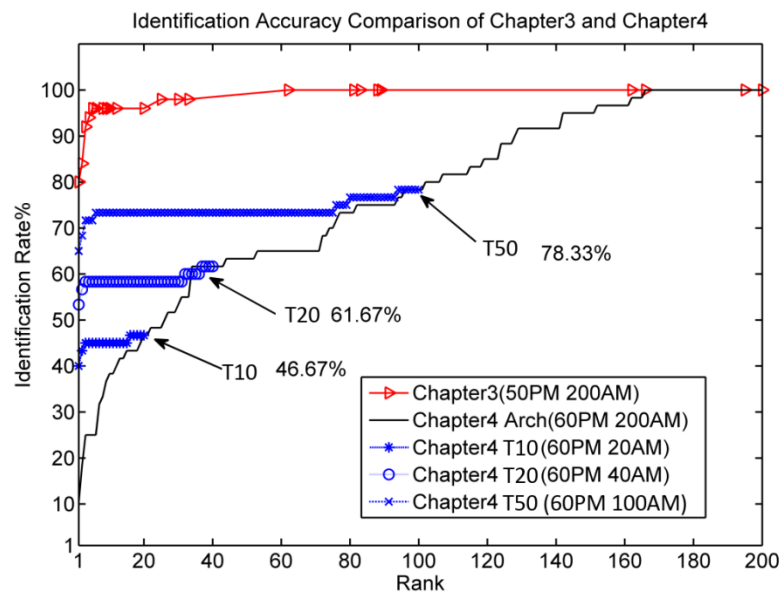


Figure 4.20 Identification accuracy comparison of total samples in Chapter 3 and Chapter 4

The following interpretations of Figure 4.20 are stated. If all types of genuine samples (complete, partial, and noisy) are considered, by using HRIS,

- 46.67% identification accuracy achieves when 90% AM data could be excluded;
- 61.67% identification accuracy achieves when 80% AM data could be excluded;
- 78.33% identification accuracy achieves when 50% AM data could be excluded.

For matching of complete samples (Figure 3.2 (a) lower row and Figure 4.4 (a)) are compared, as it is shown in Figure 4.21 that

- 90.9% identification accuracy achieved when using top 10% of arch-ranked AM data;
- 100% identification accuracy achieved when using top 20% of arch-ranked AM data;
- 100% identification accuracy achieved when using top 50% of arch-ranked AM data.

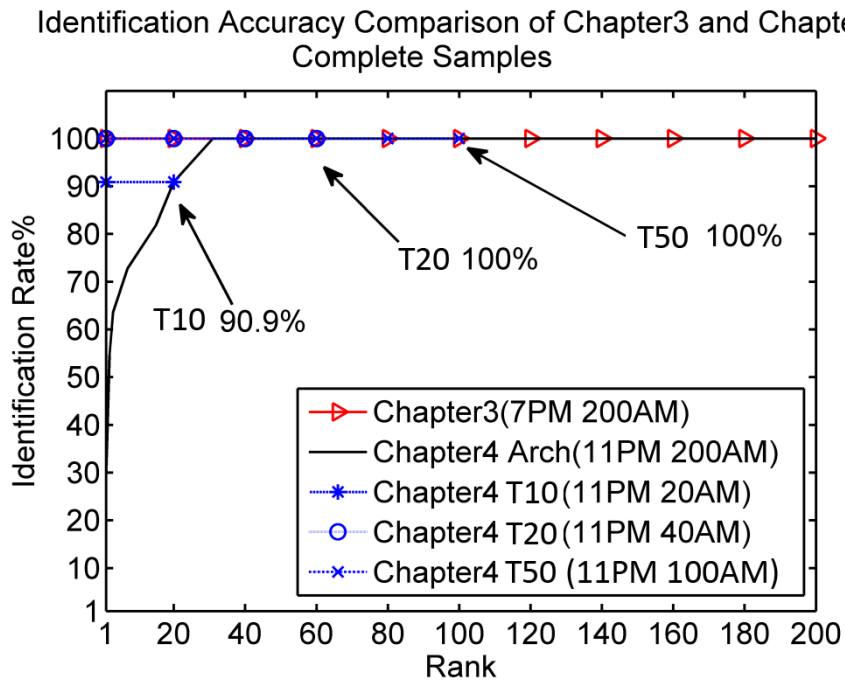


Figure 4.21 Identification accuracy comparison of only complete samples in Chapter 3 and Chapter 4

4.9 Computational Time of HRIS

The same set of complete samples in is used as those in Chapter 3. The number of complete sample has been increased from 7 to 11 as shown in Figure 4.4(b). Four new

samples PM8, PM9, PM10, and PM11 have been added. Table 4.7 is used to compare computational speed in Table 3.9 regarding identification speed for a single PM subject.

As mention before, although it is hard to compare the computational speed with that in literature work as different dataset and different hardware are used, now it is feasible to compare identification speed using the same dataset and the same hardware but different identification schemes.

As what is shown in Table 4.9 for computational time comparison in identification of complete samples between Chapter 3 and Chapter 4, it only needs about 7 minutes to achieve 90% identification accuracy while reducing more than 6 times (45/7.1) of identification speed. 100% accuracy could be achieved when eliminating 80% of the imposter samples, thus reducing about 4 times (45/11.4) of identification speed.

Comparisons of identification speed of partial and noisy samples are more or less the same except identification accuracy at each threshold decreases. Partial and noisy samples only achieve about 72.7% and 73.7% accuracy respectively when eliminating 50% of imposter samples as shown in Table 4.4-4.6.

Table 4.9 Computational time comparison in identification of complete samples [Unit: Second (s)]

Identifying 1 PM from 200 AM T10 (Accuracy 90.9%)	426.38 (7.1 minutes)
Identifying 1 PM from 200 AM T20 (Accuracy 100%)	703.78 (11.7 minutes)
Identifying 1 PM from 200 AM T50 (Accuracy 100%)	1535.98 (25.6 minutes)
Compared to Chapter 3 Identifying 1 PM from 200 AM (Accuracy 100%)	2700 (45 minutes)

Discussion

1) Sample size

Although the PM sample size in this study (60PM&200AM subjects) is rather limited compared to the actual cases, it nevertheless is considerably significant when compared to those mentioned in the literatures (e.g. 11PM &25 AM subjects [26], 29 PM&133AM subjects [34]). It also serves to test and evaluate the ability of the proposed techniques. Nevertheless, increasing AM sample size may lead to inclusion of more dentitions that are similar and thus more mismatches. More AM samples should be included in future investigation.

2) Identification accuracy

Although the dental arch matching accuracy is not sufficiently high , it is useful for providing a shortlist of ranked candidates and when judiciously selected through the use of error threshold identified, can enable the selection of suitable top percentage of the ranked list and reduce the need of complete matching of the entire AM database. Identification of the top 10% of the arch-ranked list of complete samples achieves a high 90.9% accuracy while for partial and noisy samples; accuracy achieved is a lower 72.7% and 73.7% respectively.

3) Identification speed

It takes only 11.7 minutes on average to retrieve one subject from 200 subjects with the developed HRIS framework which reduces identification speed to 26% compared to 45 minutes in Chapter 3 while achieving 100% identification accuracy. HRIS eliminates 80% of the imposter sample in the AM database.

The limitations of the proposed technique are acknowledged as well. Radial Ray Algorithm (RRA) and Hierarchical Ranking Identification Scheme (HRIS) are most applicable to complete arch matching and identification. For partial arch extraction and matching, the proposed techniques need to be improved.

4.10 Summary

Towards any automated scheme development, the automated level, identification speed and identification accuracy are three factors should be considered and be

balanced. Chapter 4 presents development of techniques for arch-based identification for a hierarchical ranking identification scheme (HRIS) that involves a faster arch-based ranking followed by a more accurate point-based ranking. Key issues for the arch-based ranking, such as dental arch extraction, arch feature description and arch matching techniques, are presented. A Radial Ray Algorithm (RRA) is proposed to extract dental arches.

PM database have been slightly increased to 60 PM samples (11 completed PM samples, 11 partial PM samples and 38 noisy PM samples) in Chapter 4. To compare with results in Chapter 3, accuracy is also calculated for the same 50 PM samples. The 7 complete samples achieved 100% rank-1 identification accuracy with a more than 6 times improved identification speed using HRIS. It takes about 7 minutes on average to identify 1 complete PM sample from 200 AM samples using HRIS compared to that of 45 minutes using the first approach alone. However, the second approach is less effective in partial and noisy sample identification. The rank-1 identification accuracy of matching 11 partial PM sample is 54.5% and 59.4% for 32 noisy PM samples.

The following contributions are made in Chapter 4:

- The proposed Radial Ray Algorithm (RRA) is free of manual calibration and arch point specification.
- The proposed fully automated Hierarchical Ranking Identification Scheme improves much of identification speed compared to Chapter 3 by excluding a large number of imposter AM samples at the arch matching level for complete samples. 90.9% identification accuracy is achieved at threshold T10 when improving more than 6 times of identification speed in identification of 11 complete samples. Partial and noisy samples only achieve about 72.7% and 73.7% accuracy respectively when eliminating 50% of imposter samples as shown in Table 4.4-4.6.

- The discovered final matching error threshold 0.8 mm in Chapter 3 has been re-evaluated for distinguishing genuine identification and imposter identification.

The sample size, identification accuracy and identification speed have been discussed. Sample size should be increased in future investigation. The limitations of the proposed technique are acknowledged as well. Radial Ray Algorithm (RRA) and Hierarchical Ranking Identification Scheme (HRIS) are fully-automated but most applicable to complete arch matching and identification. For partial arch extraction and matching, the proposed techniques need to be improved as only 72.7% accuracy is achieved at threshold T50 which eliminates 50% imposter AM samples during matching.

Chapter 5 Single Tooth Classification and Identification

The single tooth identification in this chapter is to investigate the distinctiveness of human single tooth and develop single tooth identification scheme which is useful when only very partial jaws with teeth are available. Two types of single tooth samples are used in experiments: tooth crown segmented from dental casts and entire single tooth (crown and root) reconstructed from Cone Beam CT images. Eigenteeth feature and K Nearest Neighbourhood (KNN) classifier are applied to classify tooth types – posterior (molar, premolar), anterior (canine and incisor). Then iterative closest point algorithm (ICP) is applied to match PM and AM teeth.

5.1 Introduction

There are several situations when single tooth identification becomes important:

- 1) only a few single teeth are found, e.g. at crime scene (Figure 5.1(a));
- 2) a large number of single tooth are found scattered, e.g. after a disaster;
- 3) little remained of the jaw sample, e.g. very few teeth on it or the jaw sample is heavily distorted except for one or more single teeth (Figure 5.1(b)). As shown in Figure 3.10 (b), it is difficult to align a highly partial sample such as the one in Figure 3.10 with only 4 single teeth in the jaw.
- 4) The full dental arch may change its shape due to natural growth or orthodontic surgery (Figure 5.1(d)) and the number of teeth is different but the individual tooth shape does not change much.

In chapter 5, situations 3) and 4) will be investigated. Situations 1) and 2) will be included in future work due to the lack of 3D single tooth database at present.

Although a single tooth is not as unique to a person as a single fingerprint and DNA structure, it is instrumental in forensic dentistry because the size of tooth can be used for age estimation, ethnic group differentiation, and the wear and tear of a tooth could provide invaluable clues to a person's eating habits and lifestyle, thus finally contributing to identity establishment. In anthropology and archaeology investigations as shown in Figure 5.1(c), the single tooth also plays a role in identification. A single tooth has helped in the identification of an ancient mummy as that of Queen

Hatshepsut. The archaeologist told Reuters "It is 100% definitive. It is 1.80 cm (wide) and the dentist took the measurement and studied a tooth. He found it fit exactly 100%." [85]

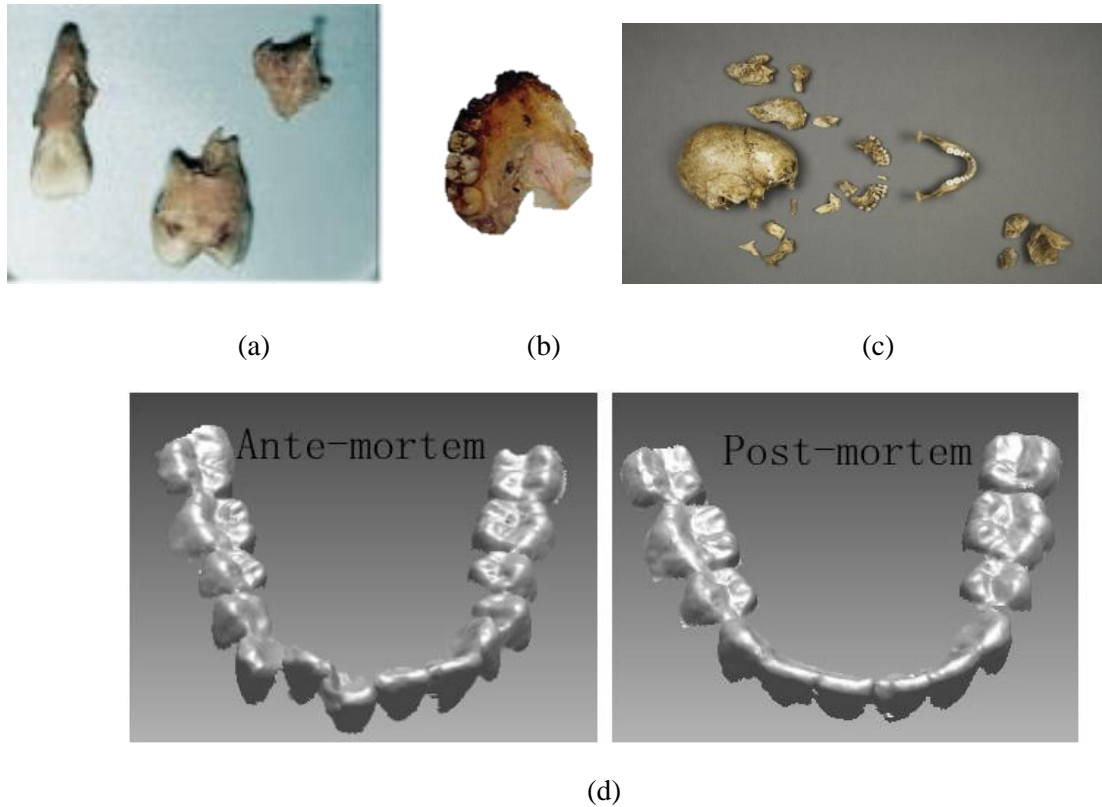


Figure 5.1 (a) a few pieces of single tooth are found at crime scene (b) a partial jaw with a few teeth (c) samples found in anthropology and archaeology investigations (d) arch shape change due to orthodontic surgery

Dental numbering system

Human teeth can be categorized into four types: incisor, canine, premolar and molar. There are multiple teeth in each type. Figure 5.2 illustrates the positions of these four types of teeth in the jaws.

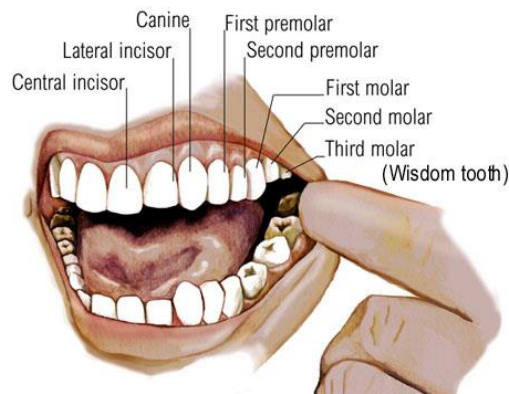


Figure 5.2 Four types of teeth in jaws [86]

- Incisors: the front four teeth in the upper (maxillary) and lower (mandibular) jaws. The two centre teeth are known as central incisors and the teeth on either side of them are known as lateral incisors. Incisors have single tooth root.
- Canines (commonly known as eyeteeth): the two teeth located distal to the lateral incisors in each jaw. These teeth form the corners of the mouth. Canines have single tooth root.
- Premolars (bicuspid): The four premolars in each jaw are located distal to each canine in the arch. These teeth are smaller than the molars. Premolars often have single root. Some have two roots.
- Molars: the large six teeth located in the back of the mouth in each jaw. Molars often have three to four tooth roots.

A unique number is used to label each tooth. There are several ways for tooth labelling. The most popular two are universal tooth numbering system (United States) and FDI (Fédération Dentaire Internationale) World Dental Federation Two-Digit Notation (International). Our study follows the universal tooth numbering system. There are 32 teeth in an adult dentition, starting with the upper-right third molar to the lower-right third molar as shown in Figure 5.3.

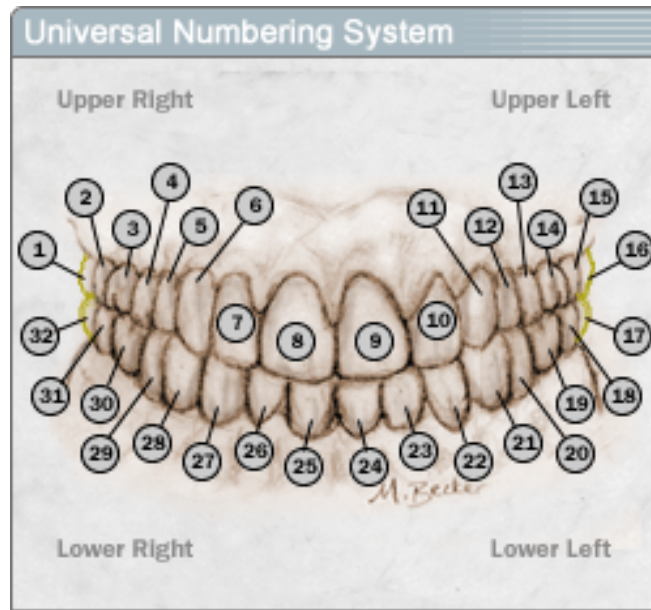


Figure 5.3 An adult dentition in universal tooth numbering system [87]

5.2 System Approach Overview

Figure 5.4 shows the single tooth identification flow chart. Input PM teeth are first classified into either anterior or posterior teeth using eigentooth feature and then indexed PM sub-database will be used to search from its corresponding indexed AM sub-database using iterative closest point algorithm (ICP). The output is the PM victim index and tooth index. The classification is useful for decreasing the search space for identification. For example, if one PM tooth is classified as anterior tooth, it will match against the indexed anterior database only during identification, excluding posterior database. The classification is also useful for establishing a large AM database automatically at later-on stage. Figure 5.4 shows the different phases

The four-tooth-type classification (molar, premolar, canine, and incisor) is also tested using the same techniques and it will be used to compare with the two-class classification (anterior teeth and posterior teeth) regarding classification accuracy, final identification accuracy and identification speed.

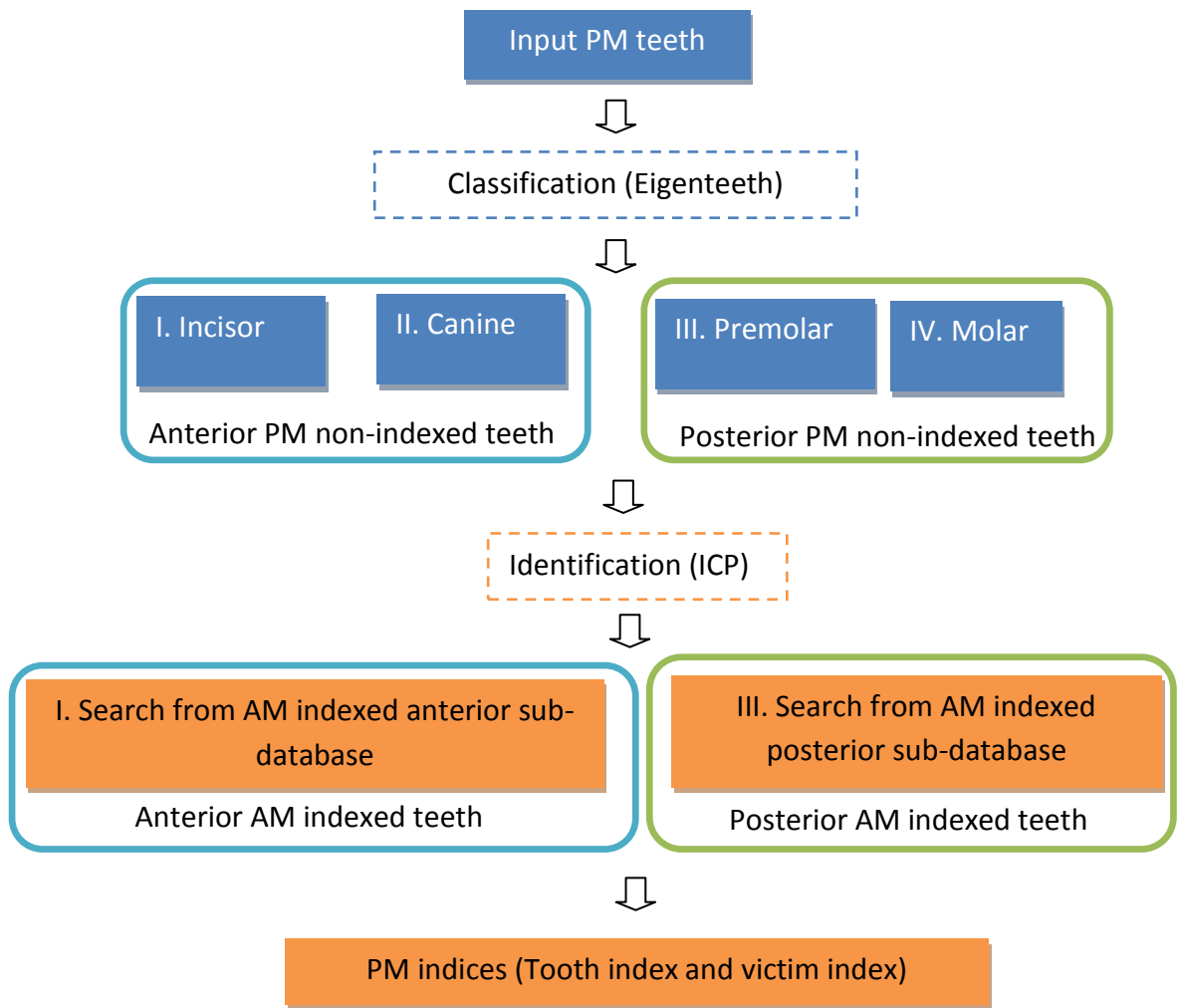


Figure 5.4 Single tooth classification and identification flow chart

5.3 Classification Algorithm Overview

Figure 5.5 shows main steps of tooth classification algorithm using eigenteeth. Details will be depicted and illustrated in Section 5.5.

The main steps list as follows.

1. Read AM set and PM set into **TrainSet** matrix and **TestSet** matrix respectively and normalize the **TrainSet** matrix and **TestSet** matrix into same dimension
2. Apply PCA to **TraniSet** matrix to calculate **EigenVector** and **EigenValue**

3. Project both **TrainSet** and **TestSet** into new vector space using the calculated **EigenVector** to form projected train set **ProTrain** and projected test set **ProTest**.
4. K Nearest Neighbourhood (KNN) Classifier is used to classify **TestSet** by using **ProTrain, ProTest and TrainClass** as input. **TrainClass** is predefined classes for **Trainset**. In this application, two **TrainClass** types are tested.
 If **TrainClass** = [1 (AM posterior teeth), 2 (AM anterior teeth)], the outcome **TestClass** = [1 (PM posterior teeth), 2 (AM anterior teeth)];
 If **TrainClass** = [1 (AM molar teeth), 2(AM premolar teeth), 3(AM canine teeth), 4(AM incisor teeth)], the outcome **TestClass** = [1 (PM molar teeth), 2(PM premolar teeth), 3(PM canine teeth), 4(PM incisor teeth)]

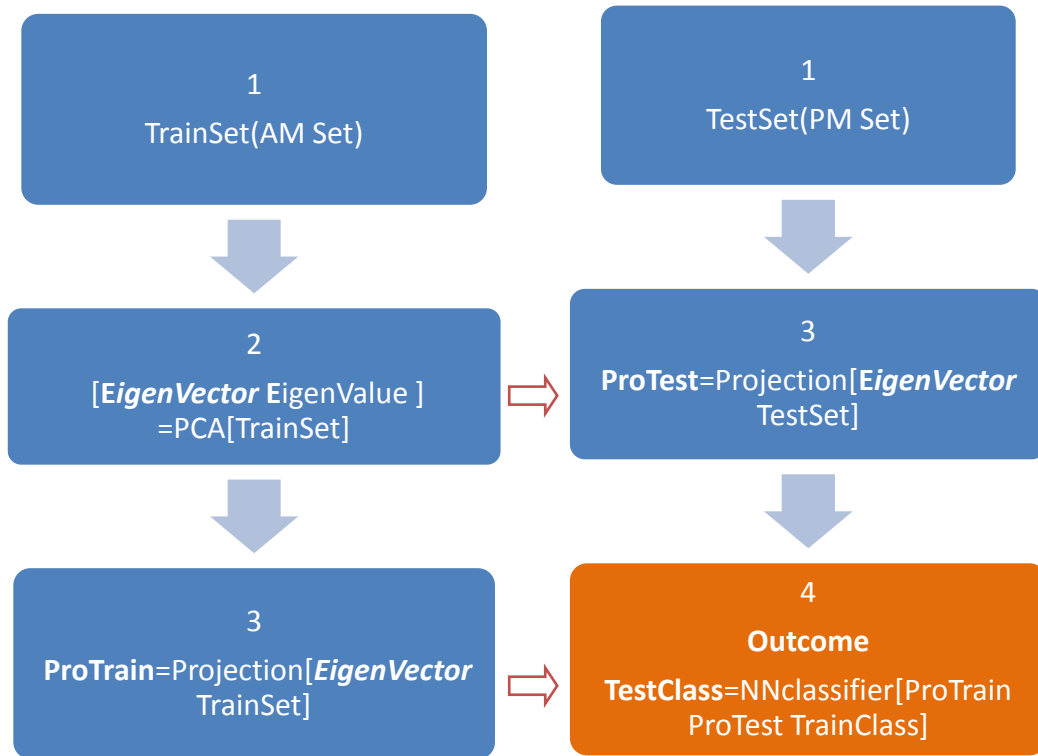


Figure 5.5 Single tooth classification algorithm

5.4 Data Preparation

Data used in Experiment I are segmented teeth from laser-scanned dental plasters, thus only containing tooth crowns as shown in Figure 5.6. Due to the deficiency of 3D single tooth database, orthodontic data are used in Experiment I as shown in Figure

5.1(d). The main goal of orthodontic surgery is to achieve a correct bite, an aesthetic face. People wear orthodontic braces for years to get their teeth arranged neatly. The elapsed time of AM sample and PM sample acquisitions can be from one to three years. Therefore, it is plausible to use orthodontic data to simulate forensic cases to some extent. The full dental arch may change its shape due to natural growth or orthodontic surgery and the number of teeth is different but individual tooth shape is usually preserved.

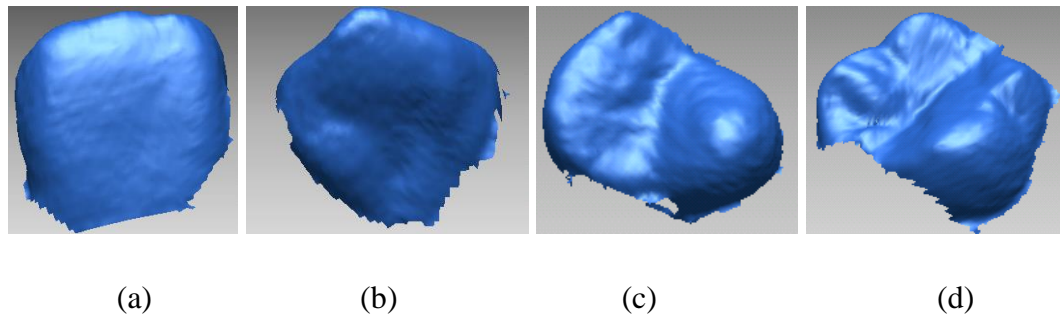


Figure 5.6 Four types of segmented teeth from laser-scanned dental plasters (a) incisor (b) canine (c) premolar (d) molar

No decimation is applied for both PM and AM samples since the tooth details needs to be kept high for single tooth crown comparison. Each tooth crown contains about 3000~5000 mesh points. An AM database containing 200 teeth and a PM database containing 50 teeth are established. Both lower jaw and upper jaw teeth and all four types of teeth are included as shown in Figure 5.6. The details of tooth crown samples are listed in Table 5.1.

Table 5.1 Tooth crown data details								
	Subject	Total	Upper	Lower	Molar	Premolar	Canine	Incisor
AM	15	200	116	84	58	60	30	52
PM	15	50	36	14	12	8	11	19

Experiment II is designed to investigate complete single tooth identification. Data are reconstructed from cone beam CT image using level set methods [88]. Tooth crown and tooth root are both available in a complete single tooth as shown in Figure 5.7. Both lower jaw and upper jaw teeth and all four types of teeth are included. An AM

database is built containing 100 single teeth and also a PM database containing 10 single teeth. Figure 5.8 shows the 3D reconstruction process. The details of complete single tooth samples are listed in Table 5.2.

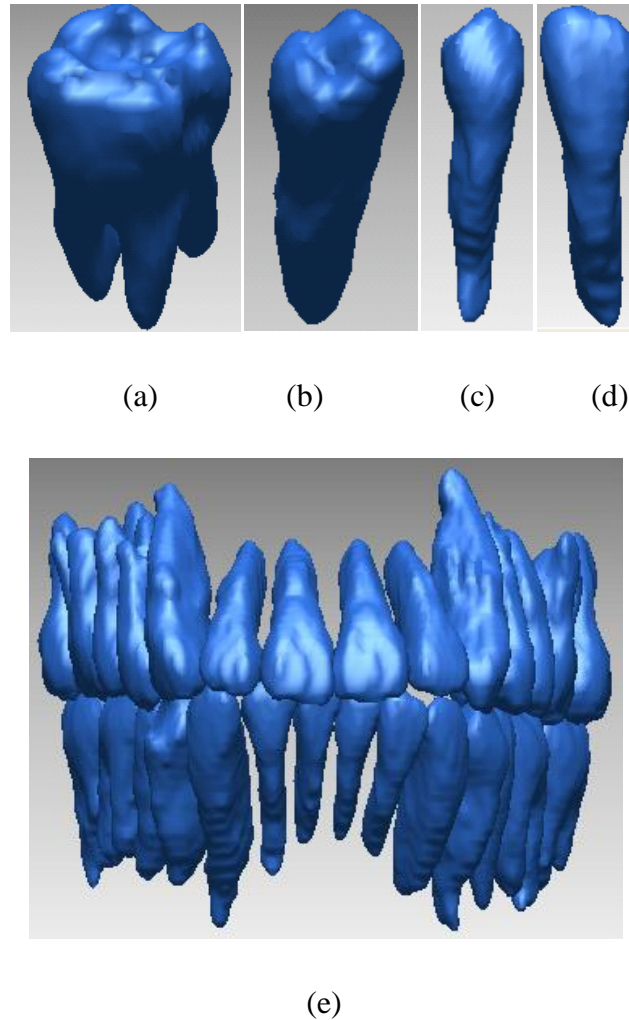
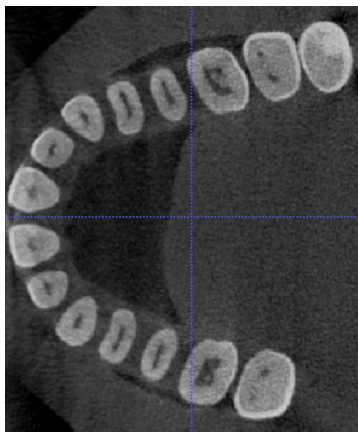


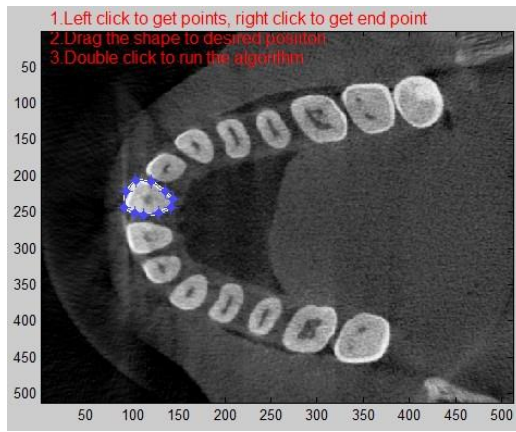
Figure 5.7 Four types of segmented teeth from laser-scanned dental plasters (a) molar (b) premolar (c) canine (d) incisor (e) upper and lower jaw teeth reconstructed from CBCT image

As shown in Figure 5.8 (a), one clear layer in CBCT is selected using Insight Toolkit (ITK) software. Insight Toolkit (ITK) is an open-source software toolkit for performing registration and segmentation [89]. Then an initial contour is specified for level set evolvement in MATLAB environment as shown in Figure 5.8 (b) and a clearly defined edge is used to segment one tooth from the whole image as shown in Figure 5.8 (c-d). Due to the overlapping of tooth regions and blurriness of CBCT

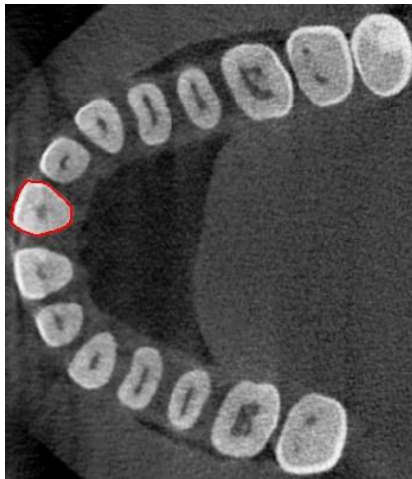
image, usually certain regions are under-segmented (root) or over-segmented (crown) where manual correction are needed. And the correction is done in ITK. The reconstructed tooth surface is usually noisy and a post-processing software RAPIDFORM is used to smooth the surface as shown in Figure 5.8 (i-j). Post-processing include smoothing and decimation. An originally reconstructed complete single tooth contains about 40,000 points and 4000~6000 points are kept after decimation.



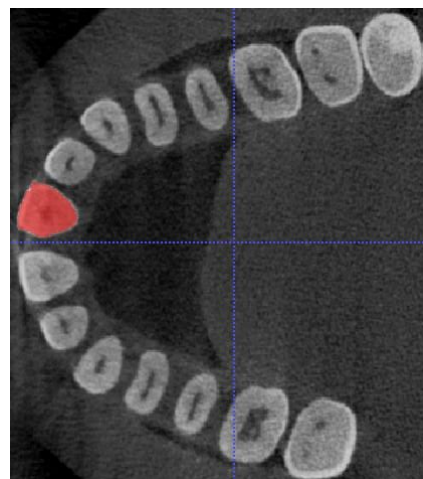
(a)



(b)



(c)



(d)

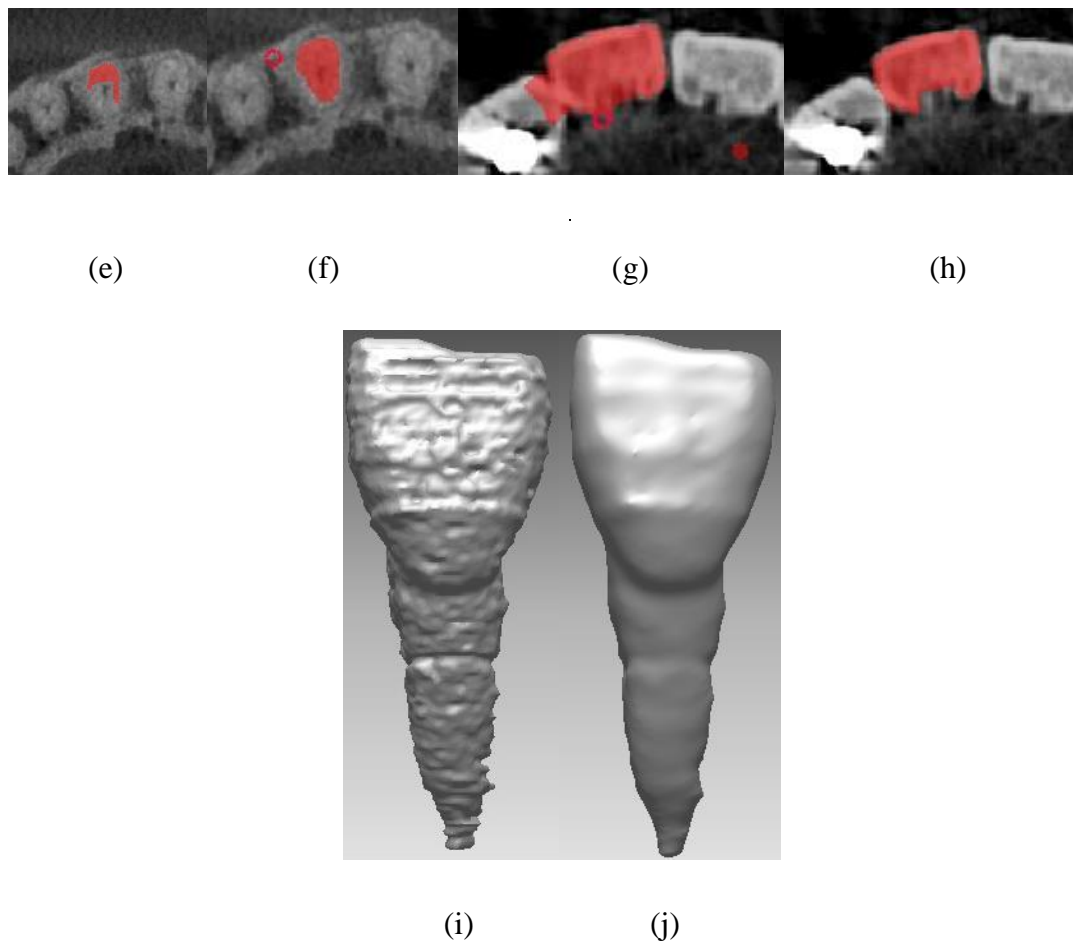


Figure 5.8 3D reconstruction of single tooth from CBCT image (a) one layer of CBCT image (b) specify an initial contour for level set evolvment (c) a clearly defined edge after level set evolvment (d) segmented part lighted in red (e) under segmentation (f) correction of under segmentation (g) over segmentation (h) correction of over segmentation (i) 3D mesh of a single tooth before smoothing (j) smoothed mesh

There are not many people who have Cone Beam CT examination before tooth treatment thus far, primarily due to the high cost. CBCT examination is much more expensive than usual dental check using radiograph examination. Thus the number of complete single tooth data is quite limited in Experiment II. The details of complete single tooth samples are listed in Table 5.2.

Table 5.2 Complete tooth data details								
	Subject	Total	Upper	Lower	<u>Molar</u>	<u>Premolar</u>	<u>Canine</u>	<u>Incisor</u>
AM	13	100	14	86	<u>10</u>	<u>9</u>	<u>28</u>	<u>53</u>
PM	2	10	10	0	<u>2</u>	<u>1</u>	<u>2</u>	<u>5</u>

5.5 Eigenteeth Calculation

Eigen feature is often used in face recognition. The term ‘Eigenteeth’ is extended from ‘Eigenfaces’ in face recognition. Eigenfaces based on 2D images have been proposed by Turk et al. in 1991[90] and applied to face recognition successfully. 3D Eigenfaces are investigated for face recognition by Xu et al. [91] to overcome problems in 2D face recognition such as the recognition accuracy is sensitive to lighting conditions, expressions, viewing position and varieties of subordinates such as hair, bear, and glasses. Later, this method was applied in dental identification based on identification of radiographs [92].

3D Eigenteeth is used for tooth classification based on 3D mesh model. The PCA method is used to obtain dominant eigen vectors, called Eigenteeth. Any new input mesh model can be represented with the linear combination of these Eigenteeth. Thus, one mesh model can be projected into the lower-dimensional space by these Eigenteeth. The K-NN (K Nearest Neighbourhood) classifier from [93] is then used to classify PM set (TestSet in Figure 5.5)

The main steps of eigenteeth calculation list as follows.

1. Read AM set and PM set into **TrainSet** matrix and **TestSet** matrix respectively and normalize the **TrainSet** matrix and **TestSet** matrix into same dimension.

Each tooth has different number of $3 \times n$ points which will be converted to a column vector to form one column in TrainSet matrix. Thus, if 100 AM teeth are used in training, the TrainSet matrix dimension is $3 \times n \times 100$ ($3 \times n$ rows, 100 columns), where n is the value of the largest number of points in TrainSet and TestSet. Blanks are filled with zeros. If 10 teeth are to be identified, the TestSet matrix dimension is $3 \times n \times 10$ ($3 \times n$ rows, 10 columns).

2. Apply PCA to **TraniSet** matrix to calculate **EigenVector** and **EigenValue**

The average 3D mesh model M_{aver} is calculated easily. Each mesh differs from the average with the vector $A_i = M_i - M_{aver}$. Then one covariance matrix is constructed as follows

$$C = AA^T \quad (5.1)$$

The matrix C is 100 by 100 and we can obtain its eigenvalues and corresponding eigenvectors by using Singular Value Decomposition (SVD). Generally, we can obtain 99 non-zero eigenvalues and 99 orthogonal eigenvectors. We can select the first e ($e < 100$) largest eigenvalues to approximate the tooth geometric space and their corresponding eigenvectors are U_1, U_2, \dots, U_e , which are called eigenteeth.

3. Project both **TrainSet** and **TestSet** into tooth geometric space using the calculated eigenvector to form projected train set **ProTrain** and projected test set **ProTest**.

$$\mathbf{ProTrain} = \text{eigenvector}^T \times \mathbf{TrainSet} \quad (5.2a)$$

$$\mathbf{ProTest} = \text{eigenvector}^T \times \mathbf{TestSet} \quad (5.2b)$$

4. K Nearest Neighbourhood (K-NN) Classifier is used to classify **TestSet** by using **ProTrain**, **ProTest** and **TrainClass** as input. K is set 5 in testing and Euclidean distance is used to measure difference of PM sample and AM sample to determine which classification the tested PM sample belongs to. **TrainClass** is predefined classes for **Trainset**. In this application, two **TrainClass** types are tested.

- If **TrainClass** = [1 (AM posterior teeth), 2 (AM anterior teeth)], the outcome **TestClass** = [1 (PM posterior teeth), 2 (AM anterior teeth)];
- If **TrainClass** = [1 (AM molar teeth), 2(AM premolar teeth), 3(AM canine teeth), 4(AM incisor teeth)], the outcome **TestClass** = [1(PM molar teeth), 2(PM premolar teeth), 3(PM canine teeth), 4(PM incisor teeth)];

5. Classification accuracy=Number of correctly classified TestClass/Total number of test sample

(5.3)

Identification accuracy= Number of correctly identified TestClass/Total number of test sample

(5.4)

Different K values (2~10) are used, however, classification accuracy does not change much.

5.6 Experiments and Discussion

Experiment I Identification of single tooth crown

In Experiment I and Experiment II, eigenteeth features are used to classify a PM tooth into 2 classes (anterior tooth crown and posterior tooth crown) and 4 classes (molar crown, premolar crown, canine crown and incisor crown) respectively. Classification accuracy, identification accuracy and computational time are then compared and discussed with reference to Table 5.3.

- **2-class classification of single tooth crown**
 - 1) 200 AM tooth crowns are indexed as anterior (incisor and canine) tooth crowns and posterior (premolar and molar) tooth crowns.
 - 2) The tested 50 PM tooth crowns are also likewise classified into anterior (incisor and canine) tooth crowns and posterior (premolar and molar) tooth crowns
 - 3) PM anterior teeth will match against AM anterior database; and PM posterior teeth will match against AM posterior database
- **4-class classification of single tooth crown**
 - 1) 200 AM tooth crowns are indexed as molar crowns, premolar crowns, canine crowns and incisor crowns.
 - 2) The tested 50 PM tooth crowns are likewise classified into PM molar crowns, PM premolar crowns, PM canine crowns and PM incisor crowns.
 - 3) PM molar crowns, PM premolar crowns, PM canine crowns and PM incisor crowns will match against AM molar crowns, AM premolar crowns, AM canine crowns and AM incisor crowns respectively.

Figure 5.9 shows the differences in alignment errors in matching genuine crowns and imposter crowns. It took less iteration to achieve a much smaller minimum alignment error in matching genuine crowns. (Yellow: PM sample; Red: AM sample)

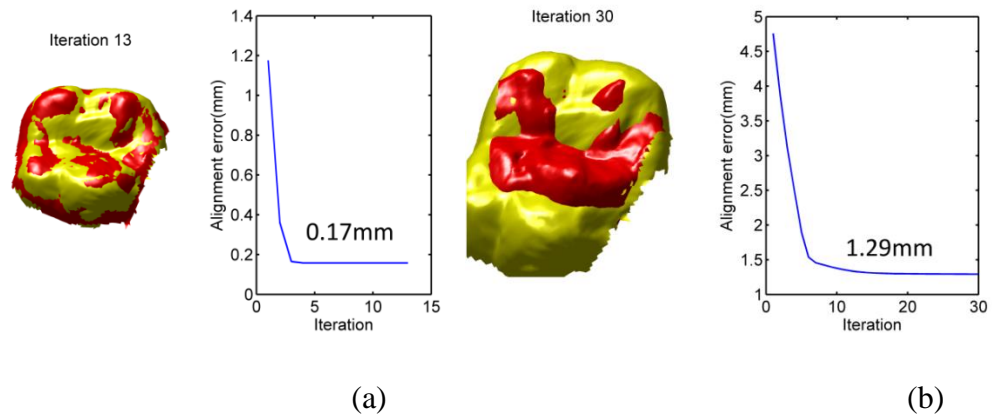


Figure 5.9 (a) genuine tooth crowns (b) imposter tooth crowns

Table 5.3 Identification of single tooth crown														
50PM 200AM	Classification Accuracy (%)	Identification Accuracy at Each Rank before Reaching Highest Accuracy (%)											Identification Speed (s)	
		R1	R2	R3	R4	R5	R6	R7	R8	R9	R10	R11	Total	Per
2 classes	96	76	82	88	92	92	92	92	94	94	94	96	3894s (~65 minutes)	78s
4 classes	88	68	72	78	82	82	82	84	84	86	88	88	2020s (~34 minutes)	40s

Table 5.3 shows that 96% and 88% classification accuracy are achieved in two classification schemes respectively. Therefore, in the later-on identification phrases, the highest final identification accuracy is 96% and 88% respectively.

Matching 50 PM single tooth crowns to 200 AM single tooth crowns, the outcome is 50*200ranks. Each PM sample has 200 ranks.

In 2-class scheme, 38 out of 50 PM samples are correctly identified at rank 1, thus it reaches $38/50=76\%$ rank-1(**R1**) identification accuracy as shown in Table 5.3. The maximum identification accuracy reaches 96% at Rank 11(**R11**), which considers

correct match in all samples from Rank 1 to Rank 11. In contrast, lower rank-1 accuracy of 68% and lower maximum accuracy of 88% is reached at Rank 10(**R10**) in 4-class scheme.

It is worth noting that maximum identification accuracy are achieved in early stage of identification since they are at top ranks ($11/200=5.5\%$; $10/200=5\%$) in both schemes. Thus top 5.5% ranks achieve 96% in 2-class scheme while top 5% ranks achieve 88% in 4-class scheme. This means that high identification accuracy could be achieved when only top 5.5% candidates' samples are selected to present to forensic experts.

Identification speed is compared as shown in the last column in Table 5.3. Total time is counted for matching 50 PM to 200AM samples. Per time is the total time divided by the total number of PM samples ($3894s/50=78s$). It is the time for matching 1 PM sample to 200 AM sample. Although 4-class scheme has lower final identification accuracy, it is about twice faster than 2-class scheme. As it is mentioned in Chapter 4, identification accuracy and identification speed are two important factors to consider in a balance manner depending on the emphasis and focus of the experiment.

Both results in the two schemes indicate there is distinctiveness in human single tooth crown with potential to establish correct identities. Enriched tooth crown database will be needed for more comprehensive future validation.

Experiment II Identification of complete single tooth

Examples of samples in Figure 5.8 are used in Experiment II. Samples contain both tooth crowns and tooth roots. The same procedure in Experiment I is followed.

- **2-class classification of complete single teeth**

- 1) 100 AM complete single teeth are indexed as anterior (incisor and canine) complete single teeth and posterior (premolar and molar) complete single teeth.
- 2) The tested 10 PM complete single teeth samples are classified into anterior (incisor and canine) complete single teeth and posterior (premolar and molar) complete single teeth

- 3) PM anterior teeth will match against AM anterior database; and PM posterior teeth will match against AM posterior database
- **4-class classification of complete single teeth**
 - 1) 100 AM complete single teeth are indexed as molar, premolar, canine and incisor.
 - 2) The tested 10 PM complete single tooth samples are classified into PM molar, PM premolar, PM canine crown and PM incisor.
 - 3) PM molar, PM premolar, PM canine and PM incisor will match against AM molar, AM premolar, AM canine and AM incisor respectively.

Table 5.4 shows that 90% and 80% classification accuracy are achieved in two classification schemes respectively.

Figure 5.10 shows the differences in alignment errors in matching genuine complete single tooth and imposter complete single tooth. It took less iteration to achieve a much smaller minimum alignment error in matching genuine complete single tooth. (Yellow: PM sample; Red: AM sample)

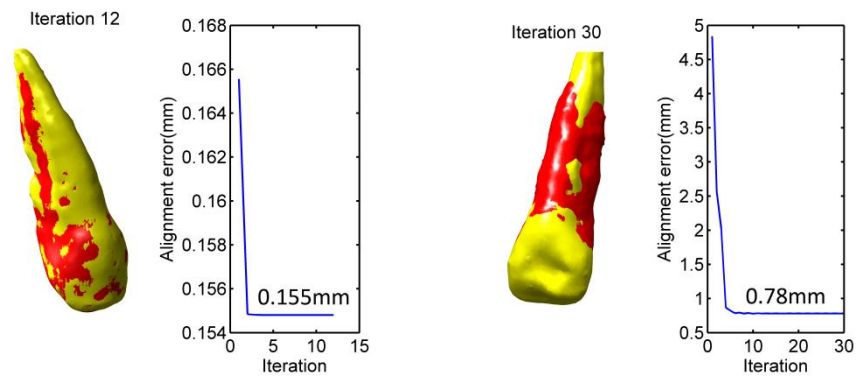


Figure 5.10 (a) genuine complete single tooth (b) imposter complete single tooth

Table 5.4 Identification of complete single tooth						
10PM 100AM	Classification Accuracy (%)	Identification Accuracy at Each Rank before Reaching Highest Accuracy (%)			Identification Speed (s)	
		R1	R2	R3	Total	Per
2 classes	90	80	80	90	613s (~10 minutes)	61s
4 classes	80	70	80	80	324s (~5 minutes)	30s

In 2-class scheme, there are 8 out of 10 PM samples are correctly identified at rank 1, thus it reaches $8/10=80\%$ rank-1 identification accuracy. The maximum identification accuracy 90% reaches at Rank 3. In contrast, lower rank-1 accuracy of 70% and lower maximum accuracy of 80% is reached at Rank 2 in 4-class scheme.

Maximum identification accuracy are achieved in early stage of identification since they are at top ranks ($3/100=3\%$; $2/100=2\%$) in both schemes respectively. Thus top 3% ranks achieves 90% accuracy in 2-class scheme while top 2% ranks achieves 80% accuracy in 4-class scheme. This means that high identification accuracy could be achieved when only top 3% candidates' samples are selected to present to forensic experts. Sample size will be increased for future validation.

Identification speed is compared as shown in the last column in Table 5.4. Total time is counted for matching 10 PM to 100AM samples. Per time is the total time divided by the total number of PM samples ($613s/10=61s$). It is the time for matching 1 PM sample to 100 AM sample. Again 4-class scheme has lower final identification accuracy, but it is about twice faster than 2-class scheme.

Single tooth samples are valuable features in forensic identification. Both results in the two schemes have indicated distinctiveness in complete single tooth. It is possible to establish correct identities particularly when a few teeth are used. Larger complete single tooth database will be needed for comprehensive future validation.

5.7 Summary

This chapter presents an exploratory investigation and development of techniques for 3D single tooth identification. Two types of single tooth samples are used: tooth crowns segmented from dental casts and entire single teeth (crown and root) reconstructed from Cone Beam CT images. Eigenteeth feature and K Nearest Neighbourhood (KNN) classifier are applied to classify tooth types – posterior (molar, premolar), anterior (canine and incisor). Then the iterative closest point algorithm (ICP) is applied to match PM and AM teeth. 50 PM tooth crowns, 200 AM tooth crowns, 10 entire PM single teeth and 100 entire AM single teeth are used in experiments.

Two classification schemes (2-class and 4-class) are tested single tooth crown identification and complete single tooth identification. The 2-class scheme classifies teeth into anterior (incisor and canine) and posterior (molar and premolar) classes. The 4-class scheme classifies teeth into molar, premolar, canine and incisor.

In tooth crown identification, classification achieves 96% accuracy as shown in Table 5.3. Rank-1 identification accuracy achieves 76% and maximum identification accuracy 96% achieves at Rank 11. In contrast, classification achieves 88% accuracy in 4-class scheme. Lower rank-1 accuracy of 68% and lower maximum accuracy of 88% is reached at Rank 10 in 4-class scheme. However, 4-class scheme is twice faster than 2-class scheme.

In complete single tooth (crown and root) identification, classification accuracy achieves 90% as shown in Table 5.4. Rank-1 identification accuracy achieves 80% and maximum identification accuracy 90% achieves at Rank 3 in 2-class scheme. In contrast, classification accuracy achieves 80% in 4-class scheme. Lower rank-1 accuracy of 70% and lower maximum accuracy of 80% is reached at Rank 2 in 4-class scheme. Also 4-class scheme is twice faster than 2-class scheme.

In both experiments, maximum identification accuracy is achieved in early stage of identification since they are at top ranks (5.5% ranks and 3% ranks).

Identification speed is fast. It takes 78 seconds in identifying 1 PM crown sample from 200 AM crown samples in 2-class scheme and 40 seconds in 4-class

scheme. It takes 61 seconds in identifying 1 PM complete single tooth sample from 100 AM single tooth samples in 2-class scheme and 30 seconds in 4-class scheme.

Single tooth crown and complete single tooth are valuable features in forensic identification. This investigation has shown that there is distinctiveness in the characteristics of single teeth that it is possible to use to establish identities. Enriched AM and PM database will be needed for more comprehensive future validation.

Chapter 6 Conclusions and Future Work

“Now this is not the end. It is not even the beginning of the end. But it is perhaps, the end of the beginning.”

-Winston Churchill

6.1 Conclusions

The primary objective of this thesis is to develop computer-based 3D identification approaches that overcome key hurdles in 2D identification. The hurdles include inaccurate tooth contour extraction from blurred radiographs and incorrect matching due to differences in imaging angles. Three approaches are proposed and presented: point-based matching and identification, arch-based matching and identification and a Hierarchical Ranking Identification Scheme (HRIS), and single tooth classification and identification. Main achievements and contributions list as follows:

1. A point-based matching and identification approach has been developed

The (PIDI) algorithms include algorithms for feature extraction, feature description and correspondence. 60 PM samples and 200 ante mortem samples are used in this study. These 60 samples consist of the 7 complete genuine samples, in addition, 11 partial genuine samples, 32 noisy genuine samples and 10 imposter samples taken from multi-ethnic Asian groups (Chinese, Indian and Malay) are also included.

The rank-1 identification accuracy of complete sample identification is 100%. The rank-1 identification accuracy of matching 11 partial PM sample is 72.7% and 78.1% for 32 noisy PM samples.

Overall accuracy of 50 genuine samples (complete, partial, and noisy) is also calculated and compared in experiments between manually segmented PM samples and auto-segmented PM samples. 94% rank-1 identification accuracy has been achieved in identification of 50 manually segmented PM samples and it

decreases to 80% in identification of 50 auto-segmented PM samples. In contrast, only 86% and 64% rank-1 accuracy have been achieved respectively in the above two identifications by applying the existing iterative closet point (ICP) algorithm alone. In addition, the proposed approach is more robust to obtain the correct identities when AM sample size is increased. Furthermore, a matching error threshold of 0.8 has been identified to differentiate genuine and imposter samples.

Compared to the literatures, this work makes the following contributions:

- Existing approaches are primarily based on 2D x-ray radiographs. Radiographs with poor contrast and exposure levels are unsuitable for identification, as it is difficult to extract tooth contours accurately with minimal geometric distortions. However, using 3D makes the identification more feasible even under large-scale decimation in noisy conditions. Samples with down to 10% of the scanned points and partial and noisy samples can be identified as demonstrated in the experiments.
- 2D images are projections of 3D objects. Differences in the radiographs arising from different imaging angles are often significant to cause incorrect matching. The extracted tooth contour which is used as an anatomic dental feature is not an accurate description of 3D tooth profile. Once different imaging angles are applied, tooth contours of the same sample are different in profiles. In contrast, no distortion of the tooth profiles occurs as projection from 3D to 2D is not required. The problem arising from different imaging angles in 3D is what we call pose variation problem. The results also demonstrate the capability of the proposed method in dealing with pose variations.
- Partial teeth identification is feasible in 3D without missing tooth detection or tooth classification.
- More salient points are extracted using the proposed feature extraction algorithm than existing work thus reducing time demand for correspondence. The feature descriptor and the correspondence algorithm are tested to be more robust to pose variations compared to existing work.

2. An Arch-based matching and identification approach and a Hierarchical Ranking Identification Scheme (HRIS) have been developed.

Key issues for the arch-based ranking, such as dental arch extraction, arch feature description and arch matching techniques, are presented. A Radial Ray Algorithm (RRA) is proposed to extract dental arches.

PM database has been slightly increased to 60 PM samples (11 completed PM samples, 11 partial PM samples and 38 noisy PM samples). To compare with results using the point-based approach, accuracy is also calculated for the same 50 PM samples. The 7 complete samples achieved 100% rank-1 identification accuracy with a more than 6 times improved identification speed using HRIS. However, the second approach is less effective in partial and noisy sample identification. The rank-1 identification accuracy of matching 11 partial PM sample is 54.5% and 59.4% for 32 noisy PM samples. In contrast, the rank-1 identification accuracy of matching 11 partial PM sample using point-based approach is 72.7% and 78.1% for 32 noisy PM samples.

The following contributions are made:

- The proposed Radial Ray Algorithm (RRA) does not require manual calibration and arch point specification.
- The proposed fully automated Hierarchical Ranking Identification Scheme improves much of identification speed compared to the point-based approach by excluding a large number of imposter AM samples at the arch matching level for complete samples. 90.9% identification accuracy is achieved with 6 times faster identification speed for 11 complete samples. With 11 partial and 38 noisy samples only 72.7% and 73.7% accuracy is achieved respectively after eliminating 50% of imposter samples.

3. 3D single tooth classification and identification schemes have been proposed.

Two types of single tooth samples are used: tooth crowns segmented from dental casts and entire single teeth (crown and root) reconstructed from Cone Beam CT images. Eigenteeth feature and K Nearest Neighbourhood (KNN) classifier are applied to classify tooth types – posterior (molar, premolar), anterior (canine and incisor). Then the iterative closest point algorithm (ICP) is applied to match PM and AM teeth. 50 PM tooth crowns, 200 AM tooth crowns, 10 entire PM single teeth and 100 entire AM single teeth are used in experiments.

Two classification schemes (2-class and 4-class) are tested single tooth crown identification and complete single tooth identification. The 2-class scheme classifies teeth into anterior (incisor and canine) and posterior (molar and premolar) classes. The 4-class scheme classifies teeth into molar, premolar, canine and incisor.

The main findings list as follows:

- In tooth crown identification scheme, classification accuracy achieved is 96%. Rank-1 identification accuracy achieved is 76% and maximum identification accuracy achieved is 96% at Rank 11 when identifying 50 PM crown samples from 200 AM crown samples. In contrast, classification accuracy achieved is 88% in 4-class scheme. Lower rank-1 accuracy of 68% is attained and a lower maximum accuracy of 88% is attained at Rank 10 in 4-class scheme. However, 4-class scheme is twice faster than 2-class scheme.
- In complete single tooth (crown and root) identification scheme, classification accuracy achieved is 90%. Rank-1 identification accuracy achieved is 80% and maximum identification accuracy achieved is 90% at Rank 3 in 2-class scheme when identifying 10 complete PM single tooth samples from 100 complete AM single tooth samples. In contrast, classification accuracy achieved is 80% in 4-class scheme. Lower rank-1 accuracy of 70% is attained and a lower

maximum accuracy of 80% is attained at Rank 2 in 4-class scheme. 4-class scheme is twice faster than 2-class scheme.

The aforementioned have testified distinctive characteristics of human single tooth and that it is possible to establish correct identities when a few teeth are found during crime scene investigation.

The following limitations are acknowledged.

1. The 3D dental image is required, which may not be available in every case at present. In addition, impressions would have to be made and 3D scanning would have to be performed, adding to the cost of the comparison technique in this study presently.
2. Radial Ray Algorithm (RRA) and Hierarchical Ranking Identification Scheme (HRIS) are most applicable to complete arch matching and identification. For partial arch extraction and matching, the proposed techniques need to be improved.
3. Compared to the number of victims in mass disasters, the number of samples used in present study is limited.

6.2 Future Work

Investigations for comprehensive formulation and more efficient algorithms of 3D dental identification are always of interest.

1. Establishment of enriched AM and PM database for future validation.

The present study and developed techniques are based on matching 200 ante-mortem samples. Increasing sample size is essential for robust validation.

2. Investigation of identification accuracy under different decimation rate.

Presently, 10% of the scanned points are kept for a faster computation. More comprehensive study on different decimation rate is needed to determine its effect on matching accuracy.

3. Development of intelligent searching scheme.

The matching error difference of rank-1 and rank-2 appears to be potential useful for identification of genuine and imposter samples. An intelligent searching approach could be developed together with a further study of these error differences.

4. Investigation of partial arch extraction and matching

Radial Ray Algorithm (RRA) and Hierarchical Ranking Identification Scheme (HRIS) are most applicable to complete arch matching and identification. Robust partial arch matching approach is needed for recognition of partial tooth regions.

5. Investigation of 3D dental work identification.

Dental work (dental fillings) is also considered a unique feature for individuals which is used in 2D radiograph identification. Dental work feature and the proposed features could be fused to achieve a more robust identification.

List of Publications

- [1] **X. Zhong**, D.P. Yu, Y.S. Wong, T. Sim, W. F. Lu, K. W. C. Foong, and H.-L. Cheng, "3D dental biometrics: Alignment and matching of dental casts for human identification," *Computers in Industry* (2013).
<http://dx.doi.org/10.1016/j.compind.2013.06.005>
- [2] D.P. Yu, **X. Zhong**, Y.S. Wong, G.S. Hong, W.F. Lu, H.-L. Cheng, An automatic form error evaluation method for characterizing micro-structured surfaces, *Measurement Science and Technology*, 22(1) (2011) 15105 (13p).
- [3] **X. Zhong**, D.P. Yu, Y.S. Wong, H. Cheng, K. W. C. Foong, Towards Automated Pose Invariant 3D Dental Biometrics, *International Joint Conference on Biometrics (IJCB)*, Washington, DC, 2011, 1-7.
- [4] **Xin Zhong**, Yoke San WONG, Wen Feng LU, Kelvin W C FOONG, and Ho-lun CHENG, A dental matching approach using partial surface features for human identification, *Proceedings of the ASME 2012 International Design Engineering Technical Conferences & Computers and Information in Engineering Conference, IDETC/CIE 2012 August 12-15, 2012, Chicago, IL, USA*.
- [5] **Xin Zhong**, Kelvin W C FOONG, Yoke San WONG, 3D Dental Biometrics: Alignment and Matching of Dental Casts, in: *47th Australian Begg Orthodontic Society Meeting, Darwin, Australia, 2011. Oral Presentation*

BIBLIOGRAPHY

- [1] Nicole. Fingerprint Identification Points. Available: <http://www.all-about-forensic-science.com/fingerprint-identification-points.html>
- [2] (2007). Genes and inheritance. Available: http://www.abpishools.org.uk/page/modules/genome/dna7.cfm?coSiteNavigation_allTopic=1
- [3] C. Marsha A. Voelker, RDH, MS. Forensic Dentistry. Available: <http://www.dentalcare.com/en-US/dental-education/continuing-education/ce401/ce401.aspx?ModuleName=coursecontent&PartID=2&SectionID=-1>
- [4] P. O'SHAUGHNESSY. (11 Sep 2002). More than half of victims IDd. Available: http://911research.wtc7.net/cache/planes/evidence/dailynews_halfvictimsidd.html
- [5] (2005). Dental records beat DNA in tsunami IDs. Available: <http://www.newscientist.com/article.ns?id=mg18725163.900>
- [6] D. R. Senn and P. G. Stimson, Forensic Dentistry, Second Edition ed. vol. Chapter 9: CRC Press, Taylor& Francis Group, 2010.
- [7] I. A. Pretty and D. Sweet., "A look at forensic dentistry-part 1: The role of teeth in the determination of human identity," British Dental Journal, vol. 190, pp. 359-366, April, 2001.
- [8] R. B. J. Dorion, Bitemark Evidence: Marcel Dekker, 2005.
- [9] C. D. Cocceianus, E. Cary, and H. B. Foster, Dio's Roman history: with an English translation: W. Heinemann, 1914.
- [10] "Body identification guidelines," J Am Dent Assoc, vol. 125, pp. 1244-1254, American Board of Forensic Odontology. 1994.
- [11] Dental radiography. Available: http://en.wikipedia.org/wiki/Dental_radiography
- [12] L. HUMPHREYS. (2011). Grim work of identification. Available: <http://www.stuff.co.nz/taranaki-daily-news/news/4741899/Grim-work-of-identification>
- [13] R. M. Lorton L, Frideman R, "The computer-assisted postmortem identification (CAPMI) system: a computer-based identification program.," Journal of Forensic Science, pp. 997-984, 1988.
- [14] M. J. (2006). WinID3 dental identification system. Available: www.winid.com
- [15] J. G. Clement, V. Winship, J. Ceddia, S. Al-Amad, A. Morales, and A. J. Hill, "New software for computer-assisted dental-data matching in Disaster Victim Identification and long-term missing persons investigations: "DAVID Web", " Forensic Science International, vol. 159, pp. S24-S29, 2006.
- [16] M. Abdel-Mottaleb, O. Nomir, D. E. Nassar, G. Fahmy, and H. H. Ammar, Challenges of developing an automated dental identification system, 2003.
- [17] D. E. M. Nassar and H. H. Ammar, "A prototype automated dental identification system (ADIS)," presented at the Proceedings of the 2003 annual national conference on Digital government research, Boston, MA, 2003.
- [18] H. Chen and A. K. Jain, "Tooth contour extraction for matching dental radiographs," presented at the Proceedings of the 17th International Conference on Pattern Recognition, 2004.

- [19] G. Fahmy, D. Nassar, E. Haj-Said, H. Chen, O. Nomir, J. D. Zhou, et al., "Towards an Automated Dental Identification System (ADIS)," in *Biometric Authentication, Proceedings*. vol. 3072, D. Zhang and A. K. Jain, Eds., ed, 2004, pp. 789-796.
- [20] G. Fahmy, D. Nassar, E. Haj-Said, C. Hong, O. Nomir, Z. Jindan, et al., "Towards an automated dental identification system (ADIS)," in *Biometric Authentication. First International Conference, ICBA 2004. Proceedings*, 15-17 July 2004, Berlin, Germany, 2004, pp. 789-96.
- [21] A. K. Jain and H. Chen, "Matching of dental X-ray images for human identification," *Pattern Recognition*, vol. 37, pp. 1519-1532, Jul 2004.
- [22] Z. Jindan and M. Abdel-Mottaleb, "Automatic human identification based on dental X-ray images," in *Biometric Technology for Human Identification*, 12-13 April 2004, USA, 2004, pp. 373-80.
- [23] M. H. Mahoor and M. Abdel-Mottaleb, "Automatic classification of teeth in bitewing dental images," in *ICIP '04. International Conference on Image Processing*, 2004, pp. 3475-3478
- [24] E. Said, G. Fahmy, D. Nassar, H. Ammar, and N. K. Ratha, "Dental X-ray image segmentation," in *Biometric Technology for Human Identification*, April 12, 2004 - April 13, 2004, Orlando, FL, United states, 2004, pp. 409-417.
- [25] M. Abdel-Mottaleb and Z. Jindan, "A content-based system for human identification based on bitewing dental X-ray images," *Pattern Recognition*, vol. 38, pp. 2132-42, 2005.
- [26] H. Chen and A. K. Jain, "Dental biometrics: Alignment and matching of dental radiographs," *IEEE Transactions on Pattern Analysis and Machine Intelligence*, vol. 27, pp. 1319-1326, Aug 2005.
- [27] A. K. Jain and C. Hong, "Registration of dental atlas to radiographs for human identification," presented at the *Biometric Technology for Human Identification II*, 28 March 2005, USA, 2005.
- [28] M. H. Mahoor and M. Abdel-Mottaleb, "Classification and numbering of teeth in dental bitewing images," *Pattern Recognition*, vol. 38, pp. 577-586, 2005.
- [29] O. Nomir and M. Abdel-Mottaleb, "A system for human identification from X-ray dental radiographs," *Pattern Recognition*, vol. 38, pp. 1295-1305, Aug 2005.
- [30] D. E. Nassar, M. Ogirala, D. Adjero, and H. Ammar, "An efficient multi-resolution GA approach to dental image alignment," in *Image Processing: Algorithms and Systems, Neural Networks, and Machine Learning*, January 16, 2006 - January 18, 2006, San Jose, CA, United states, 2006, pp. Society for Imaging Science and Technology, IS and T; SPIE.
- [31] E. H. Said, D. E. M. Nassar, and H. H. Ammar, "Image segmentation for Automated Dental Identification - art. no. 60640X," in *Image Processing: Algorithms and Systems, Neural Networks, and Machine Learning*. vol. 6064, E. R. Dougherty, J. T. Astola, K. O. Egiazarian, N. M. Nasrabadi, and S. A. Rizvi, Eds., ed, 2006, pp. X640-X640.
- [32] E. H. Said, D. E. M. Nassar, G. Fahmy, and H. H. Ammar, "Teeth segmentation in digitized dental X-ray films using mathematical morphology," *IEEE Transactions on Information Forensics and Security*, vol. 1, pp. 178-189, Jun 2006.
- [33] S. Shah, A. Abaza, A. Ross, and H. Ammar, "Automatic Tooth Segmentation Using Active Contour Without Edges," in *Biometric Consortium Conference*,

- 2006 Biometrics Symposium: Special Session on Research at the, 2006, pp. 1-6.
- [34] H. Chen, "AUTOMATIC FORENSIC IDENTIFICATION BASED ON DENTAL RADIOGRAPHS," Department of Computer Science and Engineering, PhD Thesis, Michigan State University, 2007.
 - [35] D. E. M. Nassar and H. H. Ammar, "A neural network system for matching dental radiographs," *Pattern Recognition*, vol. 40, pp. 65-79, Jan 2007.
 - [36] O. Nomir and M. Abdel-Mottaleb, "Human identification from dental X-ray images based on the shape and appearance of the teeth," *Ieee Transactions on Information Forensics and Security*, vol. 2, pp. 188-197, Jun 2007.
 - [37] O. Nomir, M. Abdel-Mottaleb, and Ieee, "Combining matching algorithms for human identification using dental X-ray radiographs," in 2007 Ieee International Conference on Image Processing, Vols 1-7, ed New York: Ieee, 2007, pp. 973-976.
 - [38] S. Chekuri, D. E. Nassar, A. Abaza, E. H. Said, A. Bahu, U. Qurashi, et al., "webADIS: A flexible web-based environment for the automated dental identification system," in 7th Annual International Conference on Digital Government Research, Dg.o 2006, May 21, 2006 - May 24, 2006, San Diego, CA, United states, 2006, pp. 348-349.
 - [39] D.Clark, "Postmortem Dental Identification in Mass Disasters," PhD, University of London, London, , 1990.
 - [40] (February 2005). Forensic identification of 9/11 victims ends. Available: http://abcnews.go.com/WNT/story?id=525937&page=1#.UAKk5E_BW4
 - [41] R. B. Friedman, K. A. Cornwell, and L. Lorton, "Dental characteristics of a large military population useful for identification," *J Forensic Sci*, vol. 34, pp. 1357-64, 1989.
 - [42] ADIS: Automated Dental Identification System. Available: <http://www.csee.wvu.edu/adis/index.html>
 - [43] L. Kang, W. Xiaodong, D. Z. Chen, and M. Sonka, "Optimal surface segmentation in volumetric images - a graph-theoretic approach," *IEEE TRANSACTIONS ON PATTERN ANALYSIS AND MACHINE INTELLIGENCE*, vol. 28, pp. 119-34, 2006.
 - [44] R.-R. Jorge and B.-C. Eduardo, "Medical image segmentation, volume representation and registration using spheres in the geometric algebra framework," *Pattern Recognition*, vol. 40, pp. 171-188, 2007.
 - [45] C. Yao-Tien, "A level set method based on the Bayesian risk for medical image segmentation," *Pattern Recognition*, vol. 43, pp. 3699-711, 2010.
 - [46] H. Chin-Chuan, L. Chang-Hsing, and P. Wen-Li, "Hand radiograph image segmentation using a coarse-to-fine strategy," *Pattern Recognition*, vol. 40, pp. 2994-3004, 2007.
 - [47] T. Zhuowen and B. Xiang, "Auto-Context and Its Application to High-Level Vision Tasks and 3D Brain Image Segmentation," *IEEE TRANSACTIONS ON PATTERN ANALYSIS AND MACHINE INTELLIGENCE*, vol. 32, pp. 1744-57, 2010.
 - [48] J. A. Sethian, *Level Set Methods and Fast Marching Methods: Evolving Interfaces in Computational Geometry, Fluid Mechanics, Computer Vision, and Materials Science*: Cambridge University Press, 1999.

- [49] M. Kass, A. Witkin, and D. Terzopoulos, "SNAKES: ACTIVE CONTOUR MODELS," in Proceedings - First International Conference on Computer Vision., London, Engl, 1987, pp. 259-268.
- [50] V. Caselles, R. Kimmel, and G. Sapiro, "Geodesic active contours," in Proceedings of IEEE International Conference on Computer Vision, 20-23 June 1995, Los Alamitos, CA, USA, 1995, pp. 694-9.
- [51] P. L. Lin, Y. H. Lai, and P. W. Huang, "An effective classification and numbering system for dental bitewing radiographs using teeth region and contour information," Pattern Recognition, vol. 43, pp. 1380-92, 2010.
- [52] D. E. Nassar, A. Abaza, X. Li, and H. Ammar, "Automatic construction of dental charts for postmortem identification," Ieee Transactions on Information Forensics and Security, vol. 3, pp. 234-246, Jun 2008.
- [53] O. Nomir and M. Abdel-Mottaleb, "Fusion of matching algorithms for human identification using dental X-ray radiographs," IEEE Transactions on Information Forensics and Security, vol. 3, pp. 223-233, Jun 2008.
- [54] O. Nomir and M. Abdel-Mottaleb, "Hierarchical contour matching for dental X-ray radiographs," Pattern Recognition, vol. 41, pp. 130-138, Jan 2008.
- [55] A. Banumathi, B. Vijayakumari, A. Geetha, N. Shanmugavadivu, and S. Raju, "Performance analysis of various techniques applied in human identification using dental X-Rays," Journal of Medical Systems, vol. 31, pp. 210-18, 2007.
- [56] L. Xiaoguang and A. K. Jain, "Deformation Modeling for Robust 3D Face Matching," Pattern Analysis and Machine Intelligence, IEEE Transactions on, vol. 30, pp. 1346-1357, 2008.
- [57] C. Hui and B. Bhanu, "Efficient Recognition of Highly Similar 3D Objects in Range Images," Pattern Analysis and Machine Intelligence, IEEE Transactions on, vol. 31, pp. 172-179, 2009.
- [58] S. Tohnak, A. J. H. Mehnert, M. Mahoney, and S. Crozier, "Synthesizing Dental Radiographs for Human Identification," Journal of Dental Research, vol. 86, pp. 1057-1062, November 1, 2007 2007.
- [59] D. Mairaj, S. D. Wolthusen, and C. Busch, "Teeth Segmentation and Feature Extraction for Odontological Biometrics," presented at the Intelligent Information Hiding and Multimedia Signal Processing (IIH-MSP), 2010 Sixth International Conference on, 2010.
- [60] W. J. Schroeder, J. A. Zarge, and W. E. Lorensen, "Decimation of triangle meshes," presented at the SIGGRAPH '92 Proceedings of the 19th annual conference on Computer graphics and interactive techniques, Chicago, IL, USA, 1992 July 27 - 31.
- [61] X. Zhong, D. P. Yu, W. C. Foong, T. Sim, Y. S. Wong, and H.-I. Cheng, "Towards Automated Pose Invariant 3D Dental Biometrics," presented at the International Joint Conference on Biometrics Washington D.C., 2011.
- [62] T. Kondo, S. H. Ong, and K. W. C. Foong, "Tooth segmentation of dental study models using range images," Medical Imaging, IEEE Transactions on, vol. 23, pp. 350-362, 2004.
- [63] T. Kronfeld, D. Brunner, and G. Brunnert, "Snake-based segmentation of teeth from virtual dental casts," Computer-Aided Design and Applications, vol. 7, pp. 221-233, 2010.
- [64] C. Lee, A. Varshney, and D. Jacobs, "Mesh saliency," presented at the SIGGRAPH '05: ACM SIGGRAPH 2005 Papers, 2005.

- [65] Y.-S. Liu, M. Liu, D. Kihara, and K. Ramani, "Salient critical points for meshes," presented at the ACM Symposium on Solid and Physical Modeling, Beijing, China, 2007.
- [66] L. Itti, C. Koch, and E. Niebur, "A model of saliency-based visual attention for rapid scene analysis," *IEEE TRANSACTIONS ON PATTERN ANALYSIS AND MACHINE INTELLIGENCE*, vol. 20, pp. 1254-9, 1998.
- [67] P. Alliez, D. Cohen-Steiner, O. Devillers, B. Levy, and M. Desbrun, "Anisotropic polygonal remeshing," presented at the ACM SIGGRAPH 2003, 27-31 July 2003, USA, 2003.
- [68] N. Gelfand, N. J. Mitra, L. J. Guibas, and H. Pottmann, "Robust global registration," presented at the Proceedings of the third Eurographics symposium on Geometry processing, Vienna, Austria, 2005.
- [69] A. Shmukler and A. Fischer, "Verification of 3D freeform parts by registration of multiscale shape descriptors," *International Journal of Advanced Manufacturing Technology*, vol. 49, pp. 1093-1106, 2010.
- [70] P. J. Besl, "A Method for Registration of 3-D Shapes," *IEEE TRANSACTIONS ON PATTERN ANALYSIS AND MACHINE INTELLIGENCE*, vol. 14, NO. 2, pp. 239-256, 1992.
- [71] Y. Chen and G. Medioni, "Object modeling by registration of multiple range images," presented at the 1991 IEEE International Conference on Robotics and Automation, 1991. Proceedings., , Sacramento, California, 1992.
- [72] G. Fahmy, D. Nassar, E. Haj-Said, H. Chen, O. Nomir, J. D. Zhou, et al., "Toward an automated dental identification system," *Journal of Electronic Imaging*, vol. 14, Oct-Dec 2005.
- [73] C. Hong and A. K. Jain, "Dental Biometrics: Alignment and Matching of Dental Radiographs," in *Application of Computer Vision*, 2005. WACV/MOTIONS '05 Volume 1. Seventh IEEE Workshops on, 2005, pp. 316-321.
- [74] O. Nomir and M. Abdel-Mottaleb, "Hierarchical Dental X-Ray Radiographs Matching," in *Image Processing, 2006 IEEE International Conference on*, 2006, pp. 2677-2680.
- [75] E. H. Said, A. Abaza, H. Ammar, and G. Fahmy, "Accurate segmentation of digitized dental X-ray records," in *Biometrics Symposium, 2008. BSYM '08*, 2008, pp. 77-82.
- [76] A. Abaza, A. Ross, and H. Ammar, "Retrieving dental radiographs for post-mortem identification," in *Image Processing (ICIP), 2009 16th IEEE International Conference on*, 2009, pp. 2537-2540.
- [77] G. Murray. (2011). Rotation About an Arbitrary Axis in 3 Dimensions. Available: <http://inside.mines.edu/~gmurray/ArbitraryAxisRotation/>
- [78] (2011). 3Shape TRIOS® Available: http://biomet3i.com/Pdf/BellaTek/ART1133_3Shape_Brochure.pdf
- [79] V. F. Ferrario, C. Sforza, A. Miani, and G. Tartaglia, "Mathematical definition of the shape of dental arches in human permanent healthy dentitions," *The European Journal of Orthodontics*, vol. 16, pp. 287-294, August 1, 1994 1994.
- [80] S. AlHarbi, E. A. Alkofide, and A. AlMadi, "Mathematical Analyses of Dental Arch Curvature in Normal Occlusion," *The Angle Orthodontist*, vol. 78, pp. 281-287, 2008.

- [81] M. Camporesi, "Thin-plate spline analysis of arch form in a Southern European population with an ideal natural occlusion," *The European Journal of Orthodontics*, vol. 28, pp. 135-140, 2005.
- [82] P.-L. Lin, Y.-H. Lai, and P.-W. Huang, "Dental biometrics: Human identification based on teeth and dental works in bitewing radiographs," *Pattern Recognition*, vol. 45, pp. 934-946, 2012.
- [83] V. F. Ferrario, C. Sforza, A. Miani, and G. Tartaglia, "Human dental arch shape evaluated by Euclidean-distance matrix analysis," *American Journal of Physical Anthropology*, vol. 90, pp. 445-453, 1993.
- [84] J. A. Kieser, V. Bernal, J. Neil Waddell, and S. Raju, "The uniqueness of the human anterior dentition: A geometric morphometric analysis," *Journal of Forensic Sciences*, vol. 52, pp. 671-677, 2007.
- [85] J. Wright. (Wed Jun 27, 2007 12:12pm BST). Tooth clinches identification of Egyptian queen. Available: <http://uk.reuters.com/article/2007/06/27/uk-egypt-queen-idUKL2776273020070627>
- [86] (2004). Adults & Kids Dental Care. Available: http://www.hazletdental.com/edu_anatomy.shtml
- [87] (2002). Tooth Numbering. Available: <http://www.simplestepsdental.com/SS/ihtSSPrint/r.==/st.31843/t.31882/pr.3/c.308449.html>
- [88] L. Chunming, X. Chenyang, G. Changfeng, and M. D. Fox, "Level set evolution without re-initialization: a new variational formulation," in *Computer Vision and Pattern Recognition, 2005. CVPR 2005. IEEE Computer Society Conference on*, 2005, pp. 430-436 vol. 1.
- [89] L. Ibáñez, W. Schroeder, V. H. Project, L. Ng, and J. Cates, *The ITK Software Guide: Kitware*, 2003.
- [90] M. A. Turk and A. P. Pentland, "Face recognition using eigenfaces," in *Proceedings. 1991 IEEE Computer Society Conference on Computer Vision and Pattern Recognition*, Maui, HI, USA, 1991, pp. 586-591.
- [91] C. Xu, Y. Wang, T. Tan, and L. Quan, "A new attempt to face recognition using 3D eigenfaces," in *The 6th Asian Conference on Computer Vision (ACCV)*, 2004, pp. 884-889.
- [92] D. E. Nassar, A. Abaza, L. Xin, and H. Ammar, "Automatic Construction of Dental Charts for Postmortem Identification," *Information Forensics and Security, IEEE Transactions on*, vol. 3, pp. 234-246, 2008.
- [93] T. M. Mitchell, *Machine Learning: McGraw-Hill, Inc.*, 1997.